ASEAN NATURAL VENTILATION STUDY: WIND PRESSURE DISTRIBUTIONS ON LONG BUILDING ROWS IN URBAN SURROUNDINGS

by

Fred S. Bauman, David R. Ernest and Edward A. Arens

ASEAN NATURAL VENTILATION STUDY:

WIND PRESSURE DISTRIBUTIONS ON

LONG BUILDING ROWS IN URBAN SURROUNDINGS

Fred S. Bauman, David R. Ernest, and Edward A. Arens

Center for Environmental Design Research
University of California
Berkeley, CA 94720

16 February 1988

ABSTRACT

To predict the performance of a naturally ventilated building, estimates of the wind-induced surface pressure distribution are needed. In urban environments, where buildings are grouped closely together, these surface pressures will be strongly influenced by the surrounding structures. In addition, the sheltering effect of the surrounding built-up environment can make it more difficult to obtain large enough pressure differences across a building necessary to produce adequate natural ventilation air flow rates.

This paper describes the results of a wind tunnel investigation of wind pressure distributions over an attached two-story shop or housing unit contained in long building rows of the variety that are commonly found in densely populated commercial centers of Southeast Asia (shophouse) and other urban settings (British row house). Surface pressure measurements were made on a 1:125 scale model as a function of wind direction, spacing between adjacent building rows, and building geometry. Simplified correlations are developed to predict the measured surface pressure coefficients and can be used to estimate the natural ventilation air flow through similar full-scale buildings in urban surroundings. The jack roof, a roof-level ventilation device, is a key architectural feature of the test model. Using the developed correlations the characteristics of the ventilation performance of the jack roof are discussed and compared to those for other flow configurations. The jack roof demonstrates significant potential to be an effective natural ventilation design for densely built-up urban areas.

INTRODUCTION

Buildings in hot and humid climates have been traditionally cooled by ventilation. Ventilative air movement in the building interior acts to cool the occupants in two ways. First, it cools the occupant directly by increasing the convective and evaporative heat transfer from the body surface. Second, it cools the occupant indirectly by removing heat stored in the building structure. Traditional buildings are operated in either or both modes depending on the climate. Internal air flows in such naturally ventilated buildings can be 1) wind-driven, resulting from the external wind pressure field, and 2) buoyancy-

driven, resulting from the temperature differences between the building interior and exterior. Even in relatively light winds wind pressure forces, rather than buoyancy forces, are the dominant cause of naturally-driven ventilation.

Traditional naturally ventilated buildings were completely energy efficient, but were unable to provide the same degree of control over the indoor environment as mechanical air-conditioning. These traditional designs had evolved through generations of experience, with little theoretical understanding of how they actually worked. As a result, it was not possible to predict with much accuracy how a building would perform once built. With the advent of mechanical air-conditioning it became accepted that designers would be able to predict and specify quite precisely the building's interior environment. There are, however, substantial energy costs associated with mechanical air-conditioning, and there is also some occupant dissatisfaction with the isolation of mechanically cooled interior spaces from the outdoors. Now ventilative cooling is being widely reintroduced as a means of improving interior comfort conditions and as an energy conservation measure, particularly in hot and humid climates, for residences, schools, factories, and low-rise offices. Because mechanical air-conditioning has given occupants higher expectations regarding the quality of their thermal environment, designers now need more quantitative information to allow them to more accurately predict the performance of naturally ventilated designs.

To predict the performance of a naturally ventilated building, a designer/engineer needs the following information:

1. The characteristics of the local climate, including the coincident occurrences of temperature, humidity, wind speed, and wind direction.

2. Changes in the local wind speed distribution and in the distribution of wind-induced pressures on exterior building surfaces (commonly described in terms of mean pressure coefficients) caused by the surroundings.

3. The relationships needed to calculate the ventilation within the building resulting from a given amount of wind on the exterior. These relationships include determining the above mentioned pressure coefficients for all wind directions of interest and determining the air flow through the building interior resulting from these pressures.

4. The rate of heat transfer to and from the building structure resulting from ventilative air flow past the building interior surfaces.

5. Criteria for human comfort under the range of combinations of temperature, humidity, radiation, and air movement found in naturally ventilated buildings. When occupant comfort is the dominant issue, human comfort models can be used to predict the magnitude of changes in the acceptability of the indoor environment.

6. Building energy analysis to estimate the energy savings consequences of the naturally ventilated design. This information is usually obtained from computer simulation of the building's energy consumption on an hourly basis, although some simplified manual methods using climatic averages are also used.

In urban environments, where buildings are grouped closely together, the wind-induced surface pressure distribution on a building, as well as the local wind velocity field around a given building, will be strongly influenced by the surrounding structures (items 2 and 3, above). In addition, the sheltering effect of the surrounding built-up environment can

make it more difficult to obtain large enough pressure differences across a building necessary to produce adequate ventilation air flow rates. Of the currently available wind pressure data a large majority have been collected 1) to determine wind loads for structural engineering purposes, in which localized and peak pressures are of greater importance than average pressure data (the quantities needed for prediction of ventilation air flow), and 2) for isolated buildings, a situation which rarely occurs in practice. Fortunately, a significant amount of the wind load pressure data is still usable for calculation of natural ventilation air flows, as studied by Vickery, et. al. (1983) and reviewed by Swami and Chandra (1987). The effect of neighboring obstructions (buildings, vegetation, or topography) on average surface pressure distributions and local wind velocities, however, is an area where additional work is still needed.

Previous related studies have looked at the effect of vegetation windbreaks and fences on wind pressures and the resulting air infiltration energy losses/gains in residential housing. The studies were done at small scale in a wind tunnel [Mattingly and Peters (1977)] and at full scale in the field [Mattingly, et. al. (1979)]. Peterka and Cermak (1975) performed a wind tunnel study of wind velocities in the wakes of freestanding buildings. The effect of a single adjacent upwind building on wind pressures on a rectangular building was the subject of a wind tunnel study by Peterka, et. al. (1979). Aynsley (1979) described the influence of a single upwind row of houses on the mean windward and leeward surface pressures of a house for a limited number of wind directions and building spacings.

The effect of a group of surrounding buildings has been studied in a series of wind tunnel experiments performed at the University of Sheffield, UK. Soliman (1973) studied a cuboid and Lee, et. al. (1979) studied a rectangular model at several geometric aspect ratios. In both studies the test model was surrounded by various arrays of identically shaped models. The results of Lee, et. al. give reductions in surface pressures on the test model as a function of building alongwind spacing, the layout of the buildings in the crosswind direction (two grid patterns were examined), and the wind approach direction over either layout. The results of the study show wind pressure reductions of up to 90% resulting from wind blockage by upwind buildings. However, there is a variability of 80% depending on the configuration of the buildings. Hussain and Lee (1980) present additional wind tunnel results on the surface pressure fields and air flow regimes between buildings for rectangular blocks representative of low-rise buildings in suburban areas.

Most recently, Wiren (1985) has performed an extensive wind tunnel study of the wind pressure effects on a 1 1/2-story single-family house surrounded by identical models in various regular arrays. Measurements were made for an isolated model, model with one upwind model, model with two adjacent models, and model within a large group of models. Unlike the previous flat-roofed models, the models used in Wiren's study had a roof pitch angle of 45 degrees. His tests indicated that the maximum reduction in ventilation air flow rate, obtained with three rows of houses surrounding the test house, was about 40%.

The above studies of simplified three-dimensional geometries have begun to address the need for mean pressure data as a function of commonly occurring surrounding building configurations. Not all possible configurations can be handled with this approach (due to time and cost constraints), but a series of well-planned wind tunnel tests should be able to provide the necessary information on building surface pressures for a large percentage of the typical urban and suburban buildings currently being designed. The resulting experimental data bases, along with complementary numerical analysis, can be used to produce correlations for surface pressure coefficients, as part of easy-to-use design calculation techniques. Such tools will improve the architect's and engineer's ability to identify and develop practical naturally ventilated design solutions.

Given a set of pressure distribution data for a building, simplified calculation techniques exist for estimating the amount of ventilation air flow through wall openings. The internal air flow is driven by the pressure difference between surfaces containing ventilation apertures. These air flow equations have been described by Aynsley (1982) for a series of openings without internal flow branching, and by Vickery (1981) for multiple openings with significant internal flow branching. The models make use of discharge coefficients derived from ventilation duct studies, obviously an approximation for typical building ventilation openings. As with the current wind tunnel study, the vast majority of available surface pressure data have been collected for solid models. The presence of flow inlets and outlets will influence the surface pressure in the vicinity of the opening. However, recent investigations by Vickery, et. al. (1983) have shown that the effect of small openings (less than 20% of total wall area) on solid-building pressure data does not significantly affect the accuracy of the above flow models, if the openings are in walls. Vickery did find that the model predictions (based on solid-building pressure data) significantly overpredicted the measured internal air flow for small roof-level outlets. More work is needed to fully understand the performance of roof-level ventilation openings.

Although the wind pressure will vary over a given building surface, particularly near the edges, for low-rise buildings these variations will not have a significant effect on ventilation air flow predictions. As a result, a single average pressure over an entire building surface is typically used in the above air flow models. Swami and Chandra (1987) found that the error produced by using average vs. local pressure data was about 5%. Similarly, Wiren (1985) indicated an error of less than 10%.

Correlations of the type reported in the current study, along with the appropriate air flow models, can be usefully incorporated into ventilation design manuals using manual methods or small computer calculation techniques. Manual design procedures for natural ventilation have been reported by Chandra (1983), Arens and Watanabe (1986), and Swami and Chandra (1987). Pressure coefficient correlations can also be added to large hourly simulation programs (e.g., ESP) containing more sophisticated internal air flow calculation subroutines [Clarke (1986)].

PRESENT INVESTIGATION

The building to be studied is a narrow attached shophouse, commonly found in the densely populated commercial centers of Southeast Asian towns and cities, as well as other urban settings (e.g., the British row house). As shown in Figure 1 [Gurstein (1985)], the typical shophouse consists of two identical two-story units separated by a central walled courtyard. Each unit has a gable roof with a small raised roof vent structure (jack roof) at the roof peak. Shophouses are contained in long rows of identical units, each separated from its adjoining units by roof parapets.

As described above, previous wind tunnel experiments on the influence of surrounding obstructions have largely focussed on three-dimensional models (typically cubical in shape) surrounded by elements of identical size and shape in some sort of grid pattern. The present study will address a configuration in which the test building unit is located near the middle of a long building row, surrounded by other parallel building rows of identical size and shape (see Figure 9). In this arrangement wind effects in the immediate vicinity of the test model will be largely independent of the ends of the building rows. In other words, the position of the unit within the building row will not be a significant parameter, which is expected to be the case for a large majority of such shophouses.

Previous studies of pressure and velocity measurements around two-dimensional rectangular roughness elements are reported in the literature by Perry, et. al. (1969) and Antonia and Luxton (1971). However, their results have limited applicability to realistic building configurations in urban environments, due to the fact that a smooth upwind boundary layer flow was utilized and only one wind direction was investigated.

A key architectural feature of the shophouse design is the jack roof, designed to promote ventilation air flow through the building. The positioning of the jack roof at the roof peak is crucial to its ventilation performance, particularly in built-up urban environments where surrounding buildings can have significant shielding effects. Proposed correction factors based on generalized shielding indicate that the ventilation air flow rates can be reduced by a factor of two to three in typical urban settings, compared to those for the same building in exposed, rural terrain [Sherman and Grimsrud (1982)].

As shown in the schematic flow diagrams of Figure 2, the jack roof can be operated in several different modes. With both sides of the jack roof open, wind-driven air flow through the jack roof will induce air to be extracted from the building (Figure 2A). The performance of roof ventilators using this principle has been studied by Wannenburg (1957). If wind entering the windward side of the jack roof is diverted down into the building (Figure 2B) its ventilation principle will resemble that of windtowers commonly found in Middle Eastern architecture [Bookhash (1981)]. If only the leeward side of the jack roof is allowed to be open, the strong negative pressures will promote the suction of air out through this surface (Figure 2C). One jack roof design of this type has been described by Fairey and Bettencourt (1981). A model of a full-scale laboratory building incorporating a jack roof has been the subject of a wind tunnel investigation by Cermak, et. al. (1981). Vickery, et. al. (1983) performed wind tunnel experiments to compare the measured ventilation air flow rates through a ridge vent (located on the leeward side of a standard gable roof) with those predicted by a simplified model for cross-flow ventilation. When little or no winds are present all jack roof configurations are effective at promoting stack-driven ventilation (Figure 2D).

The central courtyard area is also a distinguishing characteristic of the shophouse design. Smith and Wilson (1977) report the results of a series of parametric tests of wind velocity distributions on the floors of courtyard-like enclosures. The study did not examine wind pressures on the enclosure walls.

The objectives of the current study are to:

1) determine average wind pressures on the external surfaces of a shophouse located in a typical urban environment;
2) develop simplified correlations to predict the average surface pressure coefficients as a function of building spacing, wind direction, and building geometry; and
3) study the potential ventilation performance of the jack roof design.

EXPERIMENTAL METHODS

Boundary Layer Wind Tunnel

The study was conducted in the Boundary Layer Wind Tunnel (BLWT) located in the Building Science Laboratory in the Department of Architecture, University of California, Berkeley. The wind tunnel is of open circuit design with interior dimensions of 1.5 m (5 ft) high, 2.1 m (7 ft) wide, and an overall length of 19.5 m (64 ft). As shown in Figure 3, beginning with the bellmouth entry, the first 12.8 m (42 ft) of the BLWT comprise the flow processing section in which a combination of turbulence generating devices and

roughness elements covering the wind tunnel floor are used to simulate the characteristic surface roughness of the upwind terrain. Immediately beyond the flow processing section is the test area, 3.7 m (12 ft) in length, in which the scale models are placed on a 2 m diameter turntable for testing. A variable speed fan is located downwind of the test area. The data acquisition room is located adjacent to the test area.

Simulation of the Natural Wind

Boundary layer wind tunnels are used to simulate characteristics of natural wind on a scale equal to that of the model building. The simulated region of interest is known as the atmospheric boundary layer (ABL), which corresponds to the gradual increase of wind velocity with height above the ground up to a height where ground based obstacles, such as buildings, trees, and low hills, cease to affect wind characteristics. Within the ABL, the key wind features to be modeled, the vertical distributions of mean wind speed, turbulence intensity, and power spectral density, are largely determined by surface characteristics upwind of a particular building site.

To perform reliable wind tunnel studies of natural ventilation in buildings, careful attention must be paid to the modeling parameters, which can be divided into two categories described below (refer to Aynsley (1985) for a more detailed review of these parameters):

1. *Modeling parameters related to the approaching boundary layer air flow.*
   Parameters in this category describe the major features of a turbulent boundary layer over a rough surface. An acceptable wind tunnel simulation of the full-scale wind at a particular site requires that the following parameters be reproduced at the appropriate scale:

   - Mean Vertical Velocity Profile
   - Turbulence Scale
   - Vertical Turbulence Intensity Profile

2. *Modeling parameters related to the scale model and its immediate surroundings.*
   These parameters must be considered in terms of maintaining geometric similarity of all significant architectural features between the model and full-scale building at the same characteristic length scale used to simulate the atmospheric boundary layer.

   - Model Scale
   - Wind Tunnel Blockage
   - Architectural Detail
   - Surrounding Obstructions
   - Reynolds Number Criteria

Each of the above modeling parameters are discussed below in relation to the current experiments.

Approaching Boundary Layer Air Flow
The entire depth of the atmospheric boundary layer (typically 400-600 m) could not be modeled at the 1:125 model scale due to the height limitation of the wind tunnel. Fortunately, previous work has shown that acceptable results can be obtained without full-depth simulations [Cook (1973) and (1982)], and therefore, for the work described here only the lower portion of the ABL was simulated. The time-varying wind speeds which occur in a turbulent boundary layer are commonly split into a mean (U, V, and W)

and a fluctuating (u′, v′, and w′) component (for the longitudinal, lateral, and vertical directions, respectively). The variation of the mean longitudinal (along-wind) velocity component (the most important component for boundary layer flow) with height in the lower levels of the ABL (the region of greatest interest in building-related wind studies) is best represented by the logarithmic velocity profile for a thermally neutral atmosphere.

$$U(z) = (u*/k) \ln[(z-d)/z_0] \quad (1)$$

where:

$U(z)$	= mean velocity at height z
$u*$	= friction velocity
k	= von Karman's constant (0.4)
z_0	= roughness length
d	= displacement height

In Equation (1) z_0 is a measure of the retarding effect that the terrain has on the wind speed near the ground. In rough terrains (e.g., built-up or urban areas) d represents the height to which the best-fit logarithmic velocity profile is displaced above the ground. As indicated in Equation (1) all heights in the boundary layer are referenced to d, the zero-plane displacement. The value of d is generally less than the average height of the surrounding buildings and can be assumed to be zero in smoother terrains. The quantity $u*$, the friction velocity, is defined for convenience in the following way: $\tau_0 = \rho u*^2$, where τ_0 is the shear stress at the ground.

Equation (1) can be reorganized into the following form:

$$\ln(z-d) = (k/u*)U(z) + \ln(z_0) \quad (1A)$$

Thus, by plotting U(z) versus ln(z-d) the key features of Equation (1) can be visualized. As shown in Figure 4, a straight line fit to the data produces $\ln(z_0)$ as the y-intercept with the slope of the line equal to $1/2.5u*$.

The building configuration under investigation in the current experiments can be characterized as a low urban environment with long rows of relatively closely-spaced 2- to 3-story buildings extending for large distances in any direction. For this type of terrain typical values for z_0 and d in Equation (1) are: $0.3 \text{ m} \leq z_0 \leq 0.7 \text{ m}$ and $5 \text{ m} \leq d \leq 10 \text{ m}$ [ESDU (1982), (1974, 1975, and 1985)].

Turbulence intensity is a measure of the magnitude of velocity fluctuations compared to the mean velocity at a point in turbulent flow. It is a non-dimensional quantity defined below:

$$I_i = \left(\overline{i'^2}\right)^{1/2} / U(z) = \sigma_i / U(z) \quad (2)$$

where:

I_i	= i-component of turbulence intensity (i = u,v,w)
i'	= fluctuating component of velocity
σ_i	= standard deviation of i-component of velocity at height z

Turbulence intensities are always greatest near the ground, where the boundary layer flow interacts with the surface roughness and obstructions, and decreases with increasing height above the ground. Typical values for a low urban terrain are approximately 0.4 near the ground, decreasing to around 0.2 at a height of 60-70 meters [ESDU (1984)].

The approaching boundary layer flow was simulated in the wind tunnel using techniques similar to those described by Cook (1982). These methods are used to artificially accelerate the development of a boundary layer of sufficient depth in a smaller length wind tunnel, such as the one at UC Berkeley. The following wind tunnel devices and roughness elements were used to produce the desired boundary layer for the 1:125 scale models (see Figure 5):

- a square mesh turbulence grid at entrance to tunnel;
- a 0.4 m high sawtooth (0.2 m high teeth) trip fence 0.6 m downwind of grid;
- 3 m of bricks (200 mm high, 100 mm wide, 60 mm deep) placed on end at 7.5% density (density = percentage of wind tunnel floor area covered by roughness element;
- 3 m of bricks (100 mm high, 200 mm wide, 60 mm deep) placed on side at 7.5% density; and
- 4.6 m of wood blocks (88 mm high, 88 mm wide, 38 mm deep) at 7.5% density.

Under test conditions and procedures identical to those used in the model experiments (described below) velocity and turbulence intensity profiles were measured in the wind tunnel at the front edge of the turntable to document the approach wind conditions. These measured profiles are presented in Figures 6 and 7. A regression fit to the measured data ($R^2 = 0.96$) in Figure 6 produced a roughness length (z_0) of 0.48 cm (full-scale $z_0 = 0.6$ m) for a displacement height (d) of 5.0 cm (full-scale d = 6.25 m), well within the accepted range of values prescribed by ESDU. In Figure 7 the measured turbulence intensities vary between 0.46 to 0.20 for heights of 9.6 to 56 cm (equivalent full-scale heights of 12 to 70 m), corresponding well to values recommended by ESDU for the lower region of the atmospheric boundary layer.

The power spectral density function of atmospheric turbulence provides information about the energy input from different frequency ranges of the fluctuating velocity components. The von Karman spectral equations have been generally accepted as the best analytical model of isotropic turbulence. In the high frequency range ($nz/U(z) > 0.1$), which is the range most appropriate for studies of air flow around buildings, the von Karman equation takes the following functional form.

$$nS_u(n)/\sigma_u^2 = A\,(nL_x(u)/U(z))^{-2/3} \qquad (3)$$

where:

n = frequency
$S_u(n)$ = u-component spectral density function at frequency n
σ_u^2 = variance of u-component of velocity
A = parameter dependent on z and thickness of boundary layer [ESDU (1985), #85020]
$L_x(u)$ = longitudinal integral length scale

The longitudinal integral length scale, $L_x(u)$, is representative of the size of turbulent eddies in the approaching boundary layer flow. $L_x(u)$ will tend to increase in length with increasing height above the ground, as the flow is further removed from the turbulence generating effect of the surface roughness. $L_x(u)$ was determined indirectly through measurement of the power spectral density function at three different heights (8 cm, 10 cm, and 15 cm) above the front edge of the turntable. At each height 30 separate measurements were made, each consisting of 64 scans/second for a duration of 64 seconds. The time-based measurements were converted to frequency-based data by applying a Hanning window to each 4096-point data set followed by a fast Fourier

transform to produce the power spectrum. The 30 power spectrum curves were averaged together to generate the final result. In Figure 8 the measured power spectrum at a height of 15 cm is compared to the power spectrum recommended by ESDU (1974, 1975, 1985). The ESDU data is based on a large database of full-scale measurements of the atmospheric spectrum. The turbulence scale of the wind tunnel boundary layer was then determined using the following process: 1) The peak frequency of the nondimensionalized power spectrum was matched with that recommended by ESDU . 2) Using the method described by Cook (1978), the simulated turbulence scale, and therefore the most appropriate model scale, was calculated. $L_x(u)$ was calculated for each of the measurement heights: at $z = 8$ cm, $L_x(u) = 0.31$ m; at $z = 10$ cm, $L_x(u) = 0.36$ m; at $z = 15$ cm, $L_x(u) = 0.48$ m. At all three measurement heights the calculated model scale was between 1:130 to 1:140, an excellent match with the model scale of 1:125.

Scale Model and Immediate Surroundings

In selecting the length scale of wind tunnel models several factors must be considered. Depending on the details of the air flow phenomena under investigation as well as the type of measurements being made, models need to be large enough to allow key architectural features to be accurately reproduced and to accommodate the necessary instrumentation. For example, early flow visualization studies of natural ventilation performed by Smith (1951) demonstrated that small architectural details (e.g., edges of air flow inlets) can significantly influence the observed air flow patterns inside the model. On the other hand, models need to be small enough to prevent any adverse effects due to wind tunnel blockage, as well as to allow the simulated boundary layer (or partial boundary layer in the present case) to completely envelope the model. Wind tunnel blockage is the percentage of the cross-sectional area of the wind tunnel test section occupied by the models. Blockage of 2% can cause pressure measurement errors on the order of 5% (Melbourne, 1982), while blockage of 10% can cause large errors on the order of 50%. Many detailed wind tunnel studies of fluctuating surface pressures are keeping blockage below 2%. But for average surface pressure measurements, such as those being made in the current experiments, it is generally acceptable to keep the wind tunnel blockage below 5%. If larger models are necessary, some wind tunnels (including the UC Berkeley wind tunnel) have movable roofs above the test section, which can be raised to compensate for the tunnel blockage.

In the present study, the building rows (2 meters long) extended nearly across the entire width of the wind tunnel. A model height of 8 cm (corresponding to a 10-meter high full-scale building) was selected, thus producing a maximum wind tunnel blockage of 4.9%. Due to the fact that the approaching urban boundary layer was being simulated by 8.8 cm wood blocks directly upwind of the model location, the blockage effects due to the model size were actually part of the normal boundary layer flow. In this case, the continuous obstruction of the flow by the roughness elements and the models eliminates the blockage effect. No corrections were made to the pressure measurements obtained with this configuration.

When the height of the surrounding environment (adjacent structures, trees, etc.) is on the same order as the height of the subject building, as in the current study, then the surrounding buildings must also be modeled in detail. For low-rise suburban terrain the extent of this modeling is recommended to be a radius of ten building heights (Aynsley, 1985). In the current model set up, surrounding buildings were modeled to the edge of the turntable, having a radius of one meter. Further upwind of the turntable, general roughness elements on the wind tunnel floor (described above) were used to simulate the characteristics of the approaching boundary layer flow.

To perform accurate wind tunnel simulations for purposes of making pressure and velocity measurments, it is ideally required to maintain equality of the Reynolds number (Re) between full and model scale. The Reynolds number is defined as:

$$Re = UL/\nu \qquad (4)$$

where:

U = freestream velocity (m/s)
L = characteristic model length (m)
ν = kinematic viscosity of the fluid (m^2/s)

In low-speed boundary layer wind tunnels using air as the working fluid, Reynolds number equality is impossible to achieve, as demonstrated by the example of the current study (model scale = 1:125). To maintain equality of the Reynolds number in the wind tunnel simulation, the wind speed would have to be increased to 125 times its full-scale value! Fortunately, for air flow around sharp-edged objects (bluff bodies) the aerodynamics are relatively insensitive to Re. This is because separation of the surface boundary layer always occurs at the sharp corners of the object, even at low air velocities. As a result of these well-defined separation points, the relative velocity distributions and their associated surface pressure distributions remain very nearly constant over a wide range of approaching air velocities (Re). Provided a minimum Reynolds number of 2×10^4 is obtained, the above described Reynolds number independent flow around bluff buildings is usually achieved (Cermak, et. al., 1982).

For the current study, measurements were taken at an average velocity of 8.7 m/s. Using the characteristic model dimension of 8 cm and $\nu = 1.2 \times 10^{-5}$ m^2/s, it is found that $Re = 5.8 \times 10^4$, satisfying the above minimum Reynolds number criteria. This value of the Reynolds number, however, is much lower than the appropriate full-scale value (10^7 for a 12 m/s wind).

Building Models

A model containing two identical building units was designed and fabricated based on the typical shophouse configuration shown in Figure 1. The two model units were connected by a central courtyard area and, together, represent a single attached shophouse unit located within a long row of similar building units. Figures 9A and 9B show perspective drawings of how the building model is positioned within the long double rows. Each double row is separated from adjacent identical double rows by a space representative of a street or alley. The model was fabricated out of 3 mm (1/8 in) plexiglas at a scale of 1:125. Figure 10 presents a perspective cut-away drawing of the plexiglas test model (the facing building and courtyard walls are removed). The key architectural features of the shophouse model are as follows:

- The overall dimensions of each model unit are H=80 mm, L=80 mm, and W=40 mm, representative of a two-story shophouse, 10 meters high to the top of the jack roof, 10 meters long and 5 meters wide.
- The roof pitch angle (α) is fixed at 20 degrees.
- A 6 mm high jack roof (0.75 meter in full scale) is located at the roof peak and covers the top third of the roof.
- Parapets, equal in height to the jack roof, extend along both sides of the pitched roof, separating each adjacent shophouse unit.
- Both the jack roof and parapets are removable, allowing alternate roof configurations to be investigated.

- Each central courtyard is separated from adjacent courtyards by walls of variable height ($h_c/H_e = 0, 0.5, 1$). For full-height walls (extending up to eave height, H_e) an optional passageway on the second floor covers half of the courtyard and allows access between the front and back units at that level.

The surrounding building models, including the remainder of the building rows containing the plexiglas test models as well as the upwind and downwind building rows, were all constructed from blue styrofoam. Thin transparent tape was used to provide a smooth connection beteen the test models and the adjoining styrofoam models.

Note that none of the ventilation inlets and outlets (e.g., windows or jack roof openings) were included in the models. Rather, pressure taps were installed at the appropriate locations on the solid model surfaces. Figures 11A and 11B are exploded plan views of the two models showing the pressure measurement (tap) locations for the standard roof and the jack roof designs. During all tests the models were configured such that Model #1 was the upwind model and Model #2 was the downwind model. For each model unit 18 taps were monitored for the standard gable roof model, and for the jack roof design, an additional 4 taps for a total of 22 taps were monitored. Tap locations were selected to allow the measured pressures to represent averages over equal-sized areas on a given model surface.

Pressure Measurement

To make pressure measurements, pressures at the selected locations are transmitted to a pressure transducer, which converts the pressure to an analog signal. In practice, the measurement of surface pressures on scale models is complicated by the following two factors. First, since a relatively large number of measurement locations are used, simple economics makes it necessary to use a multiple pressure switch, thus reducing the number of required pressure transducers. Second, the small size of the models do not permit the pressure switches to be mounted in close proximity to the measurement locations. Instead, lengths of tubing are used to connect the various elements of the measurement system, which can alter the surface pressure by the time it reaches the transducer. These problems are addressed below in terms of the current experimental set up.

Pressure measurements were made to 1) determine average surface pressures at selected locations on the model external surfaces, and 2) monitor the free-stream dynamic and static pressures at a fixed reference location in the wind tunnel. Figure 12 presents a schematic diagram of the pressure measurement system configuration. The pressure at a point on the external surface of the model is measured by installing pressure taps [1.6 mm (0.063 in) O.D. hollow stainless steel tubing, 2.54 cm (1 in) long] through the exterior walls at the desired measurement locations on the model. The wind pressure acting on the exposed end of the pressure tap is transmitted to the pressure switch through 1.6 mm (0.063 in) O.D. vinyl tubing, connecting the inside end of the pressure tap, through an access hole in the wind tunnel floor, to the switch mounted below the tunnel. The pressure switch consists of two 24-port Scanivalve Corp. Model W0602/1P-24T fluid switch wafers, FSW (for simplicity only one is shown in the figure), allowing up to 48 pressure lines to be connected to a single transducer. Pressure measurements are made with two Validyne Model DP103 differential pressure transducers. Each transducer is connected to a Validyne Model CD15 sine wave carrier demodulator (SIG COND), which performs signal conditioning, generating an electrical analog of the pressure to be read by the PC/AT data acquisition system. As shown in the figure, Transducer #1 is connected to the output tubing from the fluid switch wafer. A

Scanivalve Model WS5-24 solenoid stepper drive (DRIVE) and Model CTLR2 solenoid controller (CTLR) permit computer-controlled switching between the pressure lines connected to the fluid switch wafers. To maintain equivalent measurement conditions for all taps, vinyl tubing lengths are all 0.6 meters (2 ft) between the taps and the fluid switch wafers, with an additional 4 meters between the wafers and Transducer #1.

Freestream static and total pressures at the stationary reference location are monitored with a Dwyer Model 166-12 pitot tube. As shown in Figure 4, the pitot tube was suspended from the wind tunnel ceiling, 0.26 meters below the wind tunnel ceiling and 0.9 meters upwind of the front edge of the turntable. The location of the reference pitot tube was selected to eliminate any interference with simultaneous building model measurements, while providing a stable characteristic reference pressure away from the influence of the models and wind tunnel roughness elements. The static pressure port of the reference pitot tube was split and connected to one side of both pressure transducers, therefore serving as the static reference pressure during the tests. The static pressure line was further split and connected to port #1 of both fluid switch wafers. The total pressure port of the pitot tube was split and connected to Transducer #2 (this transducer was dedicated to the measurement of dynamic (total minus static) pressure at the reference location) and to port position #24 on both fluid switch wafers. Connections from the pitot tube were made with 1.27 cm (0.5 in) O.D. polyflow tubing. As above, each separate run of tubing was of equal length, approximately 5 meters. Ports 2-23 on each fluid switch wafer were available for connection to surface taps in the model.

The above described pressure tubing arrangement allowed online calibration corrections to be made for Transducer #1. This was done in the following manner. Measurement of port #1 on the fluid switch wafer allowed a check of the "zero" point , or offset, of the linear calibration line for the pressure transducer. For each sequence of measurements using the fluid switch wafer, all subsequent pressure readings (ports 2-24) were corrected by the offset amount, which was generally a very small value. During the same measurement sequence, when port #24 was monitored, a check of the slope, or gain, of the calibration line for transducer #1 was made by comparison with the dynamic pressure measured by transducer #2. All such comparisons found less than a 1% difference between transducers so no further corrections were made.

Although fluctuating pressures can play an important role in structural analysis of buildings, for purposes of ventilation air flow calculations only mean pressure distributions are needed. Because of this, no additional modifications to the pressure tubing system were made, as discussed briefly below. A standard technique used in many wind tunnel studies to reduce the "pipe-organ" resonant fluctuations in the tubing system is to place a restricting insert in the tubing. This effect was observed in the current study by comparing the RMS reference dynamic pressure measured by Transducer #2 (polyflow tubing) to that measured by Transducer #1 (polyflow tubing with a small length of small diameter vinyl tubing). In the above comparison, the RMS pressure measured by Transducer #2 was significantly higher, but the mean pressures always agreed to within 1%, as described earlier.

With a mean reference velocity at the pitot tube of 8.7 m/s, each pressure measurement consisted of simultaneous readings from the two pressure transducers: Transducer #1 monitored the pressure taps on the model surfaces, and Transducer #2 monitored the dynamic reference pressure at the pitot tube. The transducers were sampled at a rate of 30 readings per second for a duration of 30 seconds. Each block of 900 data points was analyzed to produce the mean pressure and standard deviation. Upon switching to a new port location of the fluid switch wafer, a delay of 15 seconds was implemented to allow the line pressure to stabilized at its new mean value. This was based on tests which

indicated that a maximum delay of approximately 10 seconds was necessary when changing from a high (dynamic) pressure to a low (negative) building pressure.

Surface pressure data is most commonly represented in terms of a non-dimensionalized pressure coefficient, as described in Holmes (1982) and defined below:

$$C_p = (P-P_s)/(0.5\rho U_{ref}^2) = (P-P_s)/P_d \quad (5)$$

where:

C_p = mean pressure coefficient
P = mean pressure at building surface (Pa)
P_s = mean static reference pressure (Pa)
P_d = mean dynamic reference pressure = P_t-P_s (Pa)
P_t = mean total reference pressure (Pa)
ρ = density of air (kg/m^3)
U_{ref} = mean reference velocity (m/s)

During wind tunnel tests the static and dynamic reference pressures and mean reference velocity are all typically measured at the same location. As described earlier, this reference location was chosen to be at the stationary reference pitot tube. In practice, however, pressure coefficients are often normalized by the dynamic pressure at the equivalent 10-meter height, the most common weather station height. This allows the results to be related to full-scale conditions. Since simultaneous measurements at the 10-meter full-scale reference height (8 cm at wind tunnel scale) could not be made without disturbing the model measurements, the pressure coefficient was determined in two stages as defined below:

$$\begin{aligned} C_p &= (P-P_s)/(0.5\rho U_{10}^2) \\ &= (P-P_s)/P_d * P_d/(0.5\rho U_{10}^2) \\ &= C_{p,ref} * D \end{aligned} \quad (6)$$

where:

C_p = mean pressure coefficient normalized by dynamic pressure at equivalent 10-meter (8 cm) height
$C_{p,ref}$ = mean pressure coefficient normalized by dynamic pressure at stationary reference pitot tube
D = dynamic pressure height correction factor (9.47)
U_{10} = mean velocity at equivalent 10-meter (8 cm) height (m/s)

In Equation (6), $C_{p,ref}$ was measured directly as described above. The dynamic pressure height correction factor, D, was determined from a separate measurement with a hot-film anemometer placed at the equivalent 10-meter height (8 cm). The static pressure was assumed to be constant at both the reference and 8 cm heights, and no static pressure correction factor was applied in the equation. All mean surface pressure coefficients presented in this report are of the form defined by Equation (6).

Prior to wind tunnel tests the pressure transducers were calibrated by comparison with a Dwyer Model 1430 Microtector gauge. Accounting for the instrumentation error and resolution of the PC/AT data acquisition system, the estimated accuracy of the mean pressure coefficient measurements is such that a "true" measurement will fall within the following limits (for a constant reference dynamic pressure of 45.5 Pa):

$$C_{p,true} = C_{p,meas} \pm 0.065$$

In separate tests involving repeated mean pressure coefficient measurements under identical conditions, all measurements fell consistently well within the above limits.

Velocity Measurement

Air velocity measurements were used to 1) determine the boundary layer profiles of mean velocity and turbulence intensity; 2) determine the power spectral density function at selected points in the flow; and 3) determine the reference wind speed at a height (8 cm) equivalent to the full-scale reference height (10 meters). These measurements were made with Thermo Systems, Inc. (TSI) Model 1053B anemometers attached to TSI Model 1210-20 hot film probes.

To determine the characteristics of the approaching boundary layer flow, velocity measurements were made at the front edge of the turntable, immediately upwind of the scale models. Each measurement consisted of simultaneous readings from a Model 1210-20 probe, positioned at the desired height, and the stationary reference pitot tube (described above). For the mean velocity and turbulence intensity measurements the probes were sampled at a rate of 15 readings per second for a duration of 30 seconds. The height of the anemometer above the wind tunnel floor was controlled with a computer-driven probe-traversing device.

Mean wind speed measurement results are presented in terms of a velocity ratio, defined as the ratio of mean velocity at the desired location to mean velocity at the reference height pitot tube.

$$\text{Velocity Ratio} = U(z)/U_{ref} \qquad (7)$$

where:

U_{ref} = mean velocity at stationary reference pitot tube (m/s)

Prior to the wind tunnel tests, probe calibrations were performed with a TSI Model 1125 calibrator using an MKS Instruments, Inc. Model 220BD differential pressure transducer. A 13-point calibration over the range 0.1-7.5 m/s was carried out, producing the characteristic 4th-order polynomial calibration curve. Accounting for the instrumentation error and resolution of the PC/AT data acquisition system, the estimated accuracy of the calibration is such that a "true" calibration curve will fall within the following limits:

$$\begin{aligned}
U < 0.15 \text{ m/s} &\Rightarrow U_{true} = U_{cal} \pm (0.1U_{cal}) \\
0.15 \text{ m/s} \le U < 0.60 \text{ m/s} &\Rightarrow U_{true} = U_{cal} \pm (0.05U_{cal}) \\
0.60 \text{ m/s} \le U \le 3.0 \text{ m/s} &\Rightarrow U_{true} = U_{cal} \pm (0.12 + 0.05U_{cal}) \\
U > 3.0 \text{ m/s} &\Rightarrow U_{true} = U_{cal} \pm (0.02 + 0.02U_{cal})
\end{aligned}$$

Experience with repetitions of identical mean velocity measurements have indicated that the repeatability of such measurements falls consistently within a 10% margin of error.

Data Acquisition System

An IBM PC/AT-based data acquisition system was used to record the pressure transducer and anemometer measurements, to perform on-line statistical analysis, and to provide the required user interface during the wind tunnel tests. The PC/AT also controlled the

vertical position of the hot wire anemometer during the boundary layer profile measurements, and the solenoid drive for the fluid switch wafer.

Preliminary Tests

Prior to commencing the full data collection procedures, a number of preliminary tests were performed to verify the consistency and accuracy of the measurement procedures and model setup configurations. These tests are described briefly below.

The pressure measurement procedure was studied to 1) establish the optimum scan length, 2) establish the necessary delay time between individual measurements, and 3) determine the effect of tubing length and diameter. The results of these studies have been discussed earlier in *Pressure Measurement.*

The model setup configuration was studied in the following ways:

1. Localized pressures over the front and back facades of both models were studied by comparing the individual tap measurements on these surfaces (see Table 1). Due to the largely two-dimensional geometry of the building facades, with the exception of the lower front facade of Model #1, pressures showed little variation laterally across these surfaces. It was decided that a representative average pressure could be obtained from the two centrally located taps. In addition, localized pressure coefficients on both vertical surfaces facing the central courtyard were found to be very similar in magnitude for all model configurations tested. For this reason a single average courtyard pressure coefficient is reported. The combinations of individual taps used to produce the average surface pressure for each surface are identified in Table 2.
2. Pressures measured on the two shophouse models placed side-by-side were compared to verify the accuracy of the model construction and measurement procedure.
3. Pressure measurements were made as a function of number of parapets placed along the roof in either direction from the test model. It was found that a minimum of 3 parapets on both sides were needed to accurately model the effect of the parapets.
4. Pressure measurements were made as a function of number of courtyard walls placed between the building rows in either direction from the test model. It was found that a minimum of 3 walls on both sides were needed to accurately model the effect of courtyard walls, although in the tests, 9 walls were used.
5. Tests were performed to determine the level of architectural detail necessary on the adjacent upwind double-row models. The results showed that the existence of the parapets and courtyard walls had a negligible influence on downwind test models, but that the jack roof did have a significant effect. The jack roof result is discussed in *Results and Discussion.*
6. Pressure measurements obtained for equal, but opposite, wind direction angles were compared to verify the expected symmetry of these results. Agreement was found to within the previously stated experimental error. All subsequent wind direction angles were measured in only one direction from normal to the building row.
7. The length of the building rows necessary to eliminate any end effects was studied, particularly for wind angles greater than 45°, where the ends of the rows were more exposed to the approaching boundary layer flow. It was found that modeling the building rows over the extent of the turntable (2 meters in diameter) was sufficient.

PROGRAM OF STUDY

Building surface pressures were measured in response to a number of parameters varied over the ranges defined below. Refer to Figures 13A, 13B, and 13C for illustrations of the typical model layout, roof configurations, and courtyard configurations.

1) wind direction (θ):	0°, 15°, 30°, 45°, 60°, 75°, 90° from normal
2) spacing between double rows (s):	$S = s/H = 0.5, 1, 2, 3, 4, 5$
3) courtyard spacing (s_c):	$S_c = s_c/H = 0.25, 0.5, 1$
4) courtyard wall height (h_c):	$H_c = h_c/H_e = 0, 0.5, 1$
5) roof configuration	a) without jack roof, without parapet (NJ,NP) b) with jack roof, without parapet (J,NP) c) with jack roof, with parapet (J,P)

where:
H = building height
H_e = eave height (maximum courtyard height)

For each of the above three roof configurations, seven wind directions and six row spacings were investigated for a total of 42 measured pressure distributions. During each series of tests the courtyard was held at a fixed configuration. For the standard gable roof (without jack roof, without parapet) this was $S_c = 0.5$ and $H_c = 0$. For the two jack roof configurations this was $S_c = 1$, $H_c = 1$, and no second level passageway. Variations in the courtyard spacing and geometry were studied only for a fixed upwind row spacing of $S = 1$, and for the jack roof with parapet roof configuration. These procedural simplifications were justified 1) due to the observed insensitivity of courtyard surface pressures to variations in row spacing (S), 2) due to the relatively small effect of roof configuration on courtyard surface pressures, 3) due to the very repeatable dependence of courtyard surface pressures on wind direction, and 4) in the interest of reducing the number of wind tunnel tests to a manageable number.

RESULTS AND DISCUSSION

The pressure measurement results have been analyzed using STATGRAPHICS*, a PC-based data analysis and graphics program. Using a step-wise multiple linear regression fitting routine, simplified correlations have been developed, as a function of wind direction and row spacing, which predict the average pressure coefficients for many of the surfaces with a high degree of accuracy. All correlation equations took the same general form which is given below:

$$C_p = C_0 + \sum_{i=1}^{N} C_i . F_i \qquad (8)$$

where:

C_i ($i = 0,1,...,N$) are constants defined in Tables 4 and 5
F_i ($i = 1,2,...,N$) are functions defined in Tables 4 and 5

*STATGRAPHICS, STSC, Inc., 2115 E. Jefferson St., Rockville, MD 20852.

Table 4A presents the correlations for the standard gable roof building (NJ,NP); Table 4B presents the results for the two jack roof buildings ((J,NP) and (J,P)); and Table 5 presents the results for the variable courtyard configuration. It was found that for most building surfaces the pressure coefficients could be correlated with only three or fewer terms in the above equation. One term (C_0) was a constant. The "$\cos^2\theta$" term was used to account for wind angle dependence. The "$\cos\theta * S$" and "$\cos\theta * \ln(S)$" terms account for the decreasing effect of spacing at larger wind angles, when the wind is channeled down the streets. The rationales for additional terms which appear in the correlation equations for a few building surfaces are described in the appropriate sections below.

The pressure measurement results and correlation predictions are presented, compared, and discussed below in a series of graphs in which the average pressure coefficient (defined in Equation (6)) for a given surface is plotted as a function of wind direction (θ) and spacing (S). Model configurations are identified on each figure according to the key shown in Table 3.

Pressure Distribution on Model #1

Many of the observations discussed below and their relationship to one another are illustrated in Figures 14 and 15. Figure 14 shows mean pressure coefficients as a function of tap location for the front of Model #1 and Figure 15 shows the results for the back of the model. The results are for the jack roof with parapet, an upwind spacing of S = 2, and for three wind directions (0°, 45°, and 90°). The observations are as follows:

1. Pressures on the windward side of the model exhibit large differences between individual surfaces. This is due to the strong incident winds on some of the surfaces, along with flow separation at several locations (front edge of lower roof, top of jack roof, and, for wind angles of 45° and 90°, top of parapets).
2. In contrast, the pressures on the leeward side of the model are nearly constant at all tap locations, for a given wind angle. This clearly demonstrates how the wake region encompasses the entire leeward side of the model.
3. At 90° wind angle, the pressure coefficients for both sides of the model are very nearly equal and approach zero. This is an expected result as the wind is channeled between building rows on both sides of the model.
4. The largest pressures on the windward side of the model are obtained for a wind direction of 45° on the lower front roof (taps #8 and #9), and on half of the front jack roof (tap #12). In both cases the presence of the parapets strongly influences the pressures at these locations.
5. The largest negative pressures on the leeward side of the model occur on the jack roof, due to its close proximity to the strong separation from the roof peak.
6. For the 0° wind angle, all pressure coefficients on the windward side of the model are negative or zero. This indicates that even at an upwind row spacing of S = 2, the front of the model lies in the wake region of the upwind model.

Front Facade

Figures 16, 17, and 18A present measured data and the predictions of the developed correlations for the front facade of Model #1 for each of the three roof configurations. Table 4 contains the correlation equations. The observations are as follows:

1. The results follow similar trends for all three roof designs.

2. Pressure increases with increasing spacing. At small spacings and small wind angles the front facade falls in the wake region of the upwind building row, as indicated by the large negative pressure coefficients.
3. As expected, as the wind direction approaches 90°, the wind is channeled down the streets between the building rows, resulting in similar surface pressure coefficients for all three model configurations. The results approach zero at 90° for all spacings.
4. For the two models with the jack roof the existence of the parapet has very little effect.
5. The model with the standard gable roof (NJ,NP) shows slightly higher pressures compared to the two jack roof models. This is particularly evident at small wind angles, where the shielding effect of the taller upwind building row (with the jack roof) is strongest.
6. Excellent agreement was obtained between the measured data and correlation predictions. Figure 18B shows an example of the correlation fit for the results of Figures 17 and 18A.

The localized pressure coefficients on the lower front facade (tap #3) are compared with those on the upper front facade (tap #6), along with the average, in Figure 19. Results are shown for the jack roof without parapets, and are similar for the other roof configurations. Note that the average results for a spacing of 0.5 are very similar to those for a spacing of 1. The pressures are quite similar within the experimental accuracy of the measurements. However, the lower facade does consistently experience a slightly higher pressure, especially at small wind angle.

Lower Front Roof

Although the lower portion of the front roof of Model #1 (tap #8) is not a surface that would normally serve as a ventilation inlet or outlet, the measurement results are instructive in understanding the nature of the air flow over the model. Figures 20, 21, and 22 present the measured data for the three roof configurations. The observations are as follows:

1. At small spacings, pressures are low as the roof lies within the wake region of the upwind building.
2. At normal incidence, negative pressure coefficients are obtained for all spacings and model configurations, indicating the above described wake effect, or at larger spacings, separation from the front edge of the roof.
3. The influence of the parapet "catching" the wind is most evident for intermediate spacings (S = 2,3), where significantly higher (positive) pressures are obtained at an angle of 45° (see Figure 22). At larger angles the shielding effect of the upwind parapet causes the pressures to be reduced from the peak values.
4. At larger spacings a less obstructed approach flow shows a stronger separation from the front edge of the roof, as pressures decrease for all model configurations. This effect is strongest for the standard gable roof (Figure 20) due to the lower upwind building and the absence of the recirculation region in front of the jack roof.

Front Jack Roof

Figures 23 and 24A present the measured results and the correlation predictions for the front jack roof for Model #1. Table 4B contains the correlation equation. The observations are as follows:

1. The results show some of the same patterns observed for the lower front roof, although

pressures at small wind angles are larger.
2. Results are very similar for both figures, indicating that the parapet has a small effect on the average pressure for this surface.
3. Both figures indicate that for spacings in the range of 2 to 3 the measured pressures are approaching their maximum values at a wind angle of around 45°. Increasing the upwind spacing any further does not produce a significant increase in pressure on this surface. If a design objective is to maximize pressure on the front of the jack roof (presumably to increase the induced volume of air flow from the building interior out the back of the jack roof (see Figure 2A)), a spacing of S = 2-3 may be close to an optimum choice in urban areas where large spaces between buildings are not an option.
4. The influence of the more complex geometry of the jack roof made it more difficult to achieve as accurate of a correlation fit, although reasonable agreement was obtained between a single correlation and the results of both jack roof model tests (with and without parapets) (see Figure 24B and Table 4B).
5. The correlation equation contains one additional term. The "$\cos^2(\theta-\pi/4)$" term reflects the observed peak pressures near a wind angle of 45°.

The result described in item #2 above is more clearly illustrated in Figures 25, 26, and 27. Figures 25 and 26 present the individual taps and average measurements for the jack roof without parapet and with parapet, respectively. Without the parapet, all measurements are very similar. However, the shielding effect of the parapet on one tap (Jack1), and the augmenting effect on the other tap (Jack2), for wind directions other than normal are seen in Figure 26. A comparison of the average pressure coefficients for both configurations finds surprisingly similar results (Figure 27).

The potential for an optimum intermediate spacing (item #3 above) was further emphasized in a separate test of the model under fully exposed conditions (upwind building spacing much larger than 5). In this test it was found that the front jack roof experienced an average negative pressure, indicating that the strong separation from the front edge of the roof was extending over the jack roof assembly. Obviously, the roof angle (20° in the present case) will play an important role in this observed flow pattern.

The measurement results and correlation predictions for the front jack roof of Model #2 without parapet are shown in Figure 28. The correlation equation used to produce the fit in the figure is taken from Table 4B for the front jack roof of Model #1 and a spacing of one. Due to the small upwind courtyard spacing (fixed at $S_c = 1$) the results are seen to be insensitive to row spacing (S). The results for Model #2 with parapet were found to be identical to these results within the experimental accuracy of the measurements.

Back Jack Roof

Figures 29 and 30 present measured data and correlation predictions for the back jack roof on Models #1 and #2, respectively. Measurement results are shown only for one roof configuration, as again, they were identical within the experimental accuracy. Table 4B gives the correlation equation which is based on the combined data base from both roof configurations. The observations are as follows:

1. At normal wind incidence a large negative pressure is observed due to the strong flow separation from the peak of the jack roof. The generally large negative pressures on the back jack roof make it a good choice as a location for a ventilation outlet (see Figure 2C).
2. Pressure coefficients increase with increasing wind angle, approaching zero at 90°.
3. Both figures indicate that pressures on the leeward side of the jack roof for both

models are virtually independent of upwind row spacing (S). As shown in Table 4B an excellent correlation fit (dependent only on wind direction) was obtained.

Back Facade

Figures 31 and 32 present the measured results and correlation predictions for the back facade of Model #2 for two roof configurations. Table 4 gives the correlation equations. The observations are as follows:

1. The results exhibit a very similar pattern to those for all surfaces located in the wake or leeward side of the models. Nearly identical results are obtained for both roof configurations tested (J,NP and NJ,NP)
2. The results are insensitive to variations in upwind row spacing (S).
3. Beginning with a large negative pressure coefficient at 0° wind angle, the pressures increase with increasing wind angle, approaching zero at 90°.

Courtyard

Figures 33 and 34 present the measured and predicted average courtyard pressure coefficients for two roof configurations. No results are shown for the jack roof without parapet which tended to be very similar to the (J,P) results, except increased by a small constant amount. Table 4 gives the correlation equations. The observations are as follows:

1. The pattern of the results is very similar to those observed for the back of the jack roof. This is not surprising because the leeward side of the model and the entire courtyard fall within the wake region of the upwind building for $S_c \leq 1$.
2. The results are only weakly dependent on upwind row spacing (S).
3. The average courtyard pressure coefficients for the standard gable roof ($S_c = 0.5$, $H_c = 0$) are slightly higher than those for the jack roof configuration ($S_c = 1$, $H_c = 1$) due to the different courtyard configuration (see also Figure 35).
4. At close to normal wind incidence the pressures are slightly higher than those on the back of the jack roof, since the courtyard is further removed from the strong separation point at the peak of the jack roof.

Figures 35, 36, and 37 present the effect of changing the courtyard configuration on the measured pressure coefficients for the three surface areas most likely to be affected: courtyard, front jack roof of Model #2, and back jack roof of Model #1, respectively. All other model surfaces were unaffected by variations in the courtyard. Table 5 gives the correlation equations. The measured data and correlation predictions are plotted as a function of wind direction, courtyard wall height ($H_c = 0, 0.5, 1$), and courtyard spacing ($S_c = 0.25, 0.5, 1$). Separate tests indicated that the existence of the passageway with a full-height courtyard wall produced no significant effect on the measured average courtyard pressure coefficients. No results for the passageway configuration are presented here. As described in *Program of Study* these results were obtained for a fixed upwind row spacing of S = 1 for the model with the jack roof and parapets. The observations are as follows:

1. At a courtyard spacing of $S_c = 0.25$, the results are very insensitive to the existence of the courtyard wall. The sensitivity of the pressure coefficient to changes in the courtyard wall height increases with increasing courtyard spacing for both the courtyard and front jack roof of Model #2 (Figures 35 and 36).

2. At the largest courtyard spacing (S_c = 1) the full-height wall provides some amount of protection in the courtyard area, slightly reducing the pressure coefficients for all wind directions (Figure 35).
3. At the largest courtyard spacing the full-height wall also slightly reduces measured pressures on the front jack roof for oblique wind angles (Figure 36).
4. As seen in Figure 37, the courtyard configuration had a negligible effect on the back of the jack roof of Model #1.
5. One additional term was used in the correlation equation of Table 5. The "$H_c * S_c$" term accounts for the increased sensitivity to courtyard wall height with increasing courtyard spacing, as seen in Figure 35.

Use of Correlation Tables

The correlation equations contained in Tables 4 and 5 can be used to predict average pressure coefficients on similar full-scale long building rows. The predictions are applicable to building units located away from the influence of the ends of the building rows. For all surfaces except the courtyard, average pressure coefficients can be calculated directly from Table 4 for the given building configuration. For small row spacings, $0.25 \leq S \leq 1$, use the appropriate correlation with S = 1.

Example 1: Find the average pressure coefficient for the front facade of a building with a jack roof (with or without parapets) for a wind angle of 45° and an upwind row spacing of 2.

From Table 4B:

$$C_p = 0.062 - 0.945(\cos 45°)^2 + 0.237(\cos 45°)(2)$$

$$C_p = -0.075$$

The combined effects of courtyard configuration (S_c, H_c) and upwind spacing (S) can be computed using both Tables 4 and 5 as explained below. In performing this calculation it is assumed that these effects are additive. 1) Use Table 5 to determine the value of C_p for the given values of S_c and H_c. 2) Add the additional contribution due to the effect of upwind row spacing (S) from Table 4. This corresponds to only the one term in Table 4 dependent on S, and only for the contribution for S > 1, the value of S for which Table 5 was derived. 3) Add the results from steps 1 and 2.

Example 2: Find the average courtyard pressure coefficient for the following configuration: $\theta = 25°$, S = 2.5, H_c = 0.5, S_c = 0.75.

1) From Table 5:

$$C_p(5) = -0.471(\cos 25°)^2 - 0.147(0.5)(0.75)$$

$$C_p(5) = -0.442$$

2) From Table 4 (spacing contribution only):

$$C_p(4) = -0.057(\cos 25^\circ)(2.5 - 1)$$

$$C_p(4) = -0.077$$

3) Total pressure coefficient:

$$C_p = C_p(5) + C_p(4) = -0.52$$

Wind Pressure Differences: Ventilation Potential

Given a set of pressure distribution data for a building, simplified models can be used to estimate the amount of cross-ventilation air flow through inlets and outlets located on the building walls. The equation for calculating the air flow through a cross-ventilated building with one effective inlet and one effective outlet is given below [Swami and Chandra (1987)].

$$Q = C_d A_e U_{ref} (\Delta C_p)^{1/2} \quad (9)$$

where:

Q	= air flow (m^3/s)
C_d	= discharge coefficient
A_e	= effective area of inlet and outlet (m^2)
ΔC_p	= pressure coefficient difference across the inlet and outlet

Using Equation (9) as a guide, the relative ventilation effectiveness of various combinations of surfaces has been compared by calculating the square root of the mean pressure coefficient differences between the selected surfaces. Although the specific values of the discharge coefficient, inlet and outlet areas, and reference velocity will directly influence the obtained air flow volume, an analysis of $(\Delta C_p)^{1/2}$ helps to clarify the characteristic performance of the ventilation configuration. In the following series of figures the quantity, $(\Delta C_p)/|\Delta C_p|^{1/2}$, based on the developed correlation predictions, is plotted for selected pairs of surfaces on the front and back jack roof and front and back facades of Model #1. By using this quantity, negative values represent a reversal of the flow direction through the building. Note that the back facade of Model #1 is part of the courtyard.

Figure 38 presents the pressure difference coefficients between the front and back facades of the model with the standard gable roof. Without a ventilation opening on the roof, this is the most appropriate wind pressure difference to drive cross-ventilation of the building. As expected, the pressure difference increases with increasing spacing. At upwind spacings of $S \leq 1$, the ventilation potential is negligible due to the strong sheltering effect of the adjacent buildings. For comparison, the front to back facade pressure difference for both jack roof models (with and without parapets) is shown in Figure 39. The results are very similar, except at wind directions approaching 90°. For these winds the courtyard walls in the jack roof model provide added protection in the courtyard area, resulting in larger pressure differences (Figure 39) compared to those when no walls are present (Figure 38).

Since the back of the jack roof tends to have the largest negative pressures for all leeward building surfaces, using this surface as the ventilation outlet will improve the potential

ventilation air flow (see Figure 2C). Figure 40 shows pressure difference results between the front facade and back of the jack roof. The pressure differences are quite comparable to the previous results for front to back facade (Figures 38 and 39), although larger values are obtained at the smallest spacing (S=1). Figure 41 shows pressure difference results between the back facade and the back of the jack roof. The lower pressure differences are indicative of the fairly uniform pressure distribution over all leeward surfaces of the building, although some ventilation potential does exist.

In the above flow configurations as well as others incorporating the jack roof, it must be kept in mind that the accuracy of Equation (9) for roof-level openings may be unreliable [Vickery, et. al.(1983)]. In addition, the smaller size of the jack roof compared to typical windows in the building walls could reduce the effective inlet/outlet areas. However, in the example discussed above (Figures 40 and 41), both the front and back facades of the building can act as flow inlets.

If the front of the jack roof is used as a ventilation flow inlet (Figures 2A and 2B), generally higher pressure differences will be produced at small row spacings, as this surface experiences higher pressures than the more sheltered front facade of the building. Figure 42 presents the pressure difference results between the front jack roof and the back facade, and Figure 43 presents results between the front jack roof and the front facade. In both figures it is seen that higher pressure differences exist at small spacings compared to the previous flow configurations discussed above. In fact, the pressure differences between the front jack roof and the front facade attain their maximum values at the smallest row spacings, when the front facade is heavily sheltered (Figure 43). For the jack roof to be used effectively as a flow inlet the roof slope must be large enough (20° in the present study) to produce positive pressure differences between the front (windward) jack roof surface and the surface(s) containing ventilation outlets.

Figure 44 shows the pressure differences between the front and back of the jack roof. A strong air flow directly through the jack roof could be used to promote ventilation of the building by entraining air from the spaces below the jack roof (Figure 2A). If air is diverted down into the building the ventilation principle would resemble that of a wind tower (Figure 2B). The cross-ventilation flow model (Equation (9)) would clearly have limitations if applied to either of these two flow configurations. Nevertheless, an important performance characteristic of the jack roof design can be identified as the results of Figure 44 are very insensitive to building spacing. This has important implications for use of the jack roof design in urban environments where buildings are often located quite close to each other. If an adequate ventilation air flow can be achieved for this configuration, the jack roof may be quite consistent in its ability to provide ventilation over a wide range of building spacings.

CONCLUSIONS

Wind tunnel measurements have been made of the wind pressure distributions over an attached two-story shop or housing unit contained in long building rows for a range of wind directions, building spacings, and building geometries. Simplified correlations have been developed which quite accurately predict the average pressure coefficients for the configurations tested. The results have been analyzed to assess the nature of wind pressure effects caused by surrounding building rows of the same size. The jack roof along with the choice of inlet and outlet locations have been discussed in an effort to identify promising naturally ventilated designs in closely spaced buildings typical of urban environments. The major conclusions are as follows:

1. The jack roof has the potential to be an effective ventilation design for urban settings.
2. Compared to standard cross-ventilation designs the jack roof demonstrates improved ventilation potential at the small building spacings typically found in urban areas.
3. At small building spacings ($S \leq 1$) cross-ventilation designs showed no potential for providing air flow through the building.
4. Since the jack roof element is located at the top of the building, for the building configurations tested it is more consistently exposed to stronger wind conditions. As a result, the performance of the jack roof is less dependent on variations in building spacing.
5. Strong negative pressures were consistently obtained on the back of the jack roof, making it a good choice for a ventilation flow outlet.
6. The results indicate that to achieve optimal performance of a ventilation design incorporating a jack roof, different operating modes may be necessary. In other words, the best choices of flow inlets and outlets may be dependent on building spacing and wind direction.
7. The entire courtyard area was found to consistently fall within the wake flow region of the upwind building row. This was because the largest courtyard spacing tested was S_c equal to one.
8. Pressure coefficients on all leeward surfaces and the courtyard were found to be practically independent of upwind row spacing and dependent only on wind direction.

Future related work is needed to address the following important areas:

1. Development of algorithms to predict internal ventilation air flow for configurations using roof-level inlets and outlets.
2. Investigations of the effect of internal partitions and obstructions on internal air flows, and incorporation of these results into air flow prediction algorithms.
3. Measurement of building surface pressure distributions for other important building configurations for natural ventilation design.
4. Determination of microclimatic effects on ambient wind conditions.
5. Development of design methods, tools, and guidelines for natural ventilation design.

NOMENCLATURE

A_e = effective area of inlet and outlet (m^2)

C_d = discharge coefficient

C_i = correlation constants defined in Tables 4 and 5 (i=0,1,...)

C_p = mean pressure coefficient (see Eqns. 5 and 6)

$C_{p,in}$ = mean pressure coefficient at inlet

$C_{p,meas}$ = measured value of mean pressure coefficient

$C_{p,out}$ = mean pressure coefficient at outlet

$C_{p,true}$ = true value of mean pressure coefficient

d = displacement height (m)

F_i = correlation functions defined in Tables 4 and 5 (i=1,2,...)

h_c = courtyard wall height (m)

H = building height (m)

H_c = h_c/H_e

H_e = eave height (m)

I_i = i-component of turbulence intensity (i=u,v,w) (see Eqn. (2))

k = von Karman's constant (0.4)

L = building length (m)

$L_x(u)$ = longitudinal integral length scale (m) (see Eqn. (3))

n = frequency (Hz)

P = mean pressure (Pa)

P_d = mean dynamic reference pressure = P_t-P_s (Pa)

P_s = mean static reference pressure (Pa)

P_t = mean total reference pressure (Pa)

Q = ventilation air flow (m^3/s) (see Eqn. (9))

Re = Reynolds number (see Eqn. (4))

s = spacing between building rows (m)

s_c = courtyard spacing (m)

S = s/H

S_c = s_c/H

$S_u(n)$ = u-component spectral density function at frequency *n* (see Eqn. (3))

u = component of velocity in longitudinal (along-wind) direction (m/s)

u´ = fluctuating component of velocity in longitudinal direction (m/s)

u* = friction velocity = $(\tau_0/\rho)^{1/2}$ (m/s)

U_{cal} = measured value of velocity determined by calibration curve (m/s)

U_{ref} = mean reference velocity (m/s)

U_{true} = true value of velocity (m/s)

U(z) = mean velocity at height z (m/s) (see Eqn. (1))

U_{10} = mean velocity at 10-meter height (m/s)

v = component of velocity in lateral (across-wind) direction (m/s)

v' = fluctuating component of velocity in lateral direction (m/s)

w = component of velocity in vertical direction (m/s)

w' = fluctuating component of velocity in vertical direction (m/s)

W = building width (m)

z = height above ground (m)

z_0 = roughness length (m)

α = roof pitch angle

ΔC_p = pressure coefficient difference across inlet and outlet = $C_{p,in} - C_{p,out}$

ν = kinematic viscosity of air (m^2/s)

θ = wind direction

ρ = density of air (kg/m^3)

σ_i = standard deviation of i-component of velocity (i=u,v,w) (m/s)

σ_u^2 = variance of u-component of velocity

τ_0 = shear stress at ground level (N/m^2)

REFERENCES

Antonia, R.A., and Luxton, R.E. 1971. "The Response of a Turbulent Boundary Layer to a Step Change in Surface Roughness: Part 1 - Smooth to Rough." Journal of Fluid Mechanics, Vol. 48, pp. 721-761.

Arens, E.A., and Watanabe, N. 1986. "A Method for Designing Naturally Cooled Buildings Using Bin Climate Data." ASHRAE Transactions, Vol. 92, Pt. 2.

Aynsley R.M. 1979. "Wind Generated Natural Ventilation of Housing for Thermal Comfort in Hot Humid Climates." Fifth International Wind Engineering Conference Proceedings. Pergamon Press.

Aynsley, R.M. 1982. "Natural Ventilation Model Studies." International Workshop on Wind Tunnel Modeling Criteria and Techniques for Civil Engineering Applications Preprints, Timothy A. Reinhold, ed., April 14-16, 1982, pp. V.1-1 - V.1-22.

Aynsley, R.M. 1985. "Modeling Parameters for Boundary Layer Wind Tunnel Studies of Natural Ventilation." ASHRAE Transactions, Vol. 91, Part 2A.

Bookhash, F.M. 1981. "Windtower Houses of Bastakeya in Dubai." AS/ISES International Conference on Passive and Hybrid Cooling Proceedings, Miami Beach, Florida, pp. 75-79.

Cermak, J.E., Peterka, J.A., Ayad, S.S. and Poreh, M. 1981. Passive and Hybrid Cooling Developments: Natural Ventilation - A Wind Tunnel Study. Fluid Dynamics and Diffusion Laboratory, DOE Contract No. DE-AC03-80CS11510, Colorado State University, Fort Collins, Co.

Cermak, J.E., Poreh, M., Peterka, J.A., and Ayad, S.S. 1982. "Wind Tunnel Investigations of Natural Ventilation." American Society of Civil Engineers Convention and Exhibit Preprint, New Orleans, LA., Preprint 82-519.

Chandra, S. 1983. "A Design Procedure to Size Windows for Naturally Ventilated Rooms." ASES Passive Solar Conference Proceedings. Glorieta, New Mexico, September 1983.

Clarke, J.A. 1986. Energy Simulation in Building Design. U.K.: Adam Hilger Ltd.

Cook, N.J. 1973. "On Simulating the Lower Third of the Urban Adiabatic Boundary Layer in a Wind Tunnel." Atmospheric Environment, Vol. 7, 691-705.

Cook, N.J. 1978. "Determination of the Model Scale Factor in Wind Tunnel Simulations of the Adiabatic Atmospheric Boundary Layer." Journal of Industrial Aerodynamics, Vol. 2, pp. 311-321.

Cook, N.J. 1982. "Simulation Techniques for Short Test-Section Wind Tunnels: Roughness, Barrier and Mixing-Device Methods." International Workshop on Wind Tunnel Modeling Criteria and Techniques for Civil Engineering Applications Preprints, Timothy A. Reinhold, ed., April 14-16, 1982, pp. II.3-1 - II.3-12.

Engineering Sciences Data Unit. 1974, 1975 and 1985. Characteristics of Atmospheric Turbulence Near the Ground. Item Nos. 74030, 75001, and 85020, ESDU, London.

Engineering Sciences Data Unit. 1982. Strong Winds in the Atmospheric Boundary Layer. Item No. 82026, ESDU, London.

Engineering Sciences Data Unit. 1984. Longitudinal Turbulence Intensities Over Terrain With Roughness Changes for Flat or Hilly Sites. Item No. 84030, ESDU, London.

Fairey, P.W., and Bettencourt, W. 1981. "'La Sucka' - A Wind Driven Ventilation Augmentation and Control Device." AS/ISES International Conference on Passive and Hybrid Cooling Proceedings, Miami Beach, Florida, pp. 196-200.

Gurstein, P. 1985. Malaysian Architectural Heritage Survey: A Handbook. Master's Thesis, Department of Architecture, University of California, Berkeley, CA.

Holmes, J. 1982. "Techniques and Modeling Criteria for the Measurement of External and Internal Pressures." International Workshop on Wind Tunnel Modeling Criteria and Techniques for Civil Engineering Applications Preprints, Timothy A. Reinhold, ed., April 14-16, 1982, pp. III.1-1 - III.1-13.

Hussain, M., and Lee, B.E. 1980. "A Wind Tunnel Study of the Mean Pressure Forces Acting on Large Groups of Low-Rise Buildings." Journal of Wind Engineering and Industrial Aerodynamics, Vol. 6, pp. 207-225.

Lee, B.E., Hussain, M., and Soliman, B.F. 1979. A Method for the Assessment of the Wind Induced Natural Ventilation Forces Acting on Low Rise Building Arrays. Department of Building Science, University of Sheffield, Report No. BS50.

Mattingly, G.E., and Peters, E.F. 1977. "Wind and Trees: Air Infiltration Effects on Energy in Houses." Journal of Industrial Aerodynamics, Vol. 2, No. 1.

Mattingly, G.E., Harrje, D.T. and Heisler, G.M. 1979. "The Effectiveness of an Evergreen Windbreak for Reducing Residential Energy Consumption." ASHRAE Transactions, Vol 85, Part 2.

Melbourne, B. 1982. "Wind Tunnel Blockage Effects and Corrections: Scaling Implications." International Workshop on Wind Tunnel Modeling Criteria and Techniques for Civil Engineering Applications Preprints, Timothy A. Reinhold, ed., April 14-16, 1982, pp. II.7-1 - II.7-19.

Perry, A.E., Schofield, W.H. and Joubert, P.N. 1969. "Rough Wall Turbulent Boundary Layers." Journal of Fluid Mechanics, Vol. 37, pp. 383-413.

Peterka, J. and Cermak, J. 1975. "Turbulence in Building Wakes." Proceedings: 4th International Conference on Wind Effects on Building and Structures, London, September 1975, Cambridge University Press.

Peterka, J.A., Zambrano, T.G. and Cermak, J.E. 1979. "Effect of an Adjacent Building on Wind Pressures." ASCE Annual Convention and Exposition Proceedings, Atlanta, Georgia.

Sherman, M.H. and Grimsrud, D.T. 1982. "Wind and Infiltration Interaction for Small Buildings." Annual Meeting of the American Society of Civil Engineers Proceedings, New Orleans, LA, October 23-29, 1982.

Smith, E.G. 1951. The Feasibility of Using Models for Predetermining Natural Ventilation. Texas Engineering Experiment Station, The Texas A and M College System, Research Report No. 26.

Smith, F. and Wilson, C. 1977. "A Parametric Study of Airflow Within Rectangular Walled Enclosures." Building and Environment. Vol. 12, pp. 223-230.

Soliman, B.F. 1973. The Effect of Building Grouping on Wind Induced Natural Ventilation. University of Sheffield, Department of Building Science, Report BS 14.

Swami, M.V. and Chandra, S. 1987. Procedure for Calculating Natural Ventilation Airflow Rates in Buildings. ASHRAE, Final Report, FSEC-CR-163-86.

Vickery, B.J. 1981. "The Use of the Wind Tunnel in the Analysis of Naturally Ventilated Structures." AS/ISES International Passive/Hybrid Cooling Conference Proceedings, Miami Beach, Nov. 1981, pp. 728-742.

Vickery, B.J., Baddour, R.E., Karakatsanis, C.A. 1983. A Study of the External Wind Pressure Distributions and Induced Internal Ventilation Flow in Low-rise Industrial

and Domestic Structures. Boundary Layer Wind Tunnel Laboratory University of Western Ontario, Report No. BLWT-SS2-1983.

Wannenburg, J.J. 1957. "Performance Testing of Roof Ventilators." Heating, Piping & Air Conditioning (ASHAE Journal Section), March 1957, pp. 147-154.

Wiren, B.G. 1985. Effects of Surrounding Buildings on Wind Pressure Distributions and Ventilative Heat Losses for a Single-Family House. The National Swedish Institute for Building Research, Report No. M85:19.

ACKNOWLEDGMENTS

The authors wish to thank Mark Levine and Hashem Akbari of Lawrence Berkeley Laboratory for their financial support and technical assistance with this research. We also wish to acknowledge Davide Garda of the UC Berkeley Architecture Department for his help with preparation of model construction drawings and figures for the final report. The IBM personal computer equipment used for data acquisition and analysis throughout this study was provided through an IBM DACE Grant.

TABLE 1

Individual taps Cp measurements and averages

Tap Location	Left	Center	Right	Average
Lower Front Facade Taps:	2	**3**	4	
Measured Cp:	0.24	0.17	0.12	0.18
Upper Front Facade Taps:	5	**6**	7	
Measured Cp:	0.07	0.06	0.09	0.07
Upper Courtyard Taps, Model #1:	18	**19**	20	
Measured Cp:	-0.63	-0.60	-0.62	-0.62
Lower Courtyard Taps, Model #1:	21	**22**	23	
Measured Cp:	-0.53	-0.54	-0.52	-0.53
Lower Courtyard Taps, Model #2:	26	**27**	28	
Measured Cp:	-0.54	-0.52	-0.52	-0.53
Upper Courtyard Taps, Model #2:	29	**30**	31	
Measured Cp:	-0.62	-0.64	-0.62	-0.63
Upper Back Facade Taps:	42	**43**	44	
Measured Cp:	-0.34	-0.36	-0.36	-0.35
Lower Back Facade Taps:	45	**46**	47	
Measured Cp:	-0.29	-0.28	-0.27	-0.28

Notes

1) Refer to Table 2 and Figure 11 for definition of surface tap locations.
2) Pressure coefficients were measured for S=3, θ=45°, S_c=1 and H_c=1.
3) The pressures were only measured for tap locations in **bold** in subsequent tests.

TABLE 2

Tap Locations for Average Pressure Measurements

Surface	Tap Locations	
	Model #1	Model #2
Front Facade	3 + 6	27 + 30
Back Facade	19 + 22	43 + 46
Front Jack Roof	11 + 12	35 + 36
Back Jack Roof	13 + 14	37 + 38
Courtyard	19 + 22 + 27 + 30	

TABLE 3

Key to Figures and Correlations

#1 - Model # 1 or Windward Model
#2 - Model # 2 or Leeward Model
P - with Parapets
NP - without Parapets
J - with Jack Roof
NJ - without Jack Roof

TABLE 4

Correlations For Average Surface Pressure Coefficients*

Correlation Equation: $C_p = C_o + \sum_{i=1}^{N} C_i.F_i$

A) Model Configuration: No Jack Roof and No Parapet (NJ,NP); $S_c = 0.5$; $H_c = 0$

Independent Variables (F_i)	Front Facade C_i	Courtyard C_i	Back Facade C_i
Constant	0.095	0.107	--------
$Cos^2\theta$	-0.519	-0.436	-0.602
$Cos\theta * S$	--------	-0.067	--------
$Cos\theta * Ln(S)$	0.571	--------	--------
R^2 (ADJ)	0.980	0.982	0.990

B) Model Configuration: Jack Roof (J,NP) and (J,P); $S_c = 1$; $H_c = 1$

Independent Variables (F_i)	Front Facade C_i	Front Jack C_i	Back Jack C_i	Courtyard NP C_i	Courtyard P C_i	Back Facade C_i
Constant	0.062	-0.240	--------	0.091	-0.082	--------
$Cos^2\theta$	-0.945	-0.098	-0.832	-0.512	-0.512	-0.690
$Cos\theta * S$	0.237	--------	--------	-0.057	-0.057	--------
$Cos\theta * Ln(S)$	--------	0.095	--------	--------	--------	--------
$Cos^2(\theta-45°)$	--------	0.539	--------	--------	--------	--------
R^2 (ADJ)	0.954	0.843	0.985	0.958	0.986	0.993

* **Notes**

1) Roof slope is $\alpha = 20°$.
2) Refer to Table 2 for definitions of surface tap locations.
3) Correlations for Front Facade and Front Jack, are reported for Model #1 only.
4) Correlations for Back Jack are reported for Models #1 and #2.
5) Correlations for Back Facade are reported for Model #2 only.
6) Ranges of applicability for these correlations are:
   $0 \leq \theta \leq 90°$
   $1 \leq S \leq 5$

TABLE 5

Correlation For Average Surface Pressure Coefficients : Courtyard Effects*

Correlation Equation: $C_p = C_o + \sum_{i=1}^{N} C_i.F_i$

Model Configuration: Jack Roof and Parapets (J,P); S = 1

Independent Variables (F_i)	Courtyard C_i
Constant	--------
$Cos^2\theta$	-0.471
$H_c * S_c$	-0.147
R^2 (ADJ)	0.989

* **Notes**

1) Roof slope is $\alpha = 20°$.
2) Refer to Table 2 for definitions of surface tap locations.
3) Ranges of applicability for this correlation are:
$0 \leq \theta \leq 90°$
$0.25 \leq S_c \leq 1$
$0 \leq H_c \leq 1$

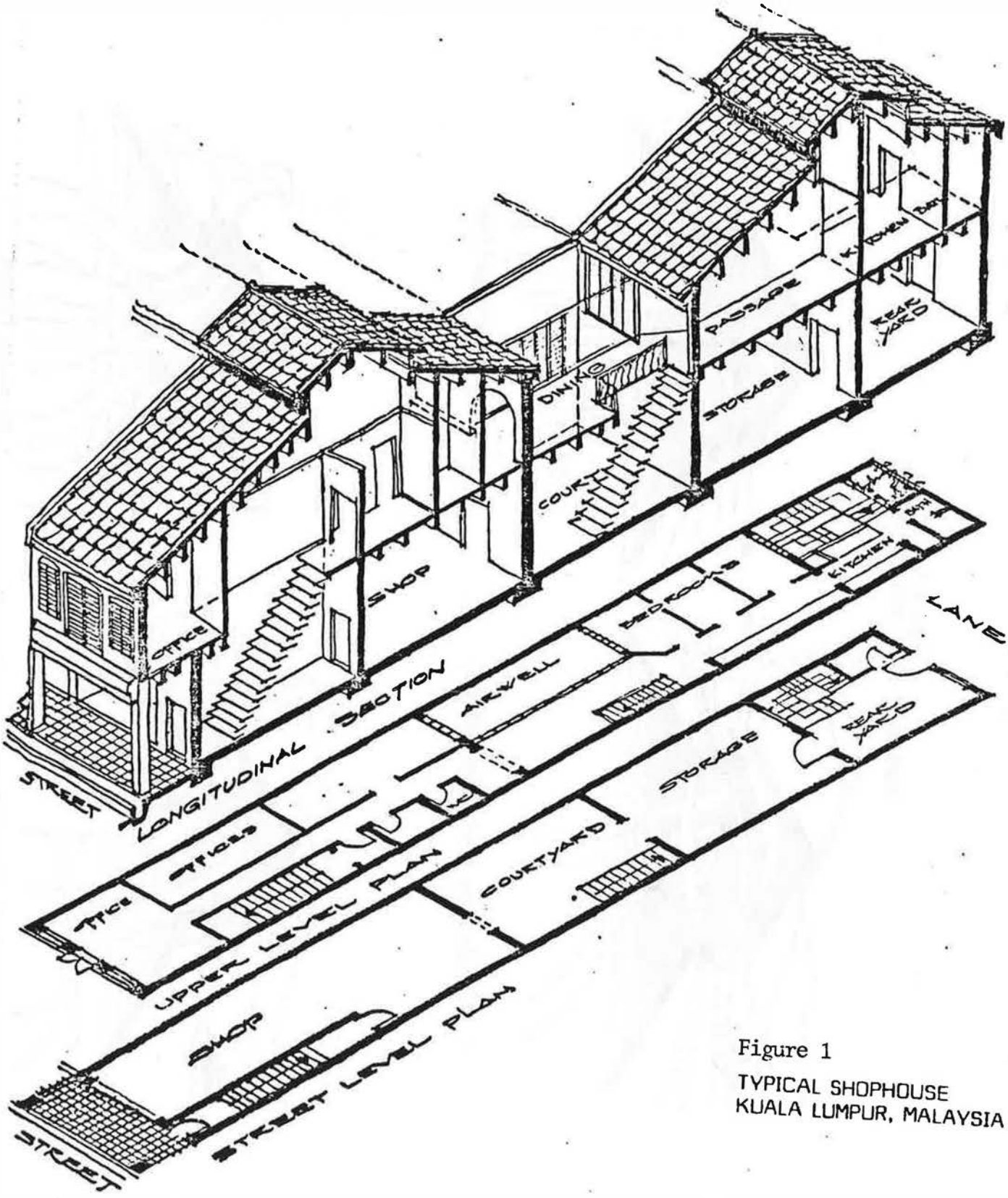

Figure 1

TYPICAL SHOPHOUSE
KUALA LUMPUR, MALAYSIA

Figure 2
JACK ROOF FLOW CONFIGURATIONS

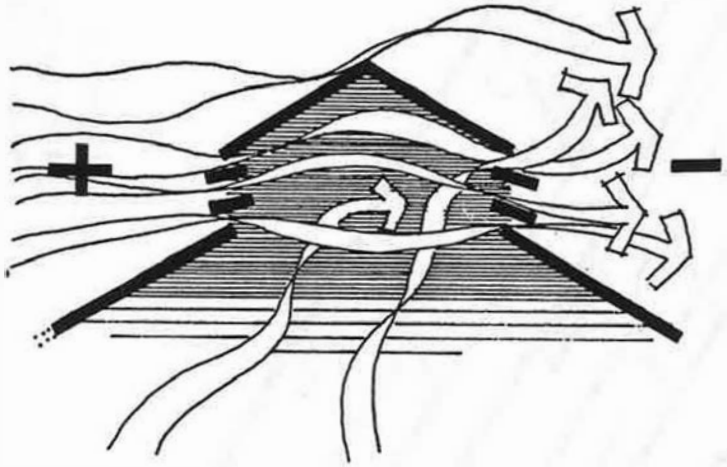

A) Through-Flow (Induction Effect)

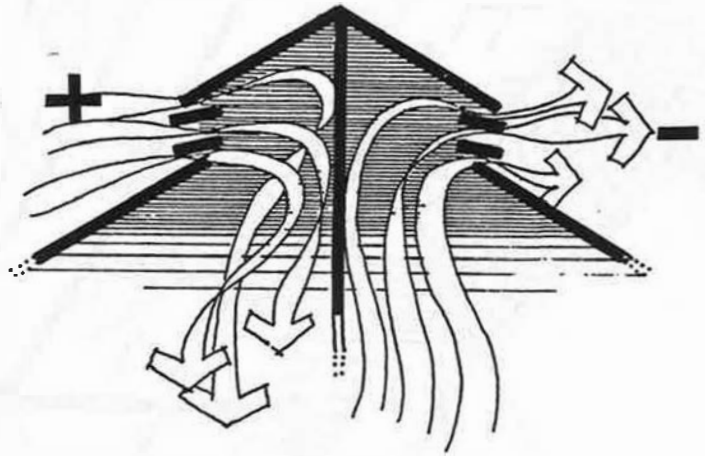

B) Diverted Through-Flow

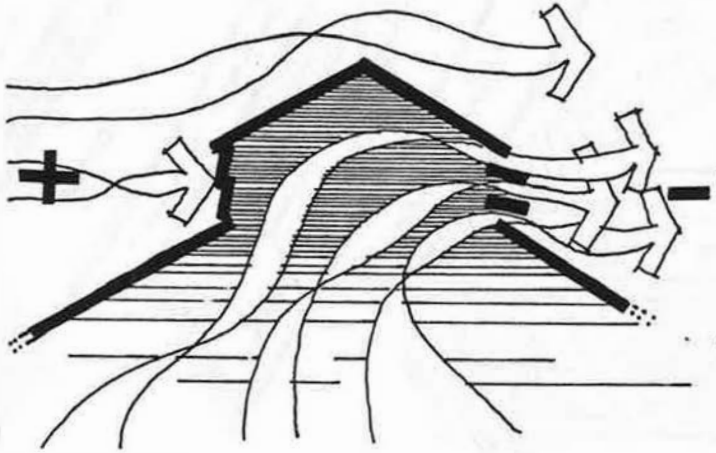

C) Suction Effect

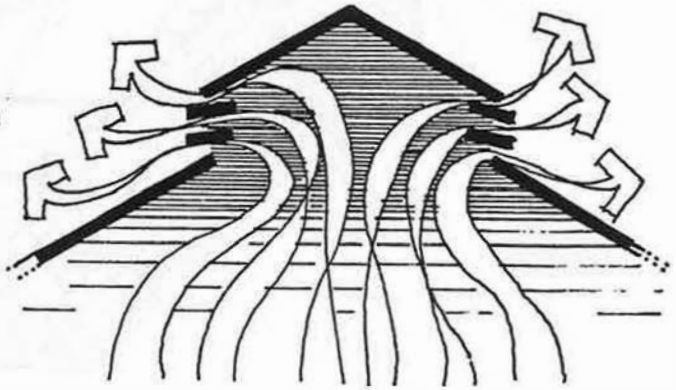

D) Stack Effect

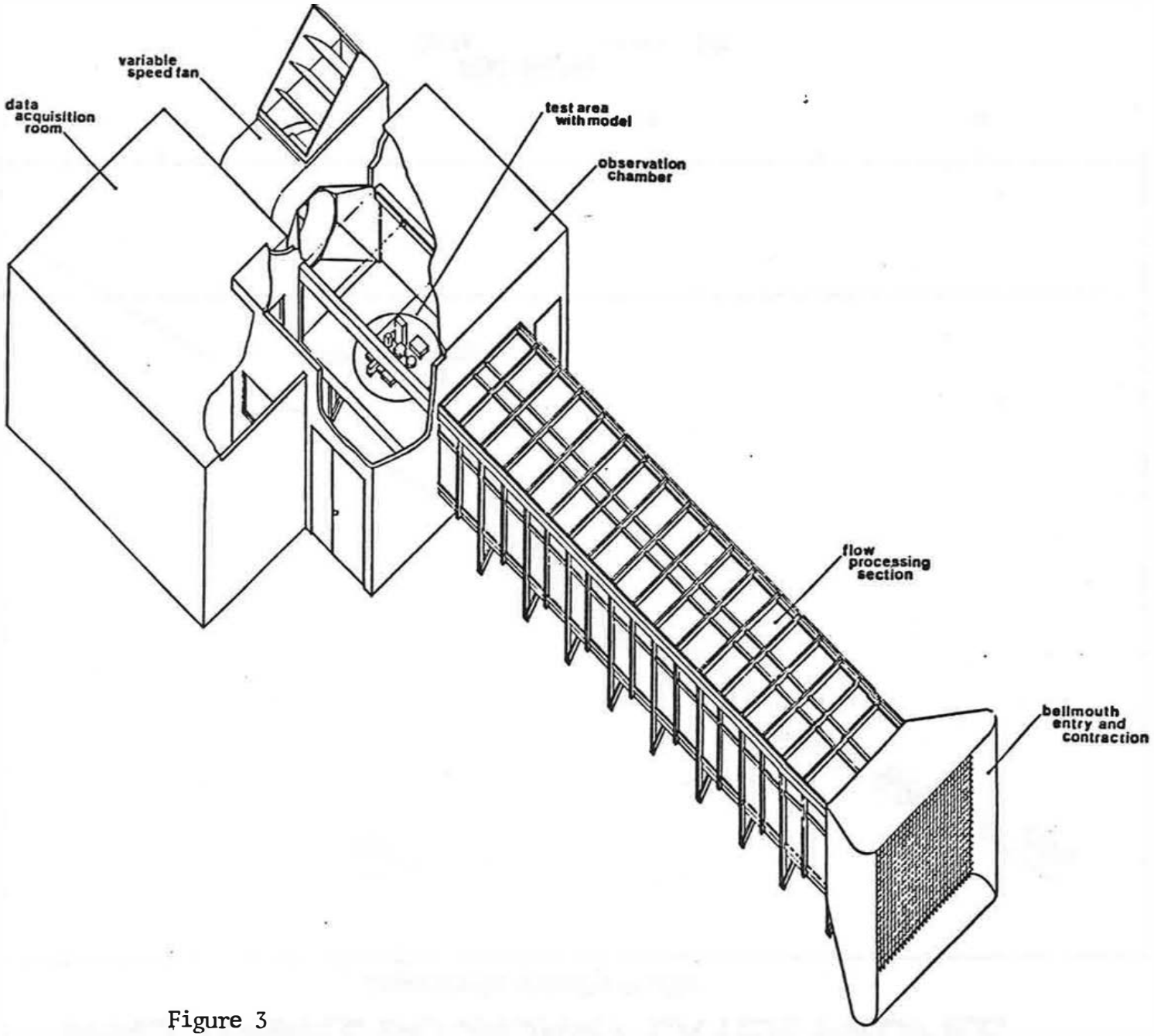

Figure 3

BOUNDARY LAYER WIND TUNNEL

Figure 4

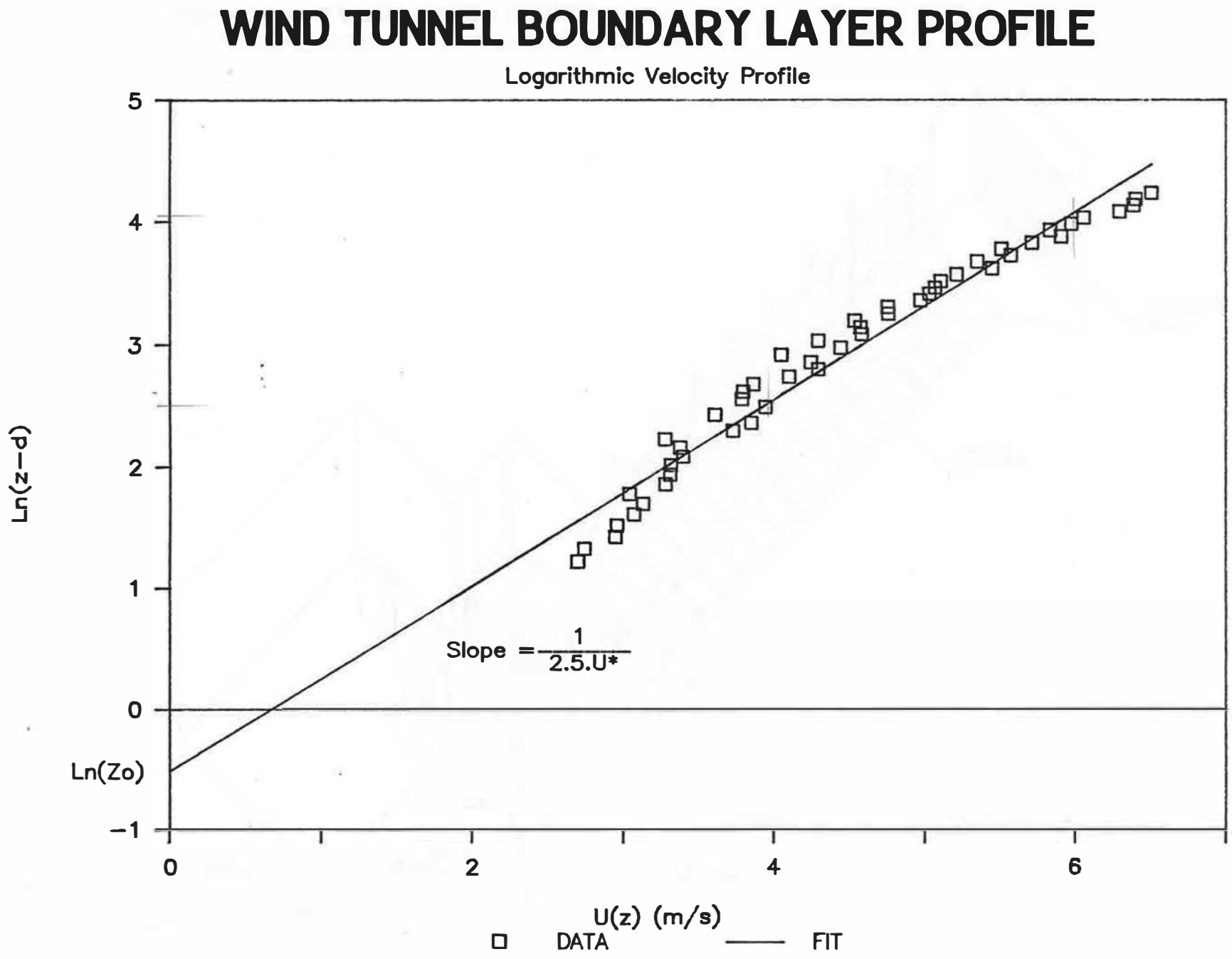
WIND TUNNEL BOUNDARY LAYER PROFILE
Logarithmic Velocity Profile
Ln(z-d)
5
4
3
2
1
0
Ln(Zo)
-1
Slope = 1 / 2.5.U*
0
2
4
6
U(z) (m/s)
DATA
FIT

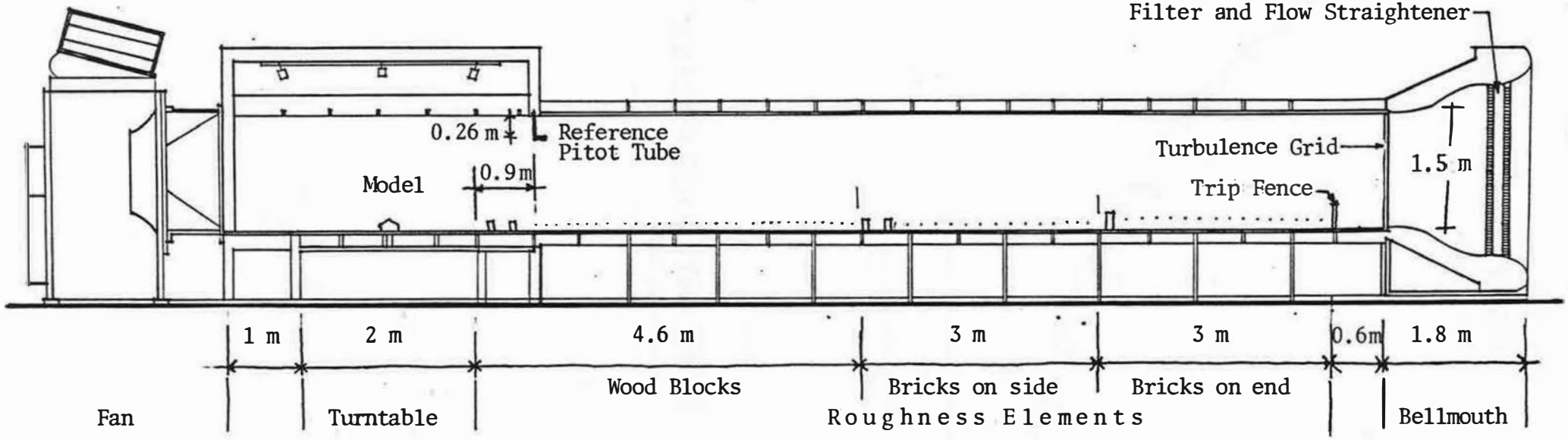

Figure 5
Boundary Layer Wind Tunnel Configuration

For ASEAN Study

Figure 6

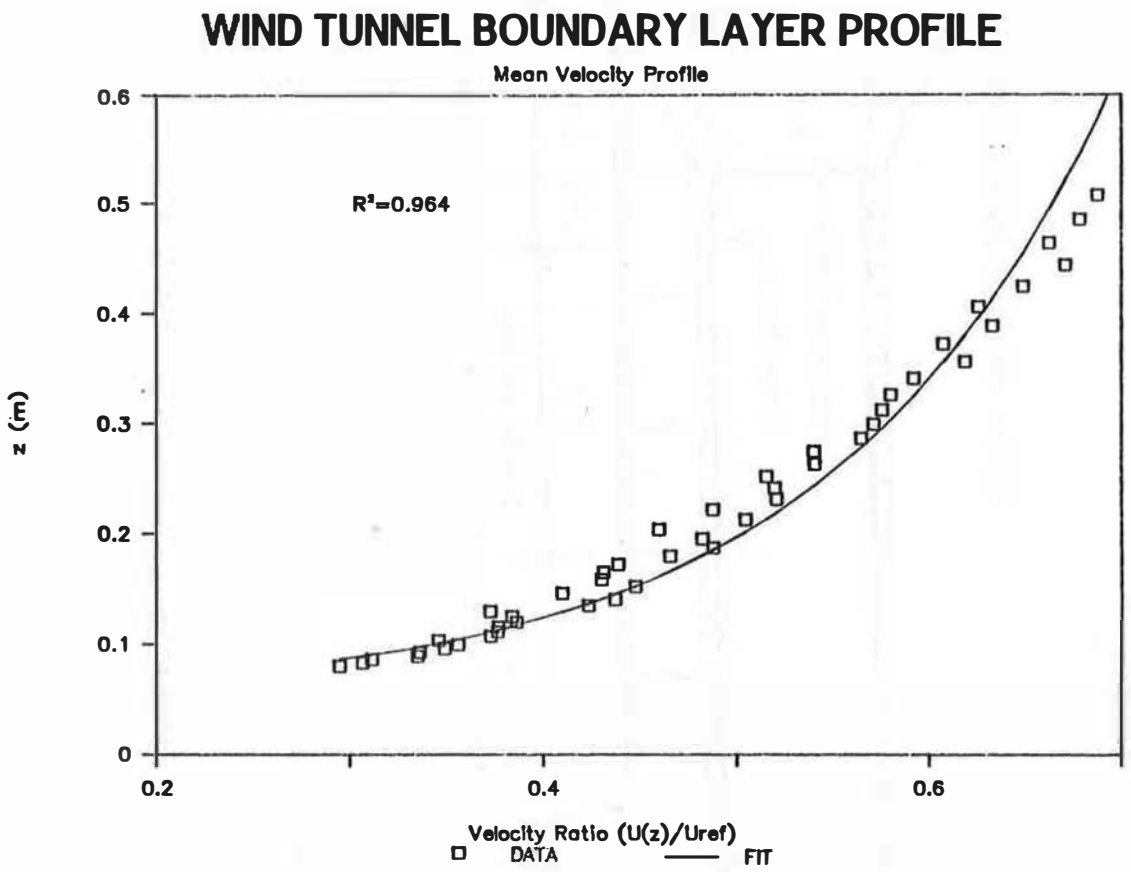

Figure 7

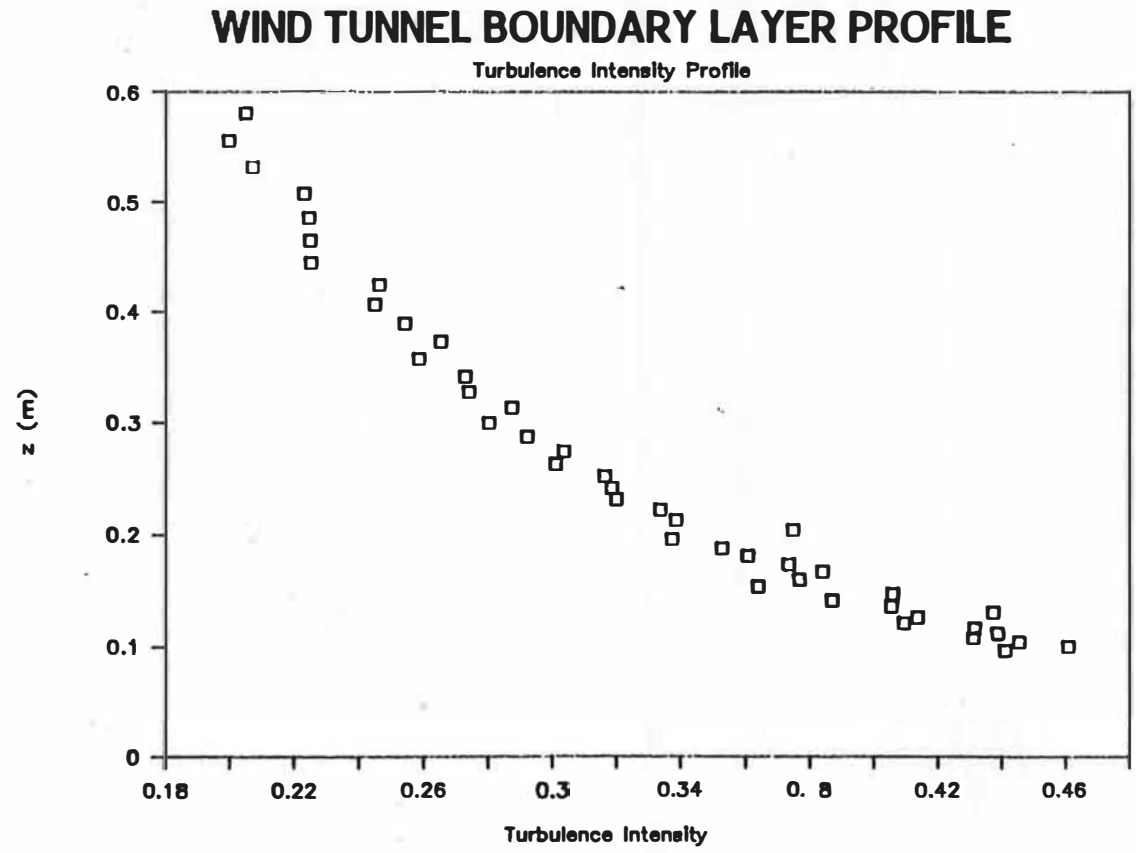

Figure 8

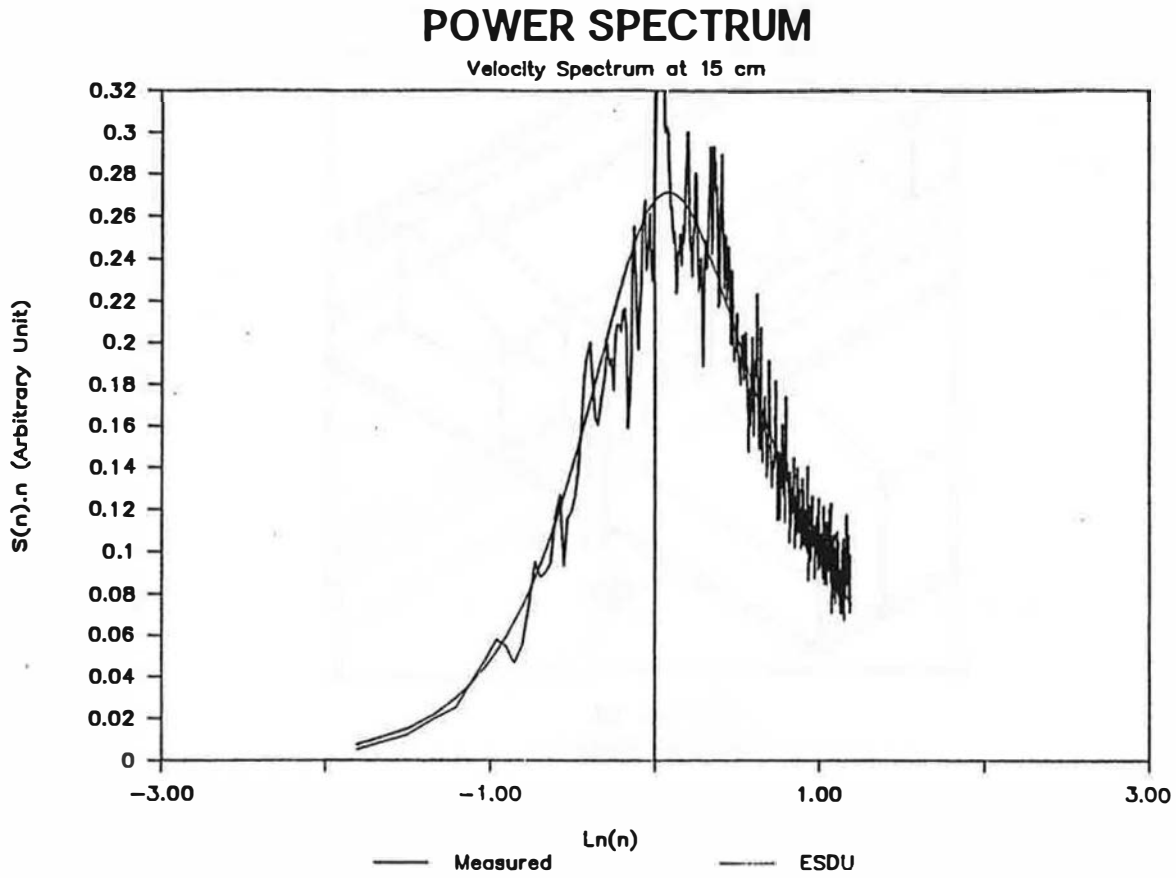
POWER SPECTRUM
Velocity Spectrum at 15 cm
S(n).n (Arbitrary Unit)
0.32
0.3
0.28
0.26
0.24
0.22
0.2
0.18
0.16
0.14
0.12
0.1
0.08
0.06
0.04
0.02
0
-3.00
-1.00
1.00
3.00
Ln(n)
Measured
ESDU

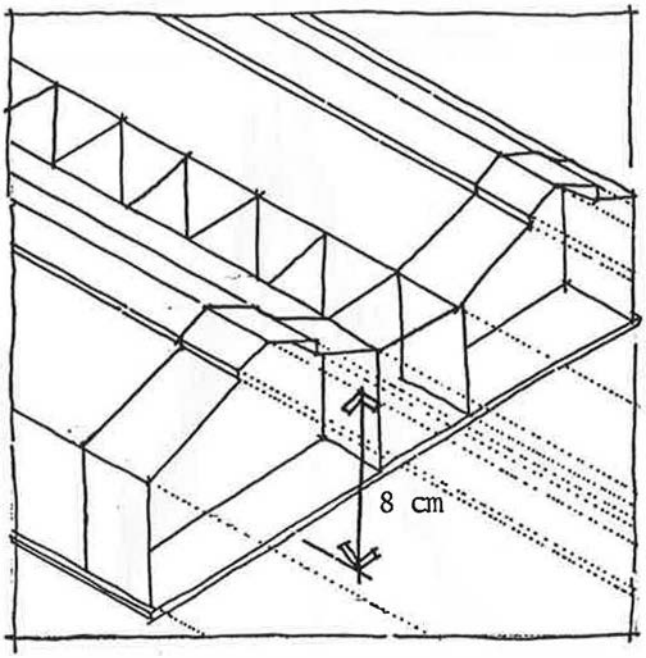

Figure 9A
Generic Model

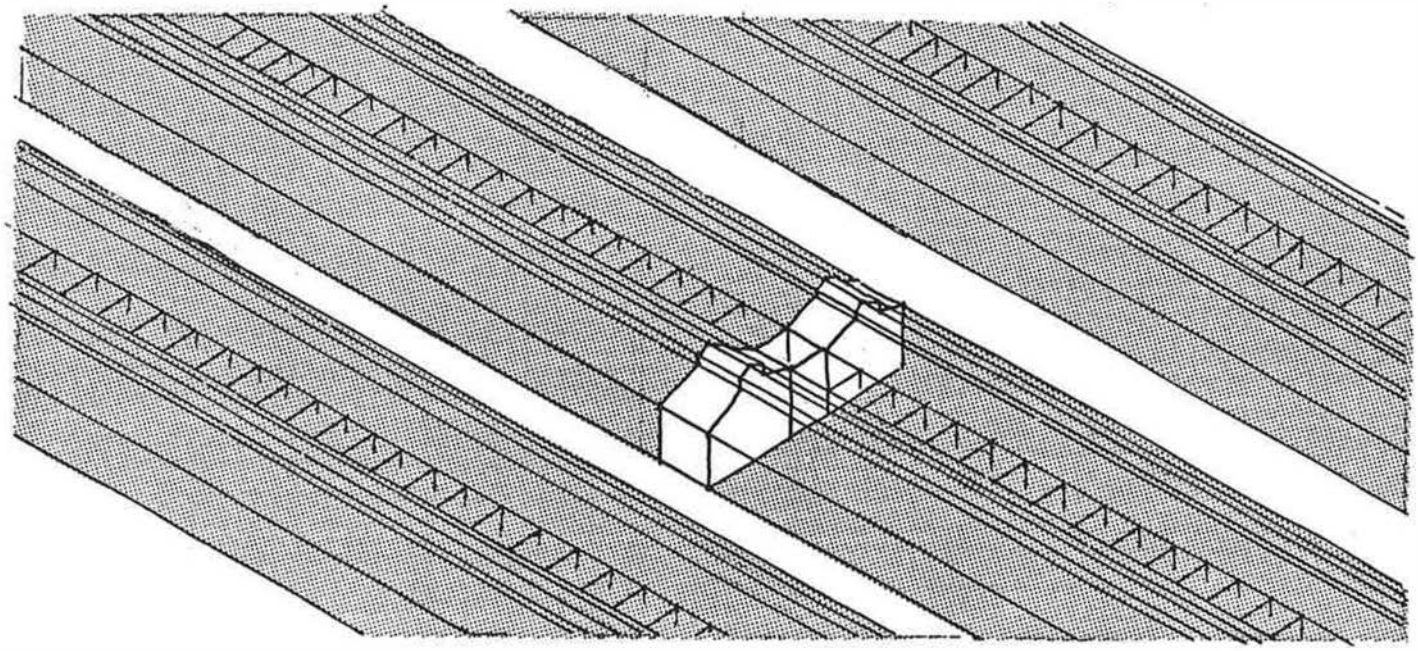

Figure 9B
Test Unit in Row

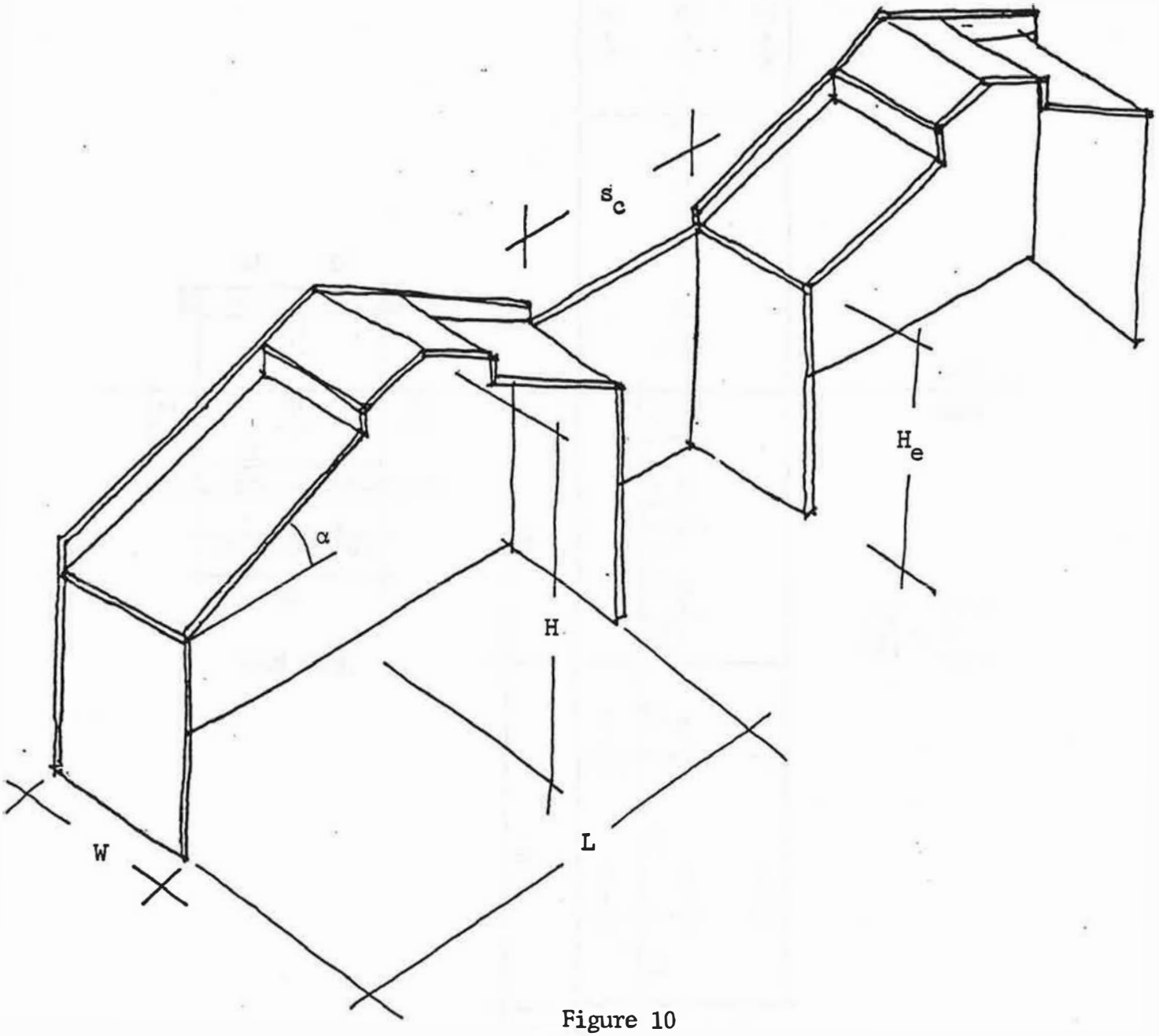

Figure 10
SHOPHOUSE TEST MODEL

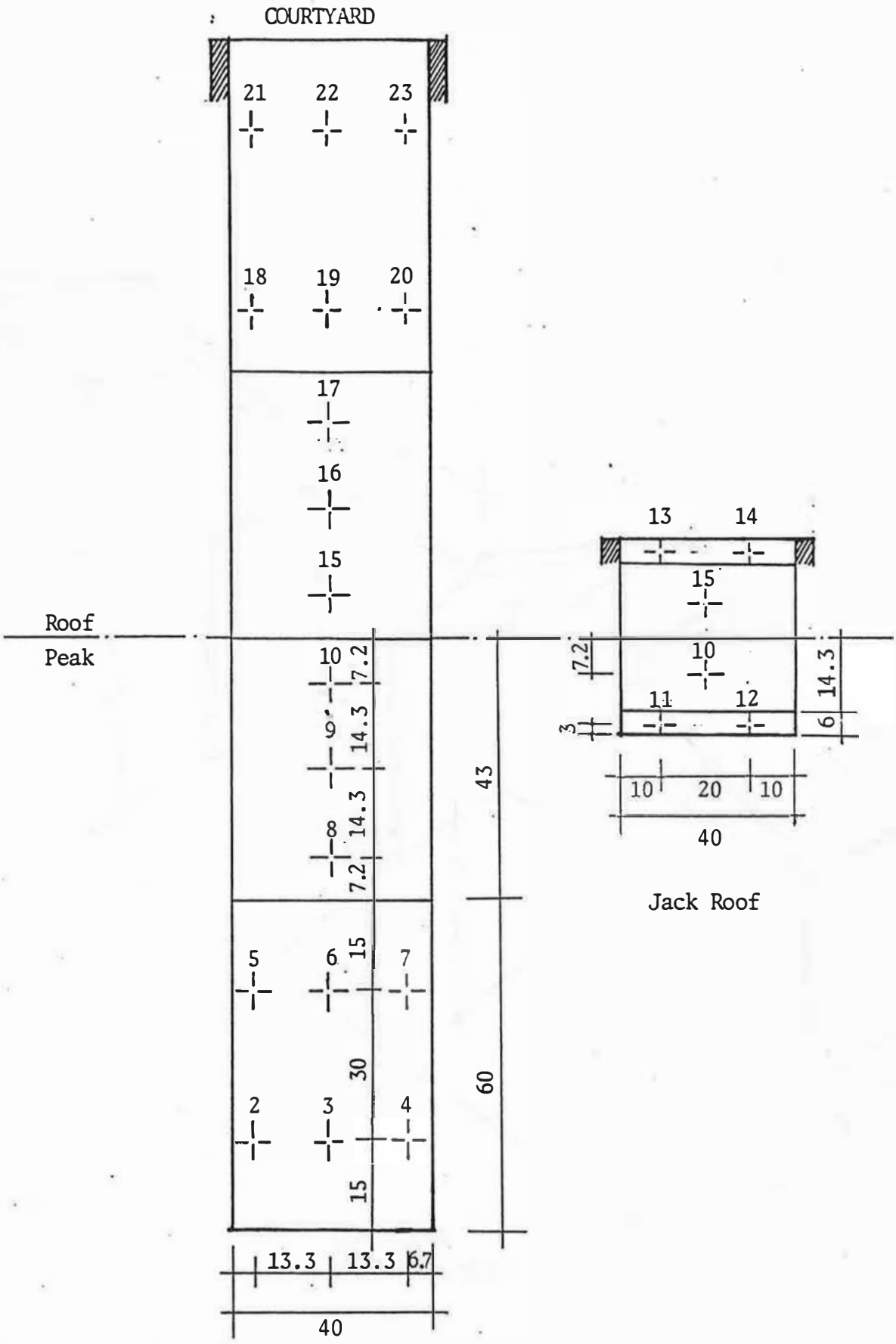

Figure 11A
TAP LOCATIONS FOR MODEL #1 (dimensions in mm)

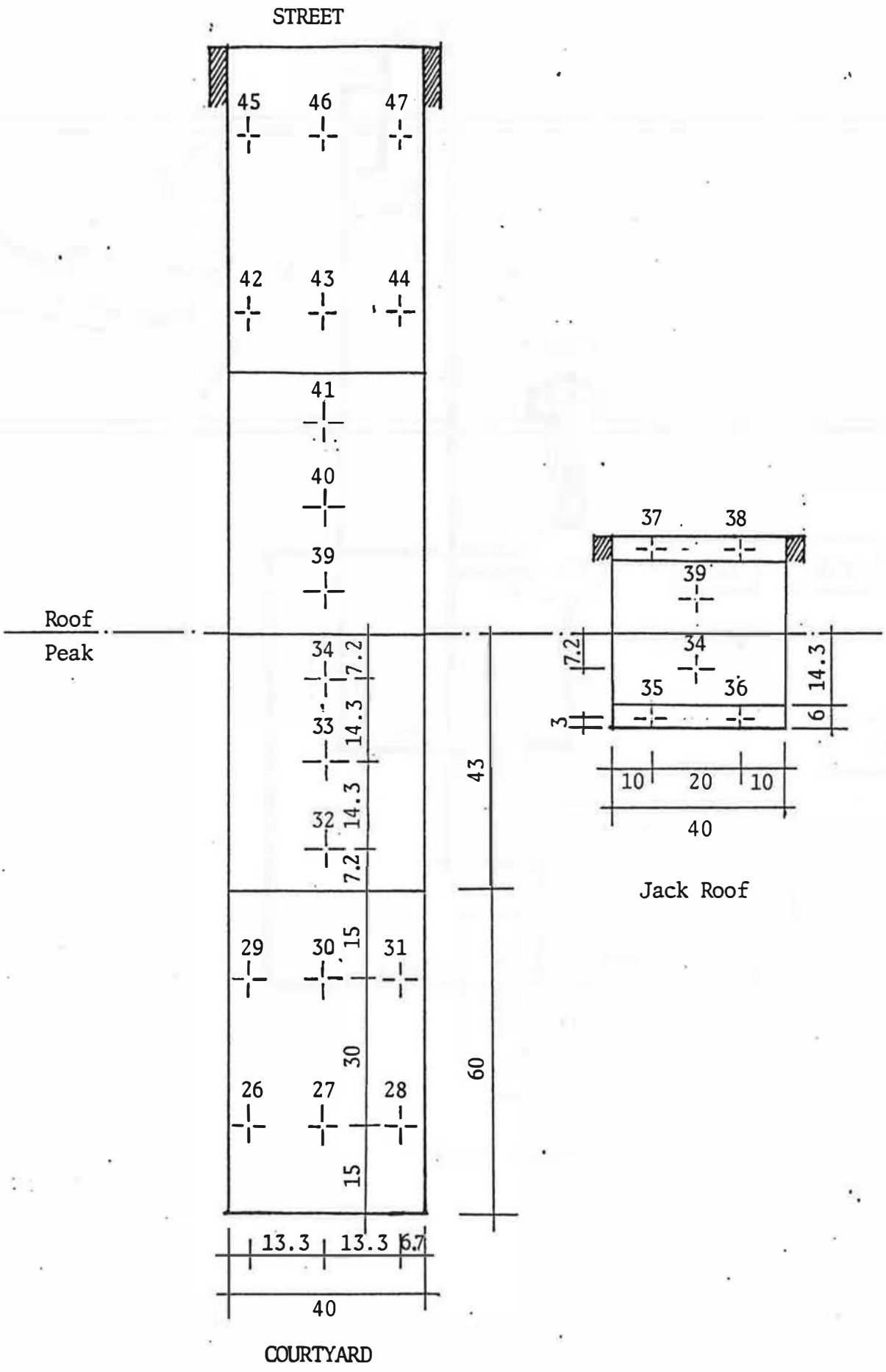

Figure 11B
TAP LOCATIONS FOR MODEL #2 (dimensions in mm)

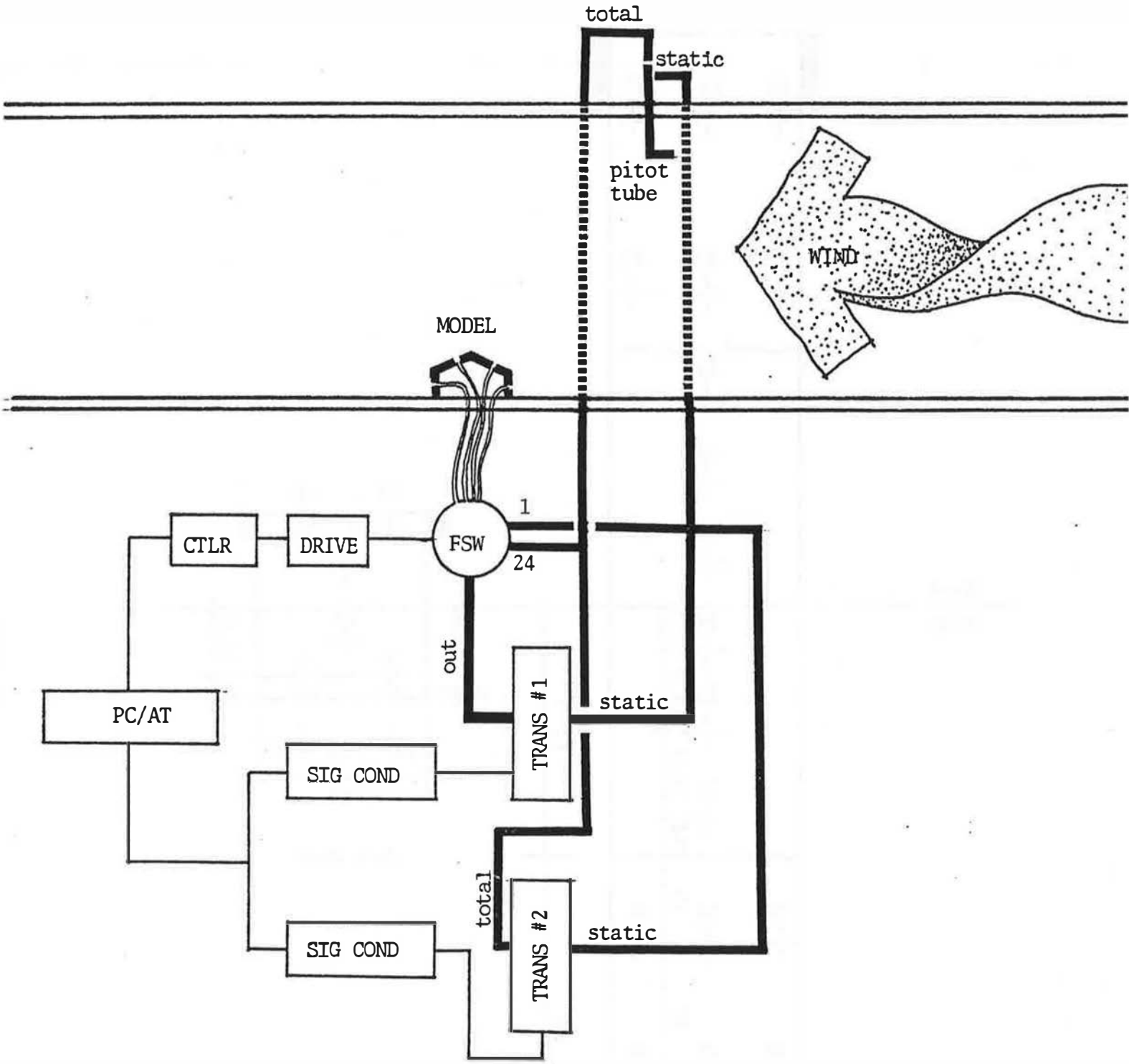

Figure 12
PRESSURE MEASUREMENT SYSTEM

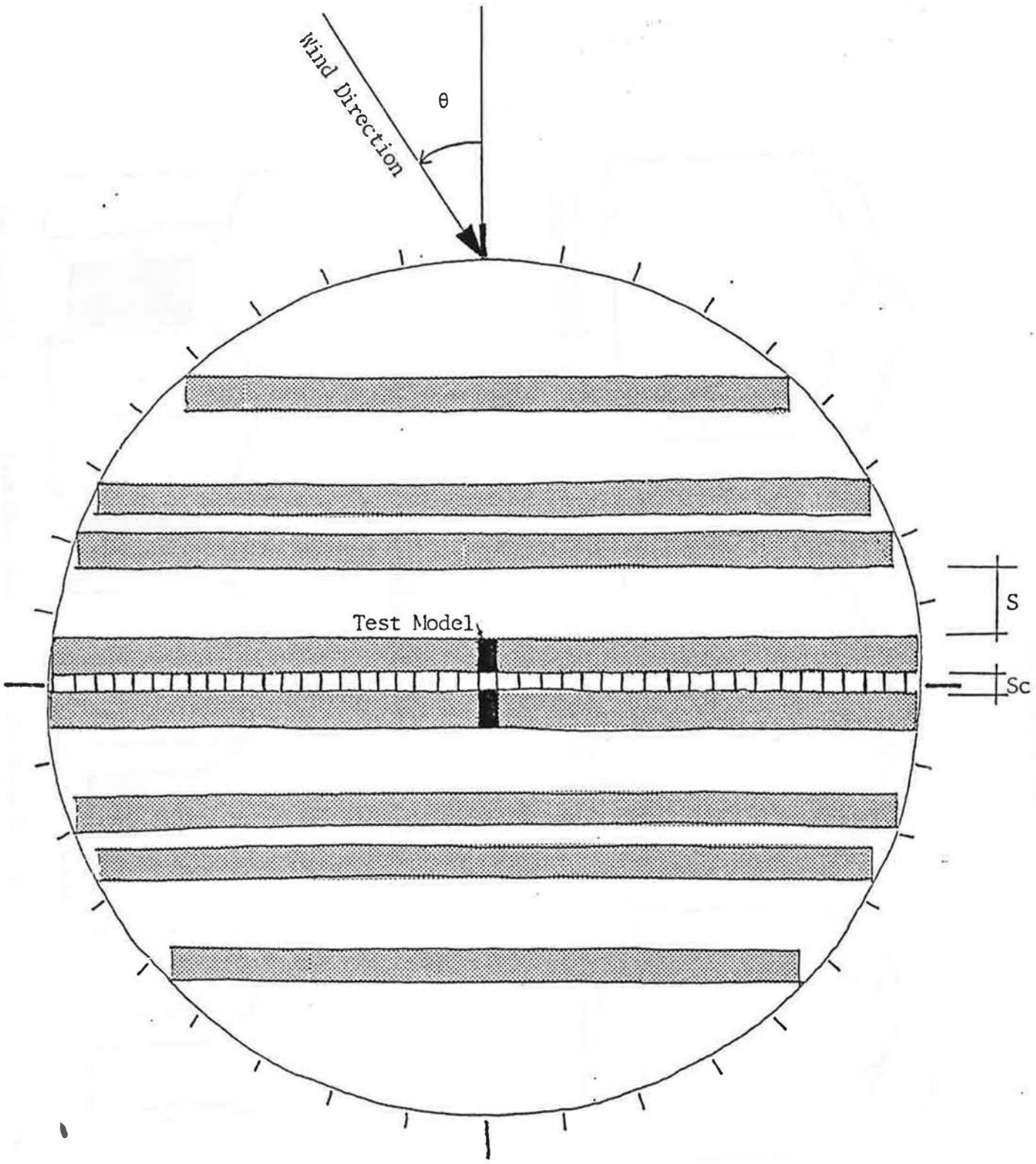

Figure 13A
Model Spacing Configuration and Wind Direction

Figure 13B
Roof Configurations

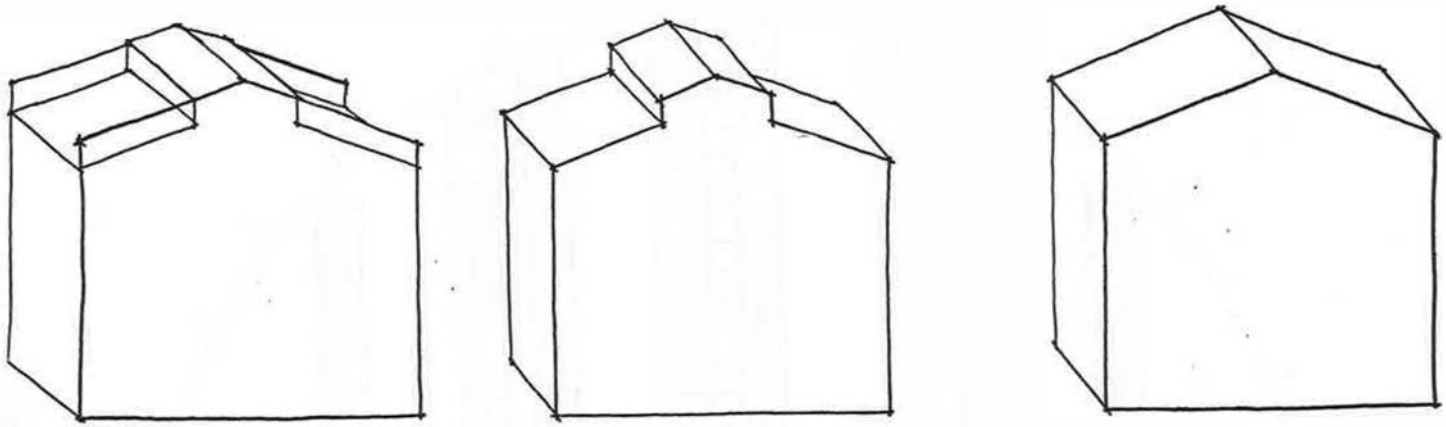

a) With Jack Roof and Parapets

b) With Jack Roof Without Parapets

c) Without Jack Roof Without Parapets

Figure 13C
Courtyard Configurations

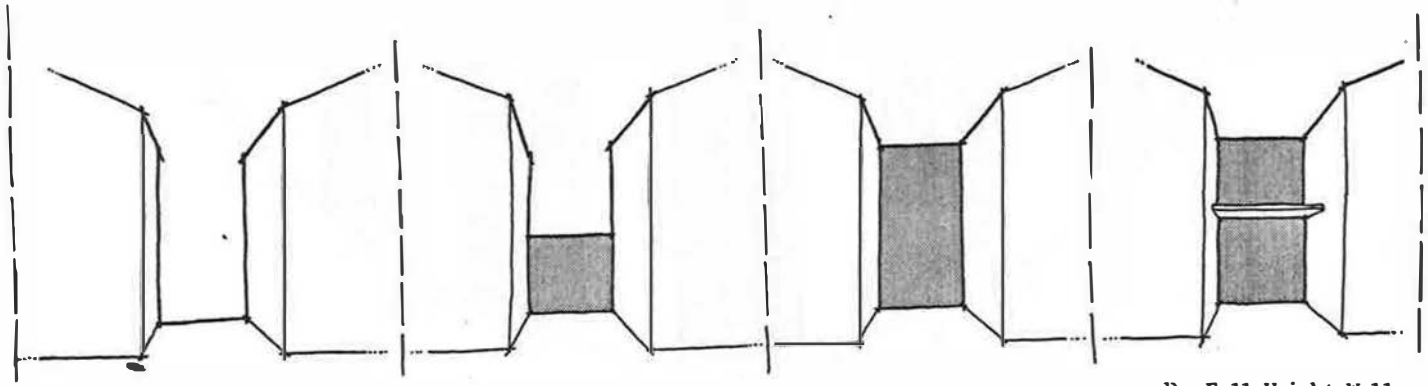

a) No Wall
Hc = 0

b) Half Height Wall
Hc = 0.5

c) Full Height Wall
Hc = 1

d) Full Height Wall
With Passage Way

Figure 14

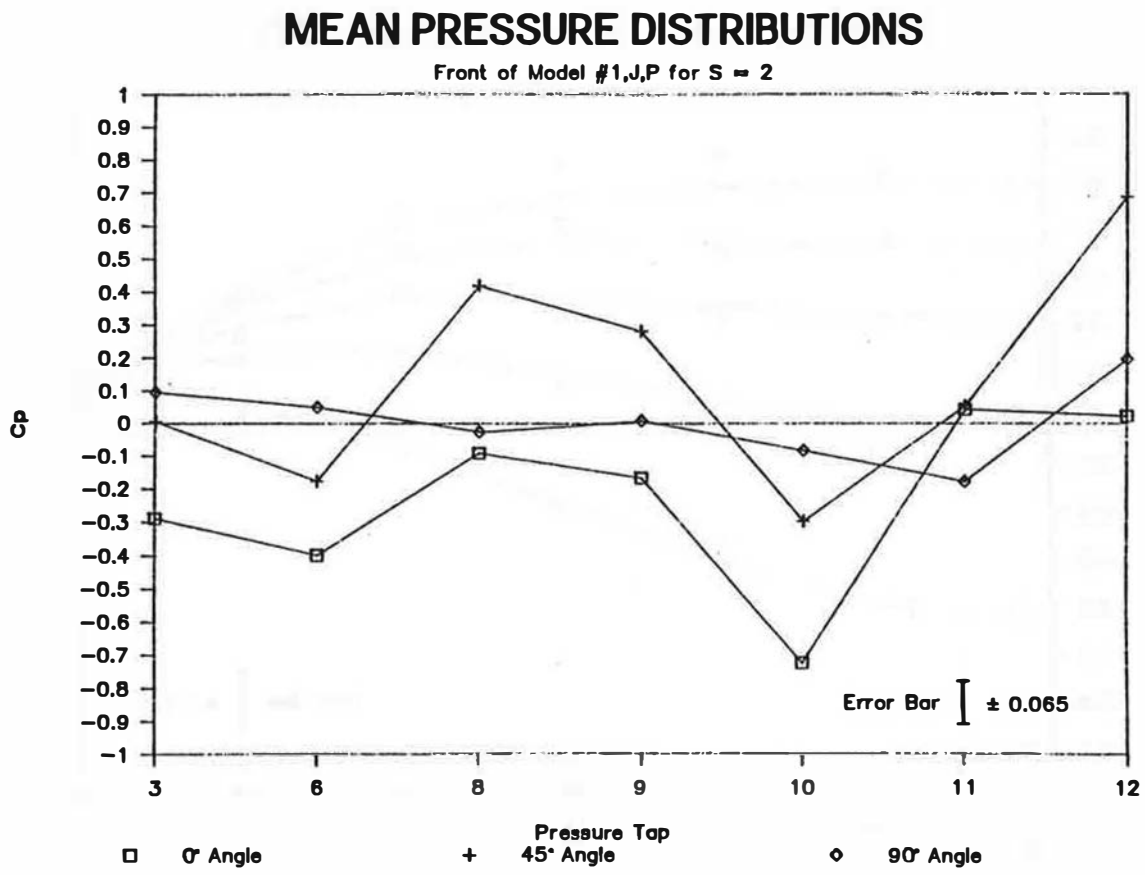

Figure 15

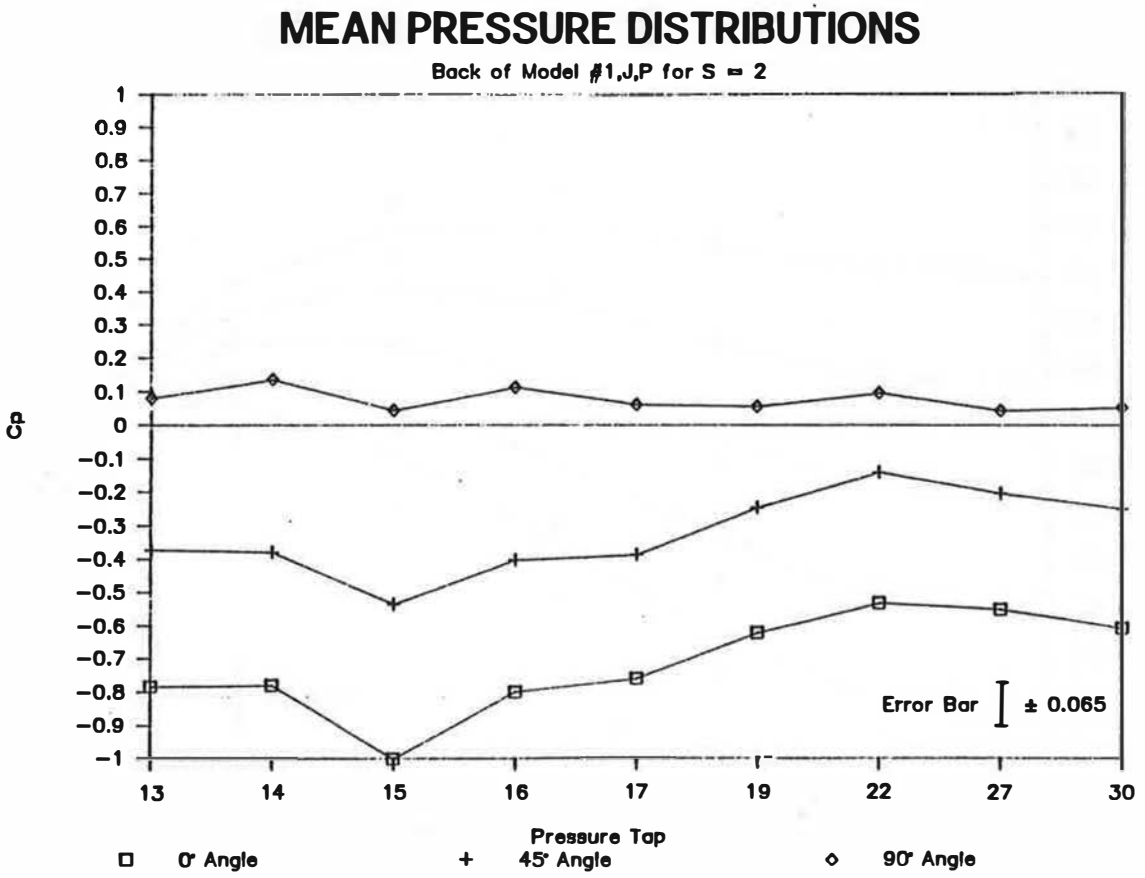

Figure 16

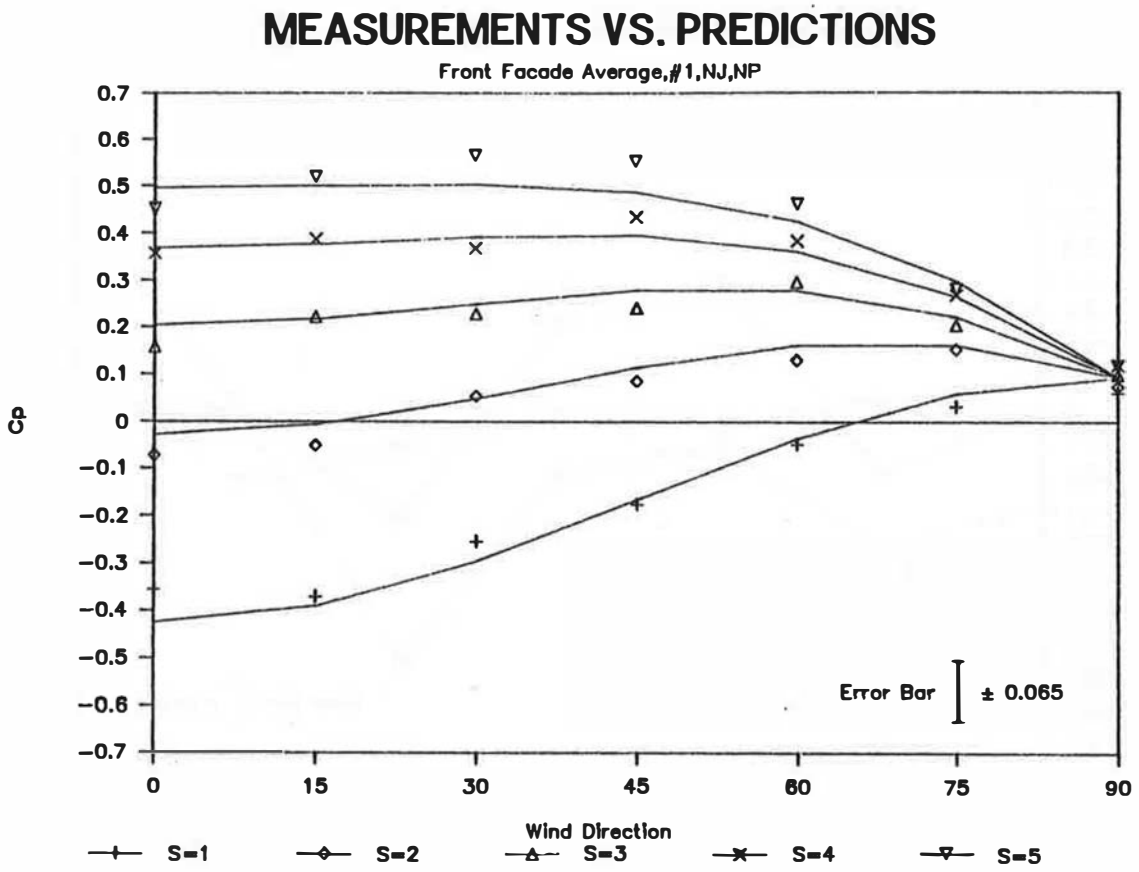

Figure 17

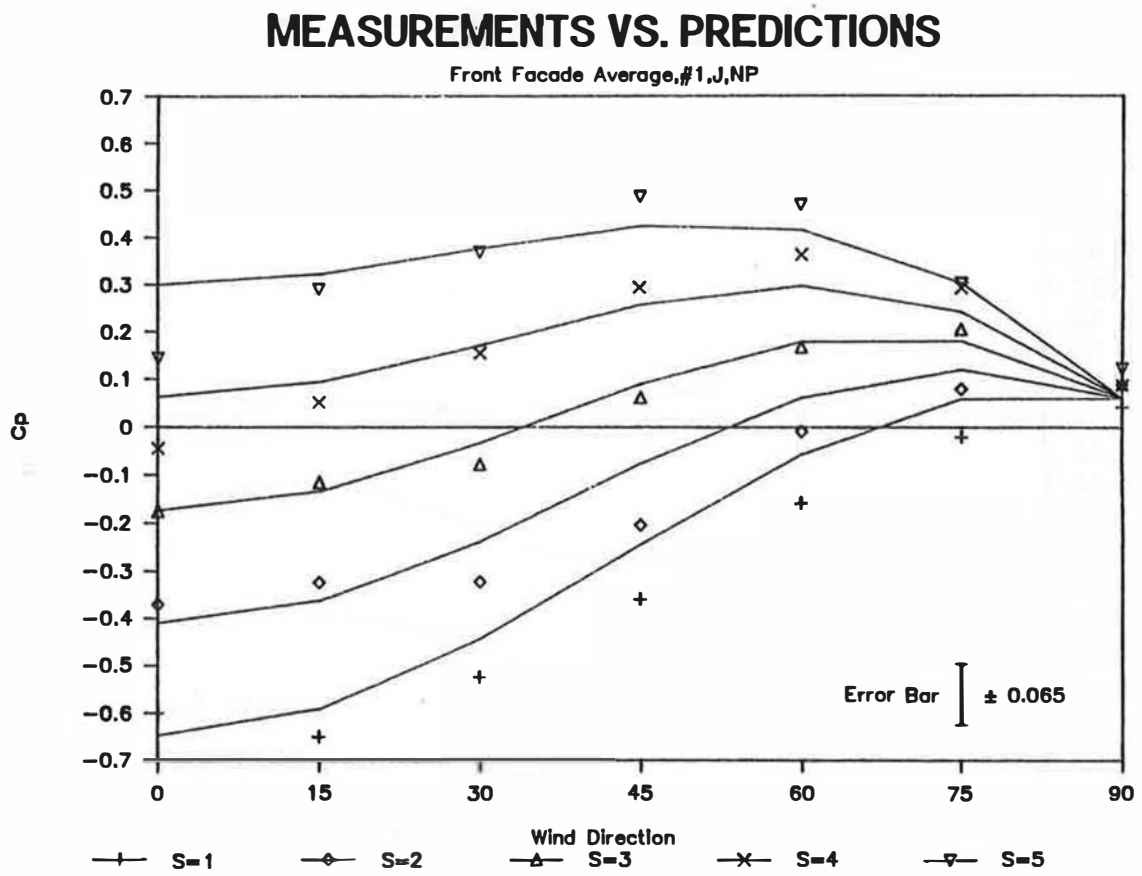

Figure 18A

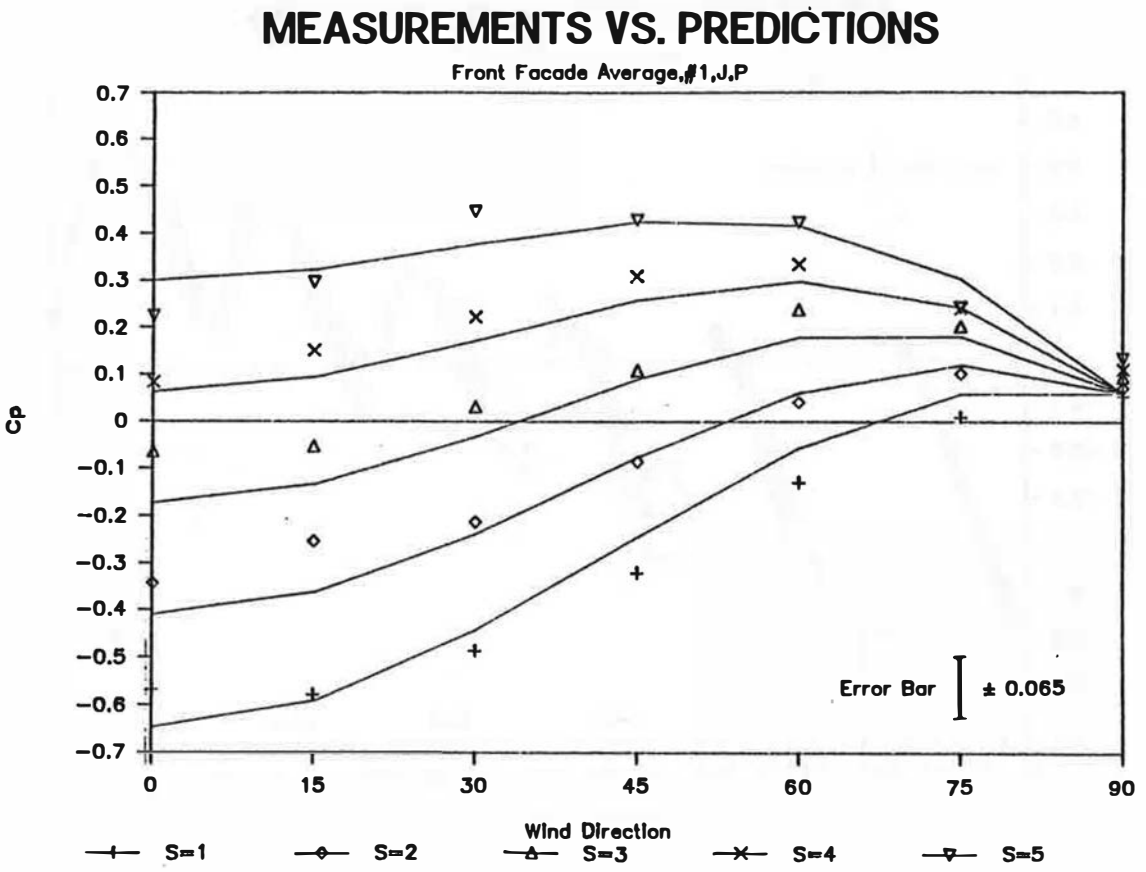

Figure 18B

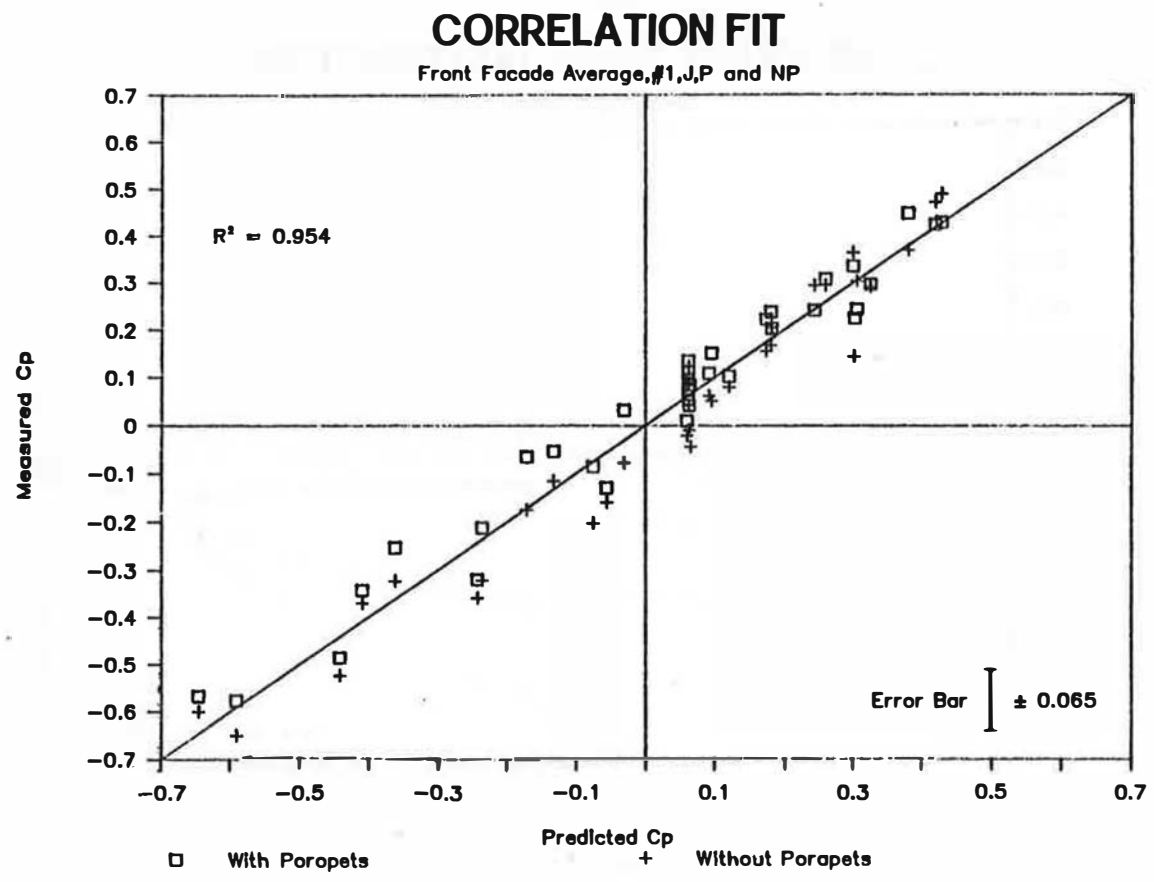

Figure 19

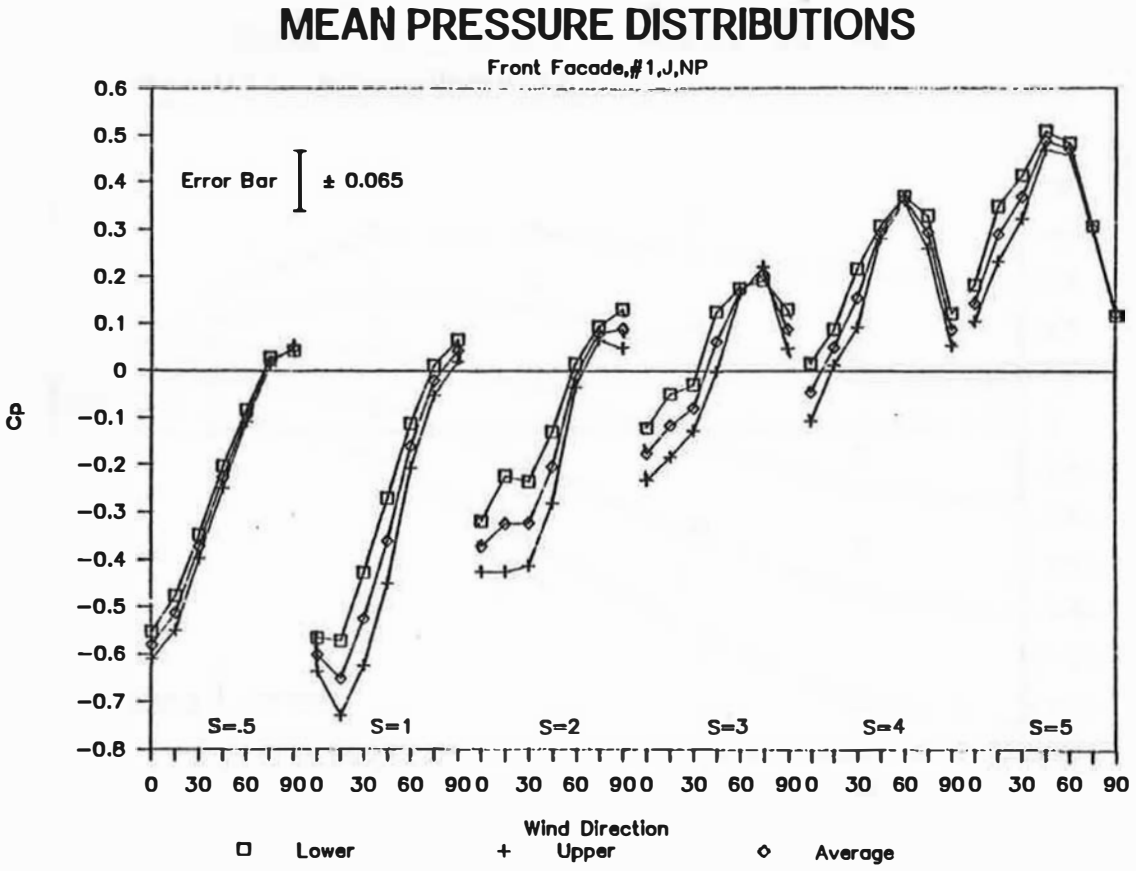

Figure 20

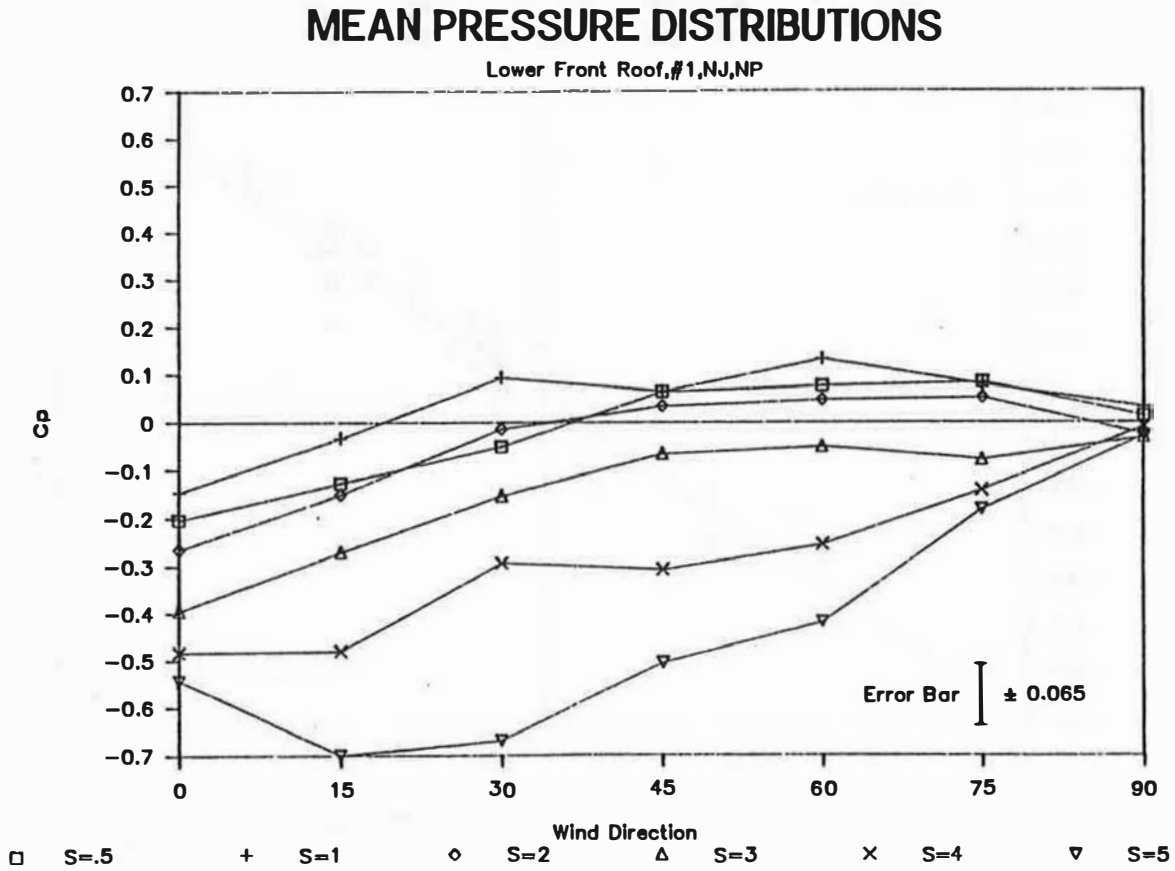

Figure 21

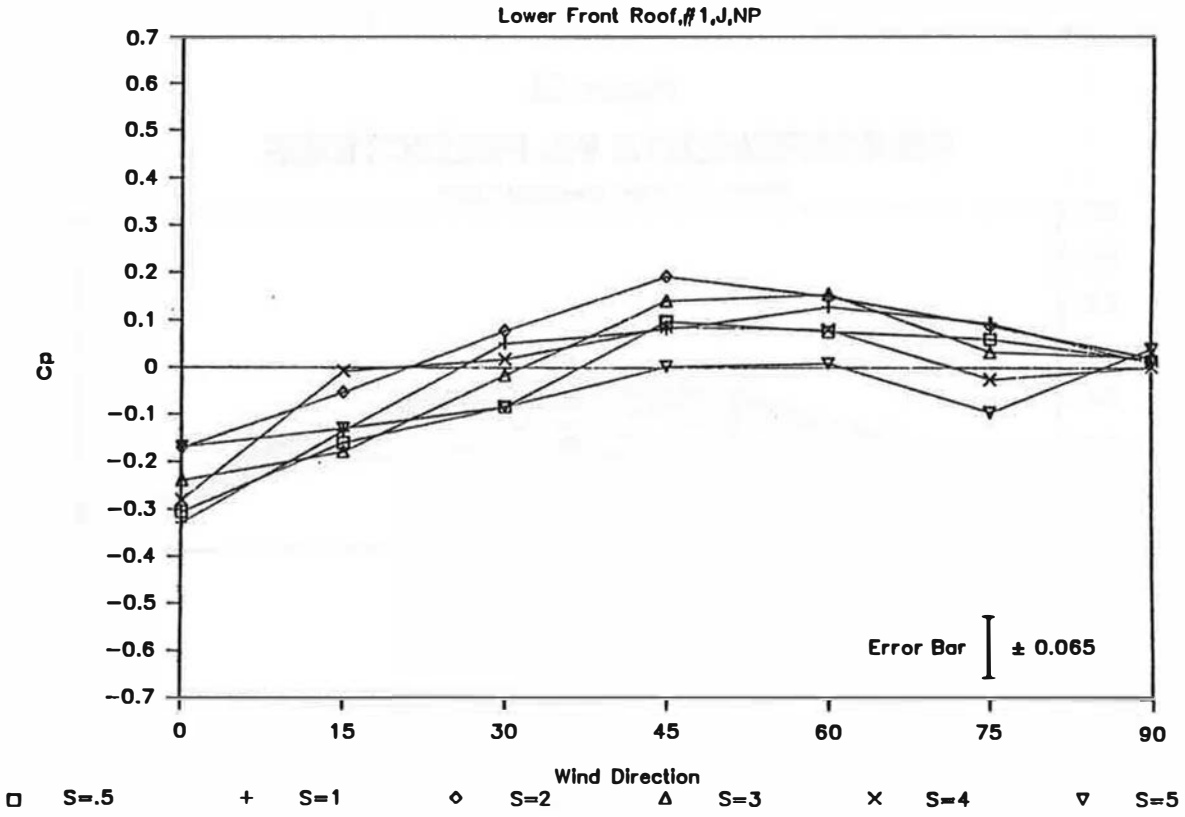

Figure 22

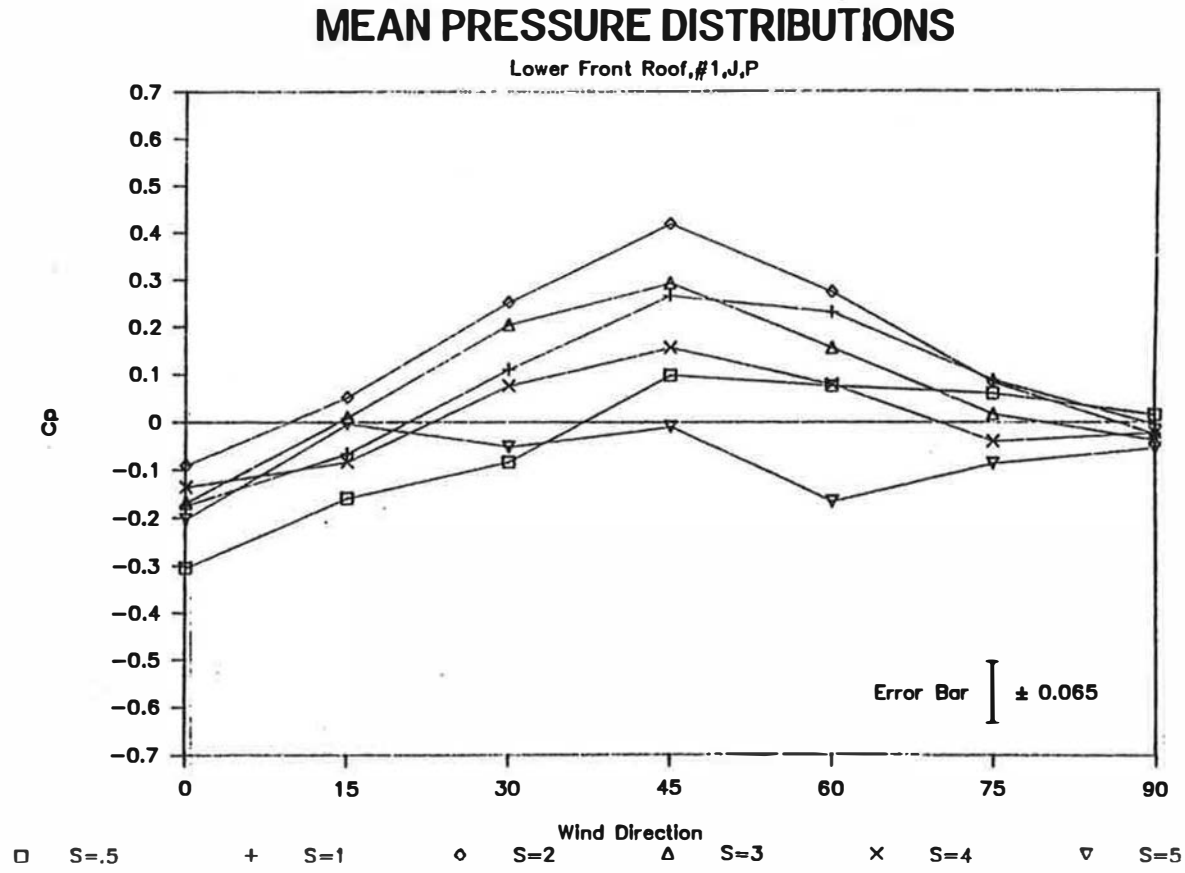

Figure 23

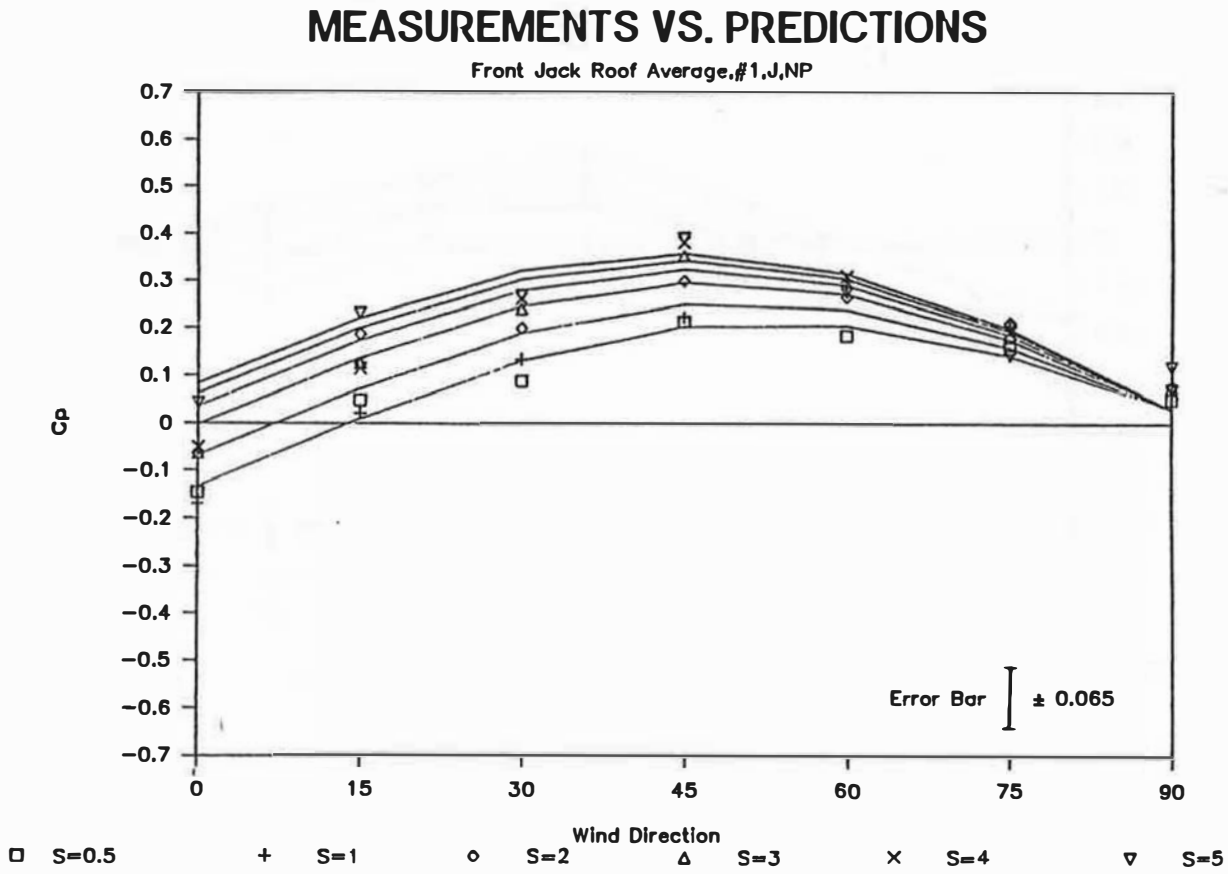
MEASUREMENTS VS. PREDICTIONS
Front Jack Roof Average,#1,J,NP
Cp
0.7
0.6
0.5
0.4
0.3
0.2
0.1
0
−0.1
−0.2
−0.3
−0.4
−0.5
−0.6
−0.7
0
15
30
45
60
75
90
Wind Direction
Error Bar
± 0.065
S=0.5
S=1
S=2
S=3
S=4
S=5

Figure 24A

MEASUREMENTS VS. PREDICTIONS

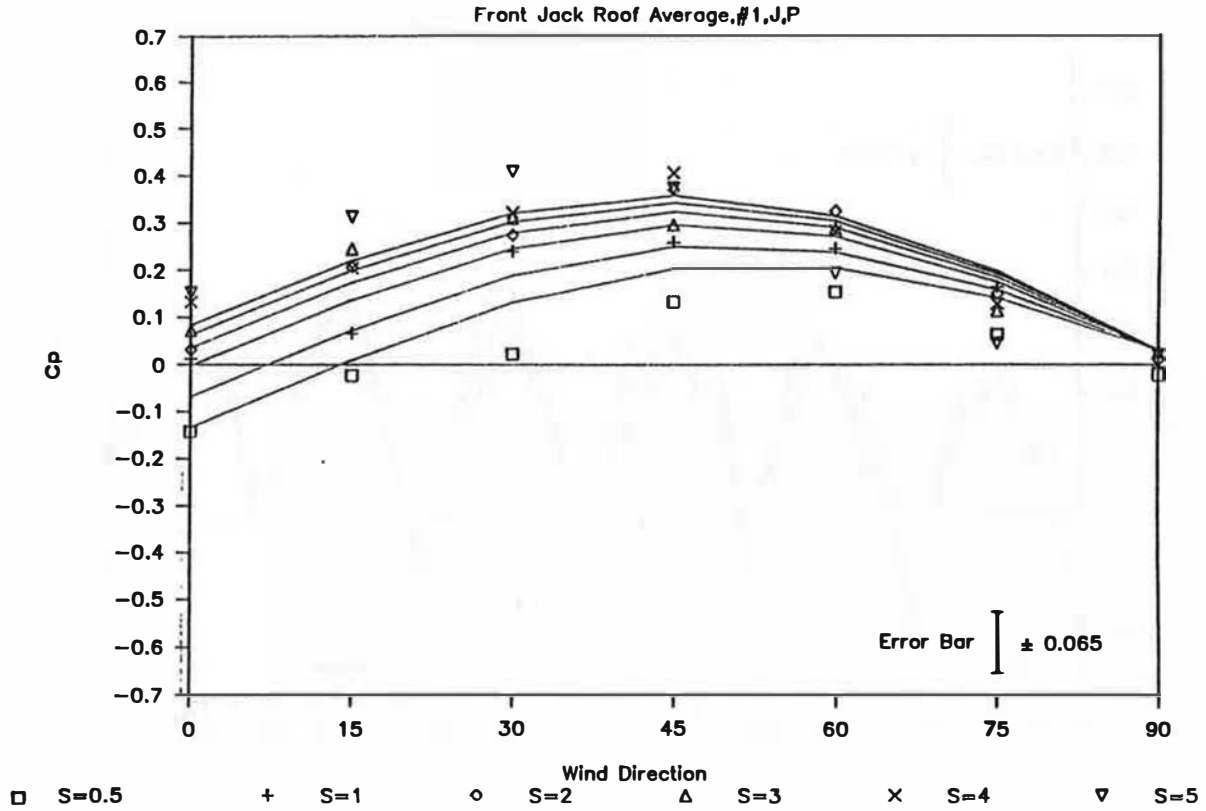

Figure 24B

CORRELATION FIT

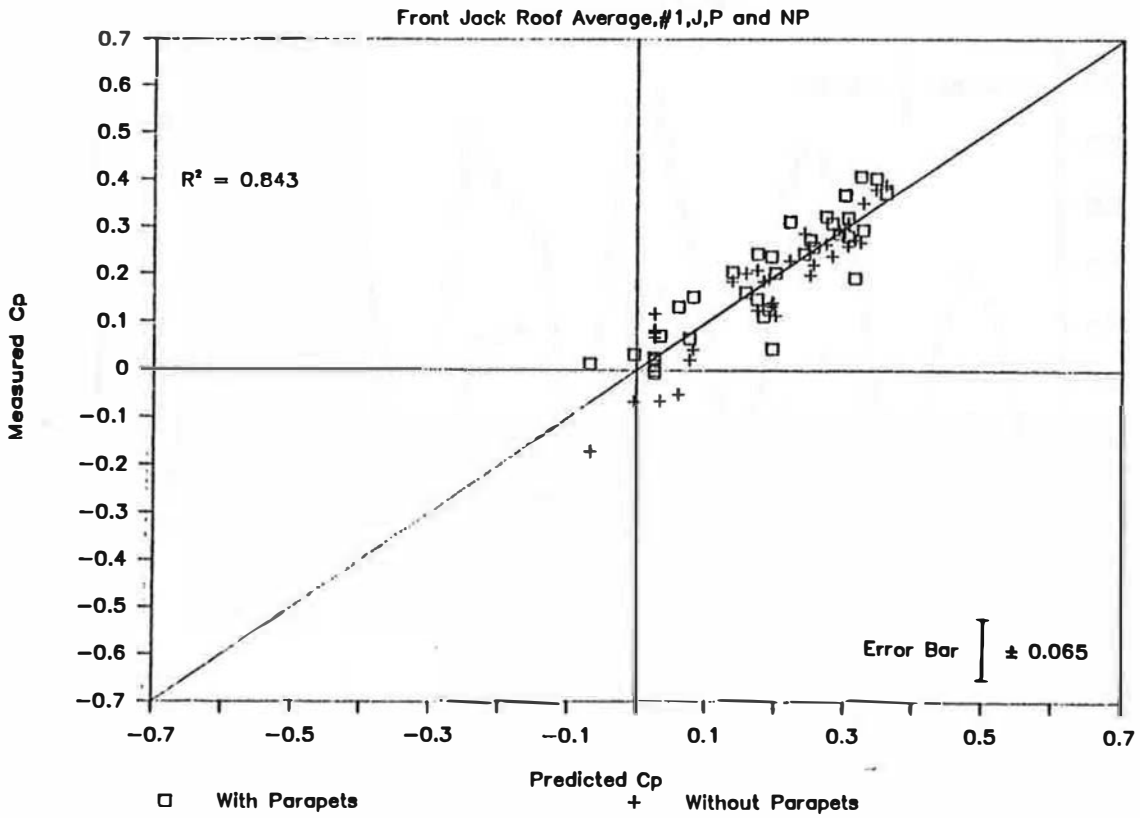

Figure 25

MEAN PRESSURE DISTRIBUTIONS

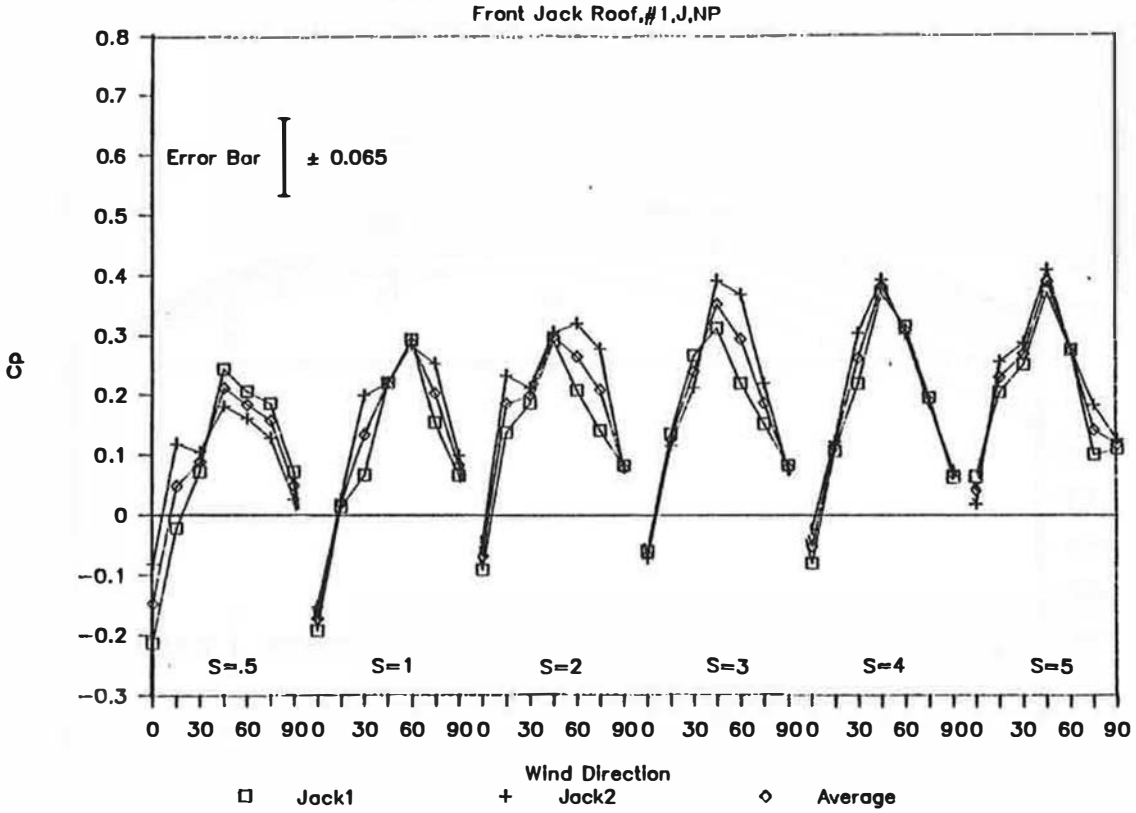

Figure 26

MEAN PRESSURE DISTRIBUTIONS

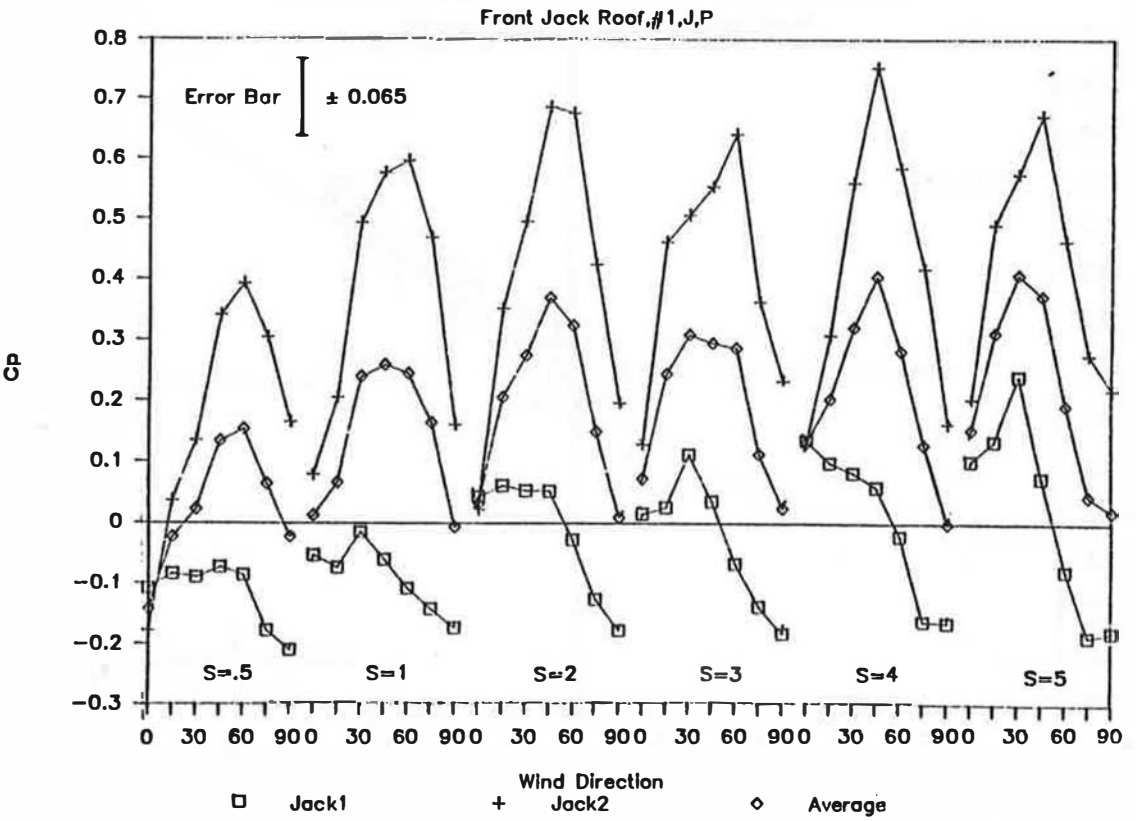

Figure 27

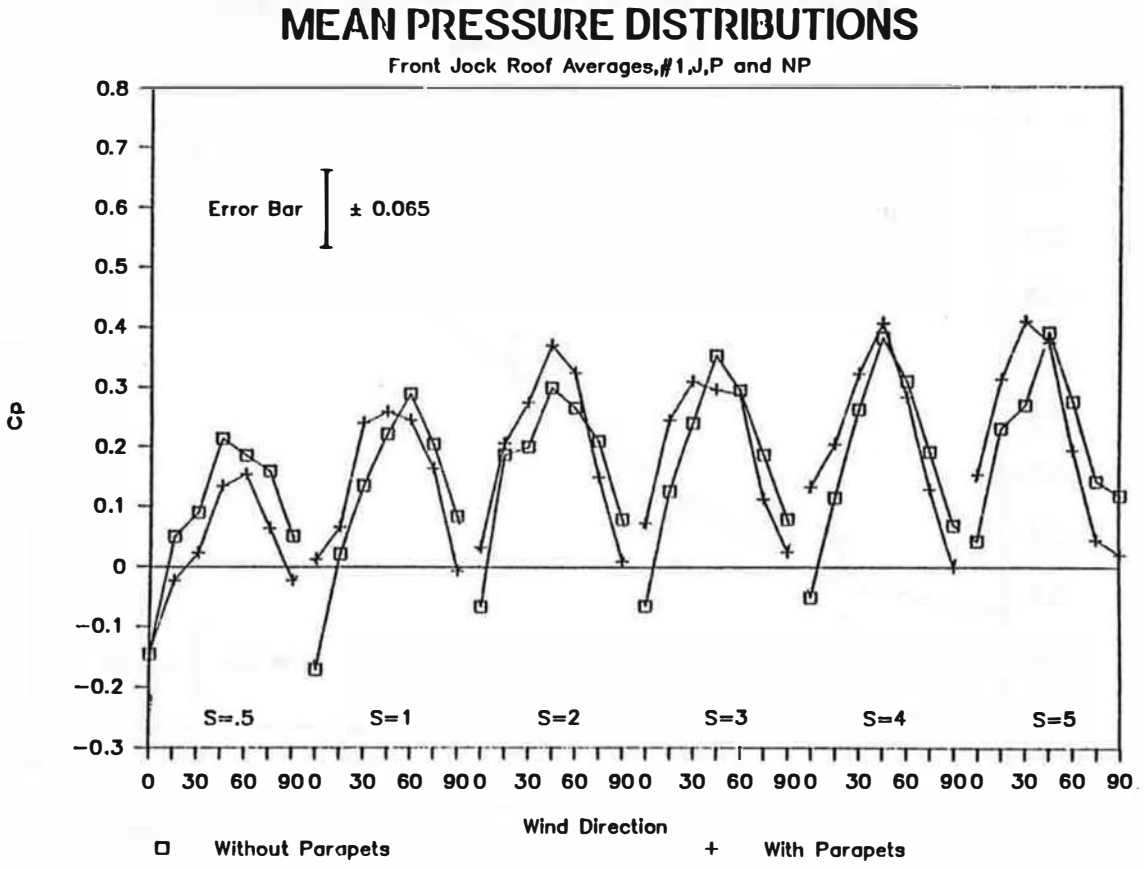

Figure 28

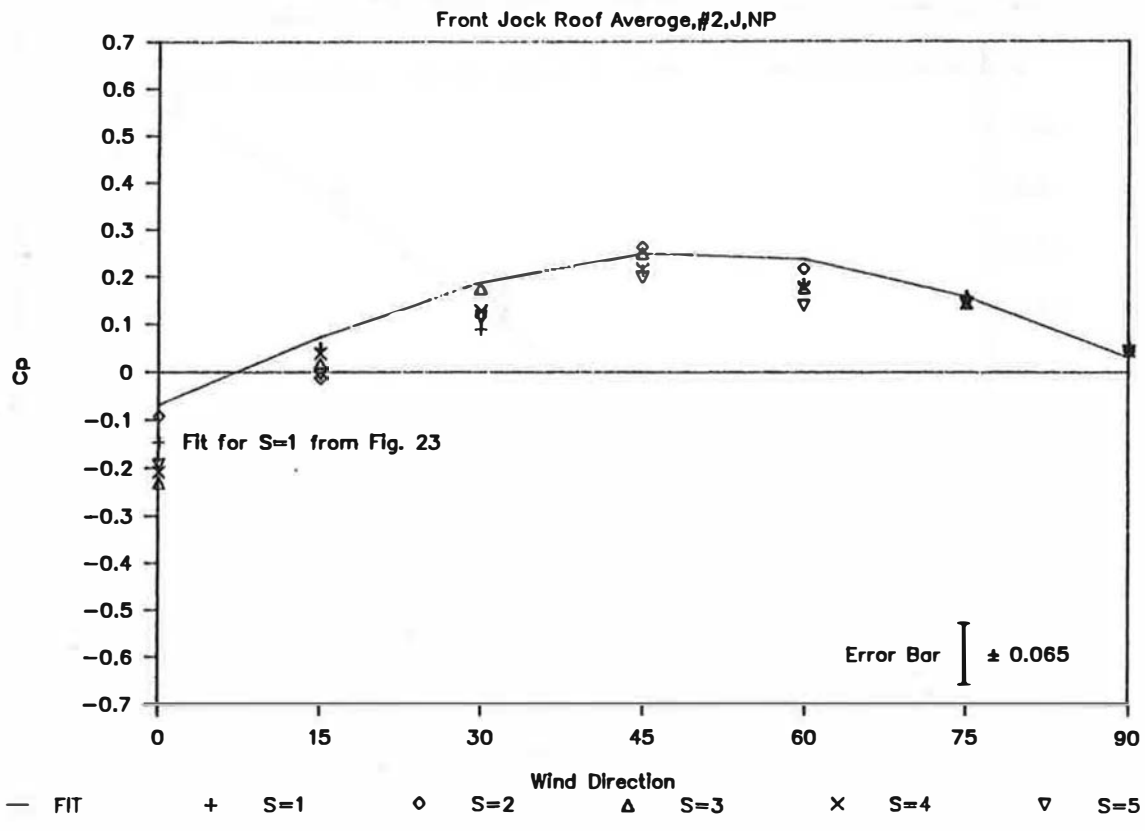

Figure 29

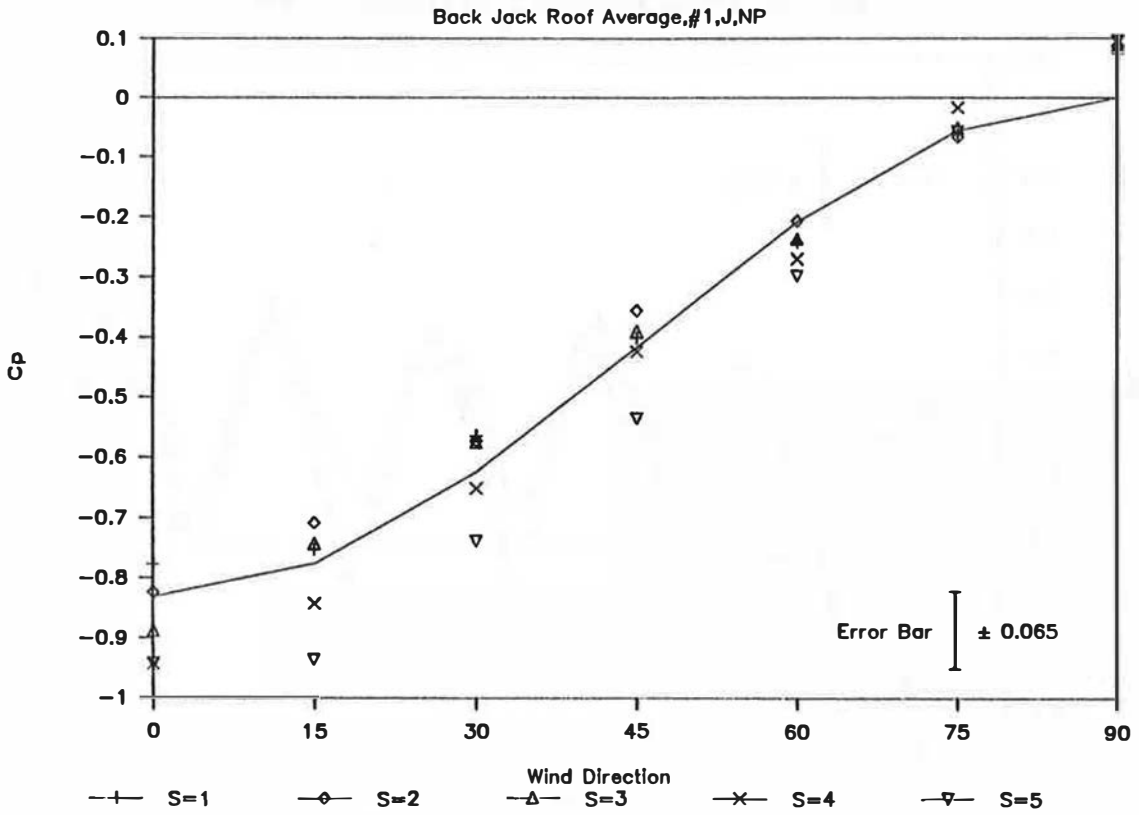

Figure 30

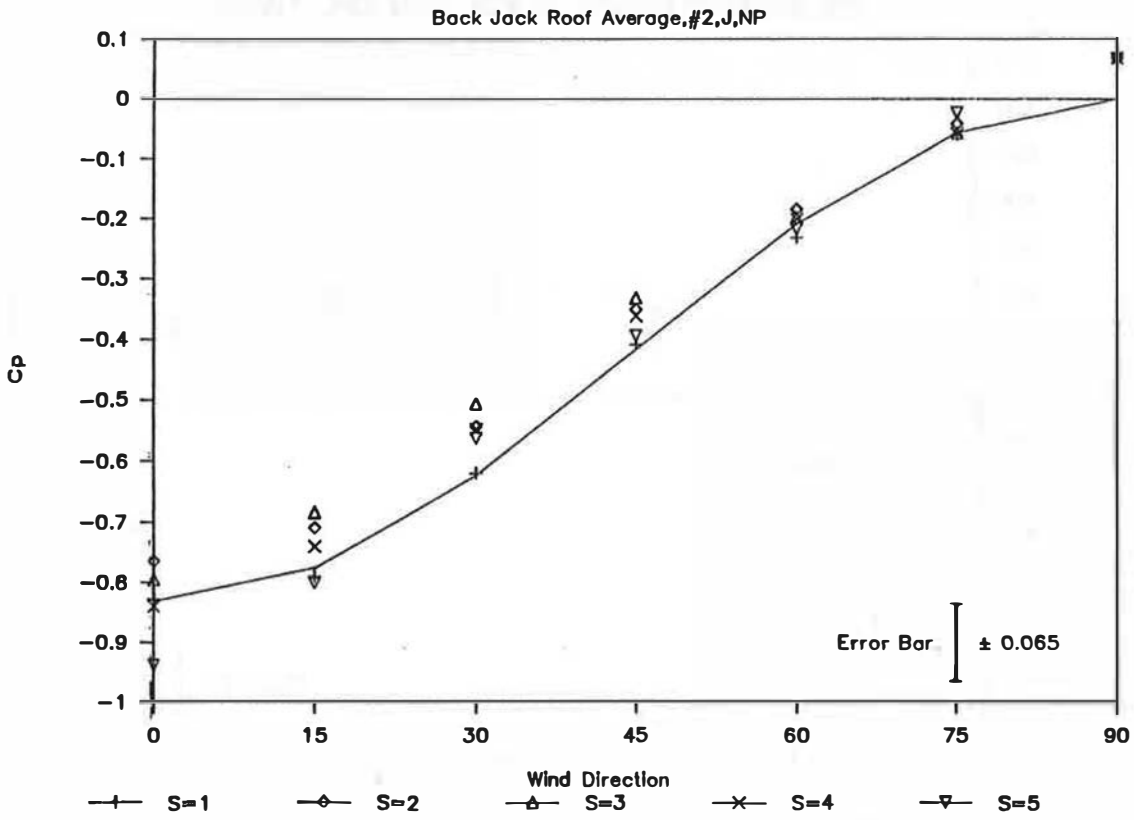

Figure 31

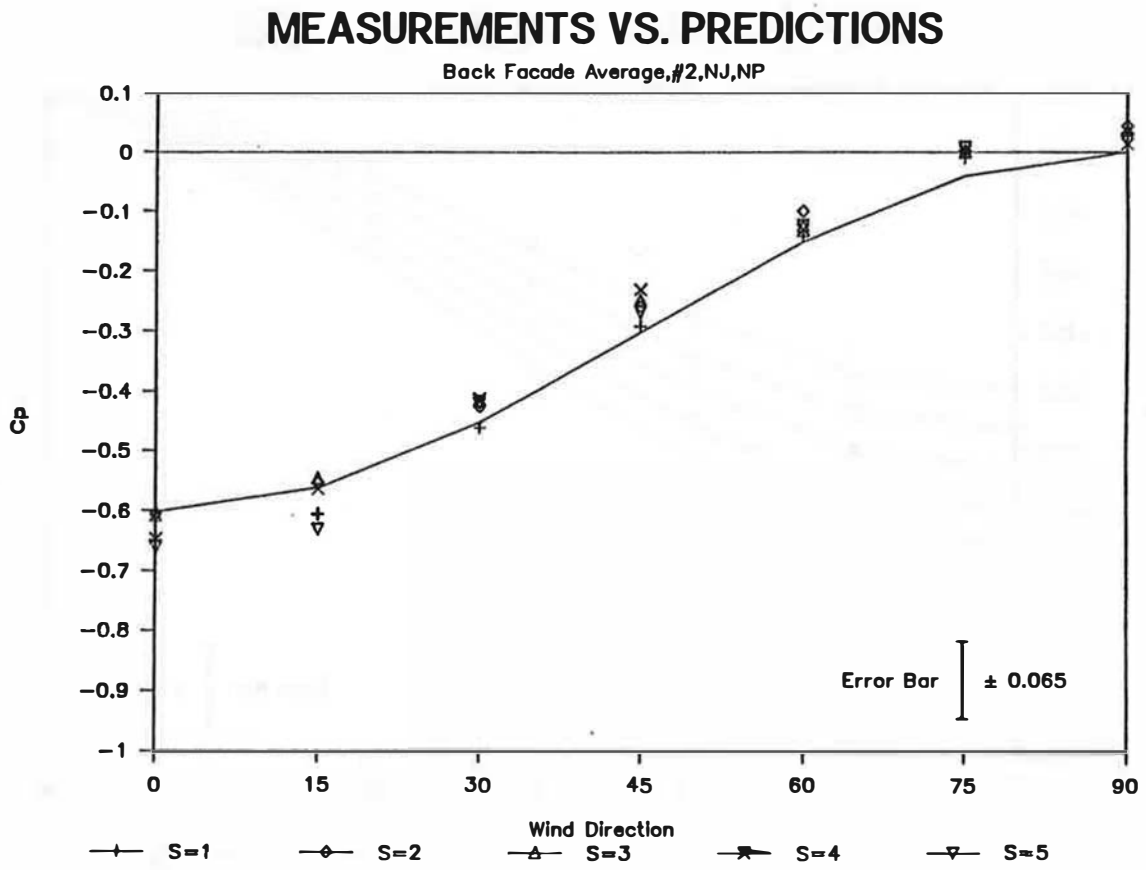

Figure 32

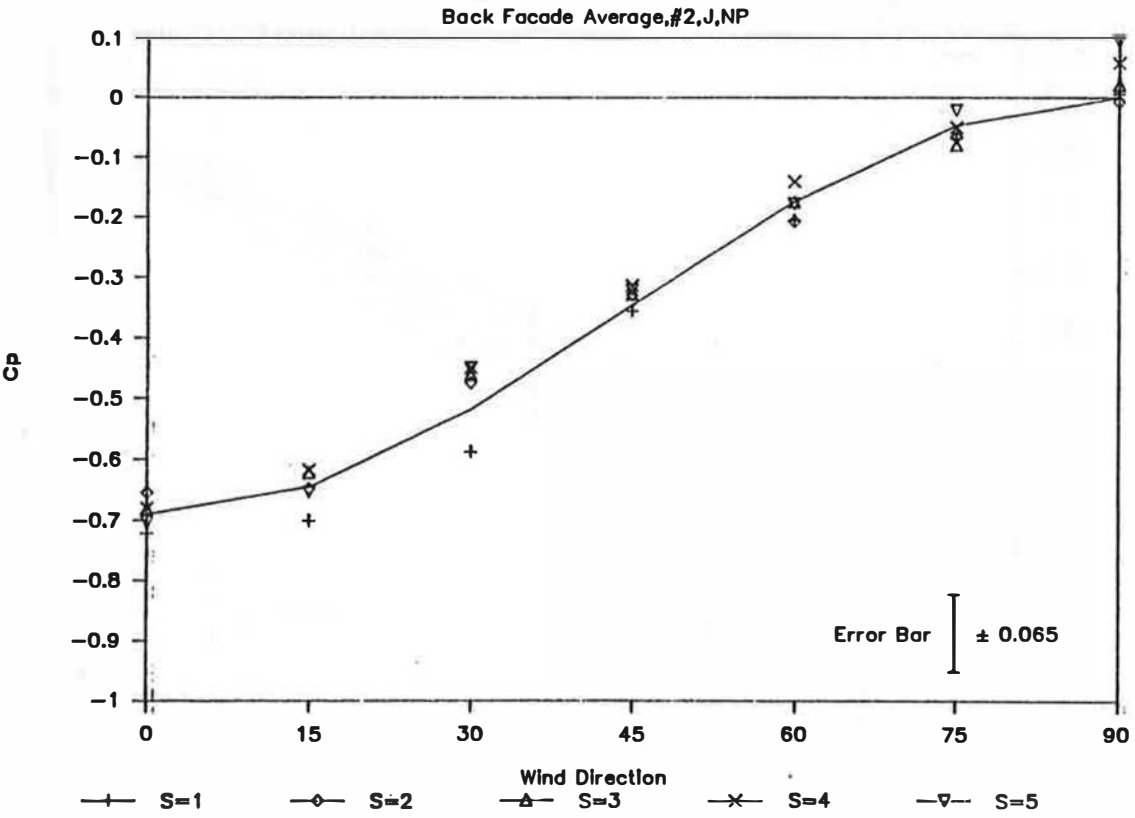

Figure 33

MEASUREMENTS VS. PREDICTIONS

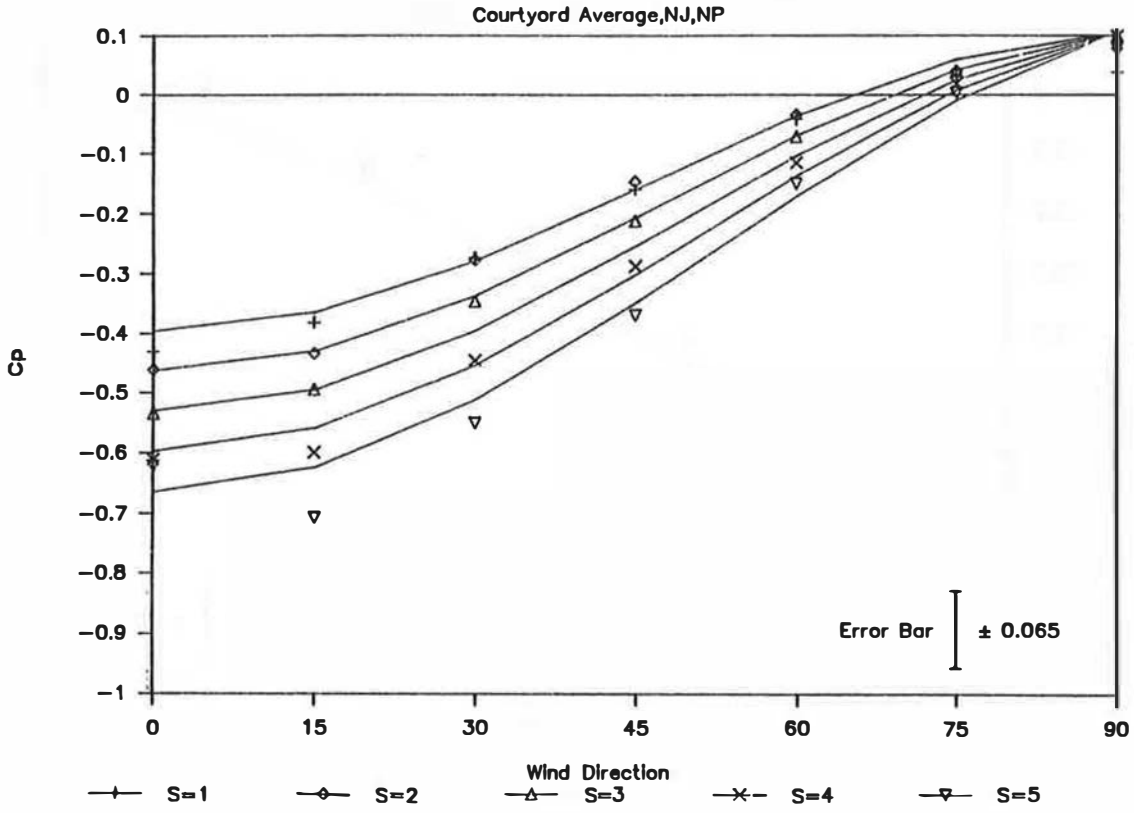

Figure 34

MEASUREMENTS VS. PREDICTIONS

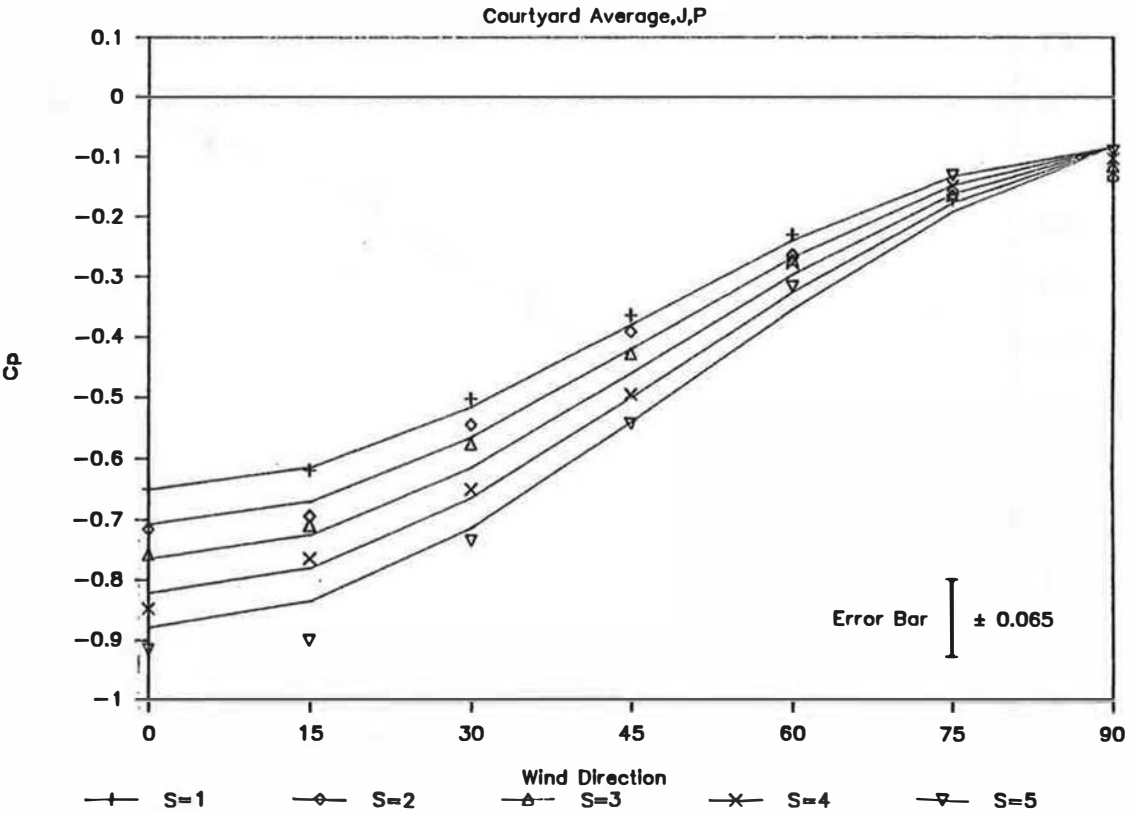

Figure 35

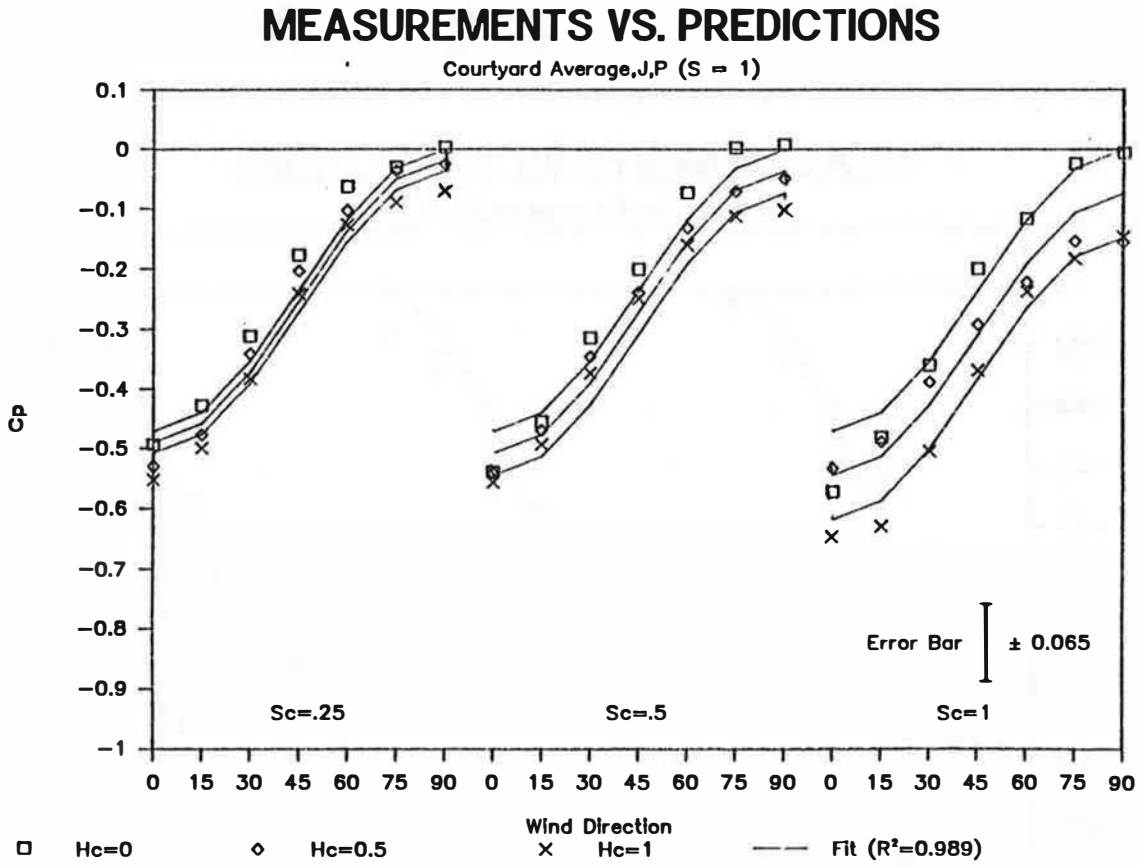

Figure 36

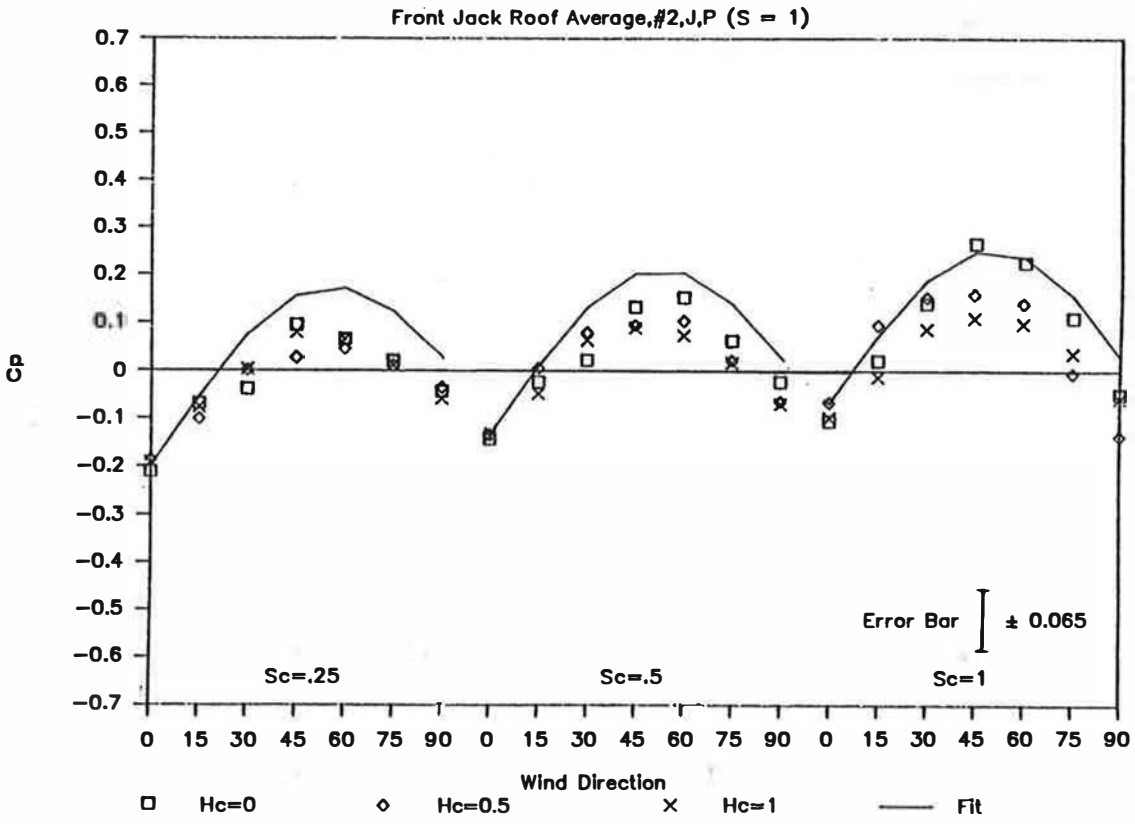

Figure 37

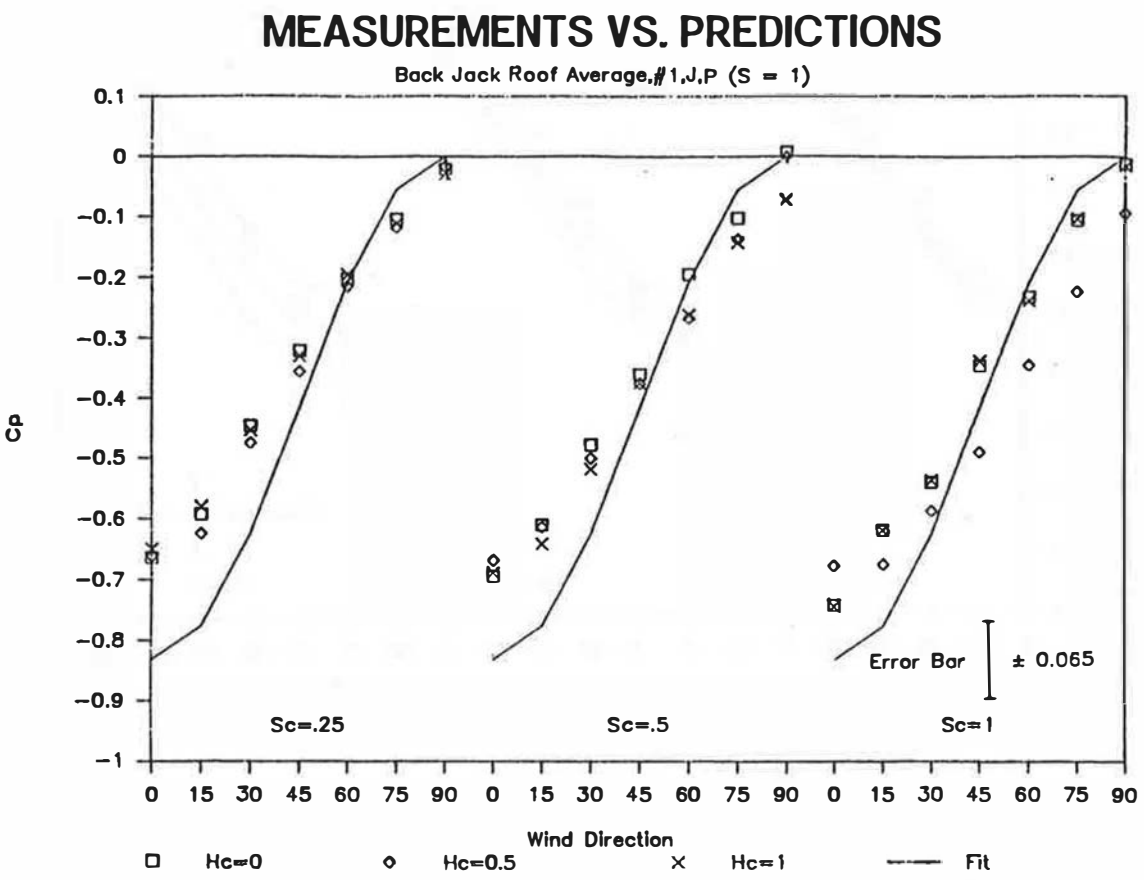
MEASUREMENTS VS. PREDICTIONS
Back Jack Roof Average,#1,J,P (S = 1)
Cp
0.1
0
-0.1
-0.2
-0.3
-0.4
-0.5
-0.6
-0.7
-0.8
-0.9
-1
0 15 30 45 60 75 90 0 15 30 45 60 75 90 0 15 30 45 60 75 90
Wind Direction
Sc=.25
Sc=.5
Sc=1
Error Bar
± 0.065
Hc=0
Hc=0.5
Hc=1
Fit

Figure 38

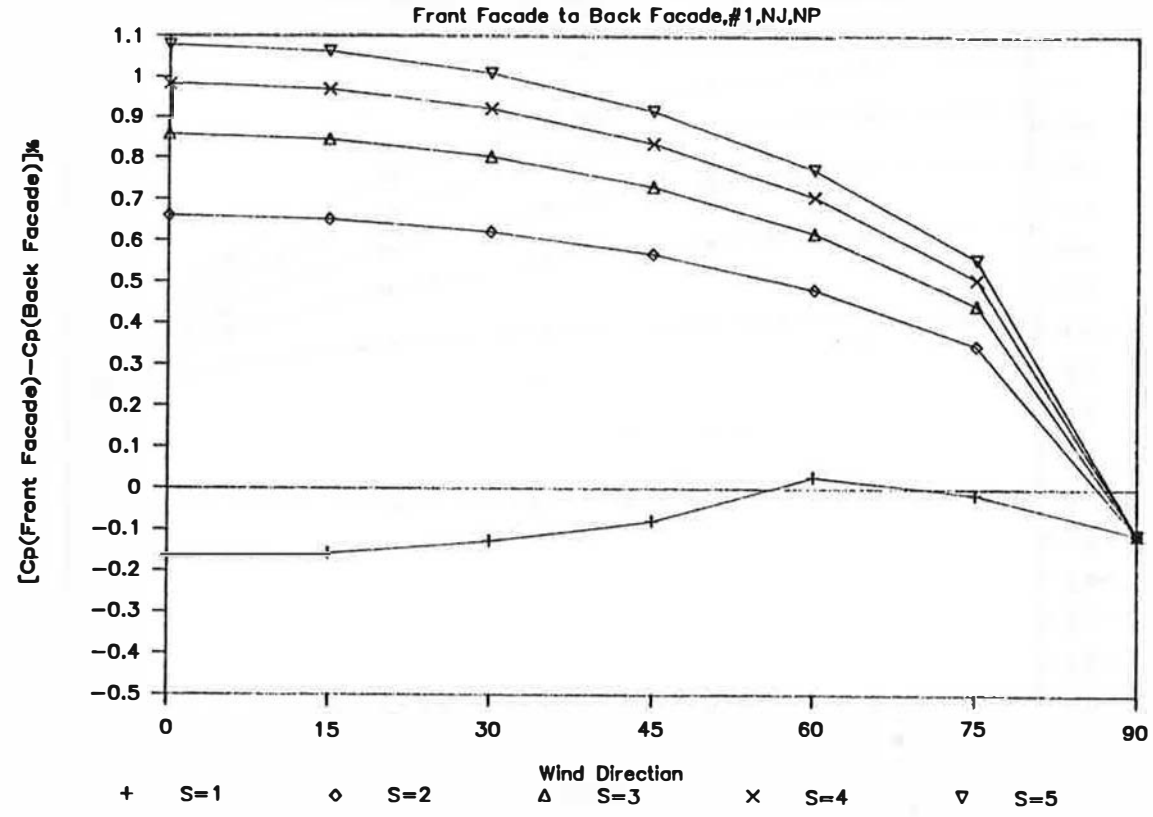

Figure 39

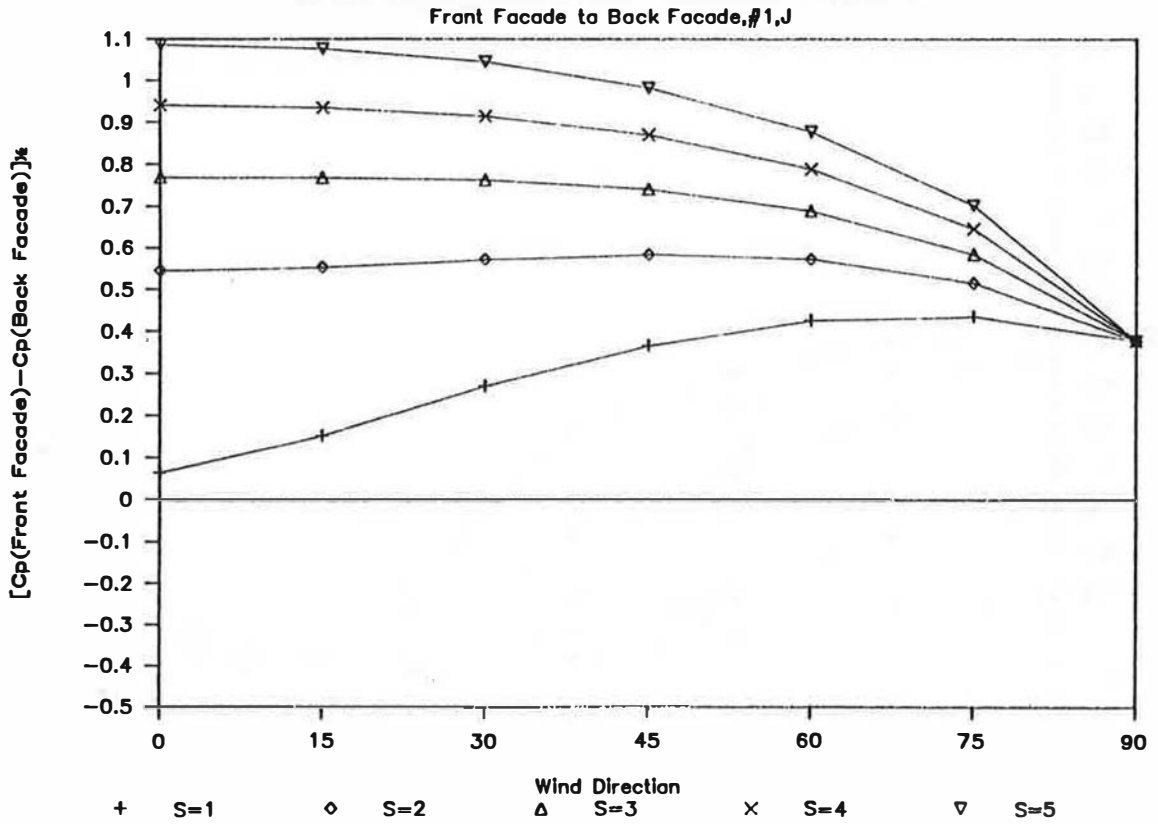

Figure 40

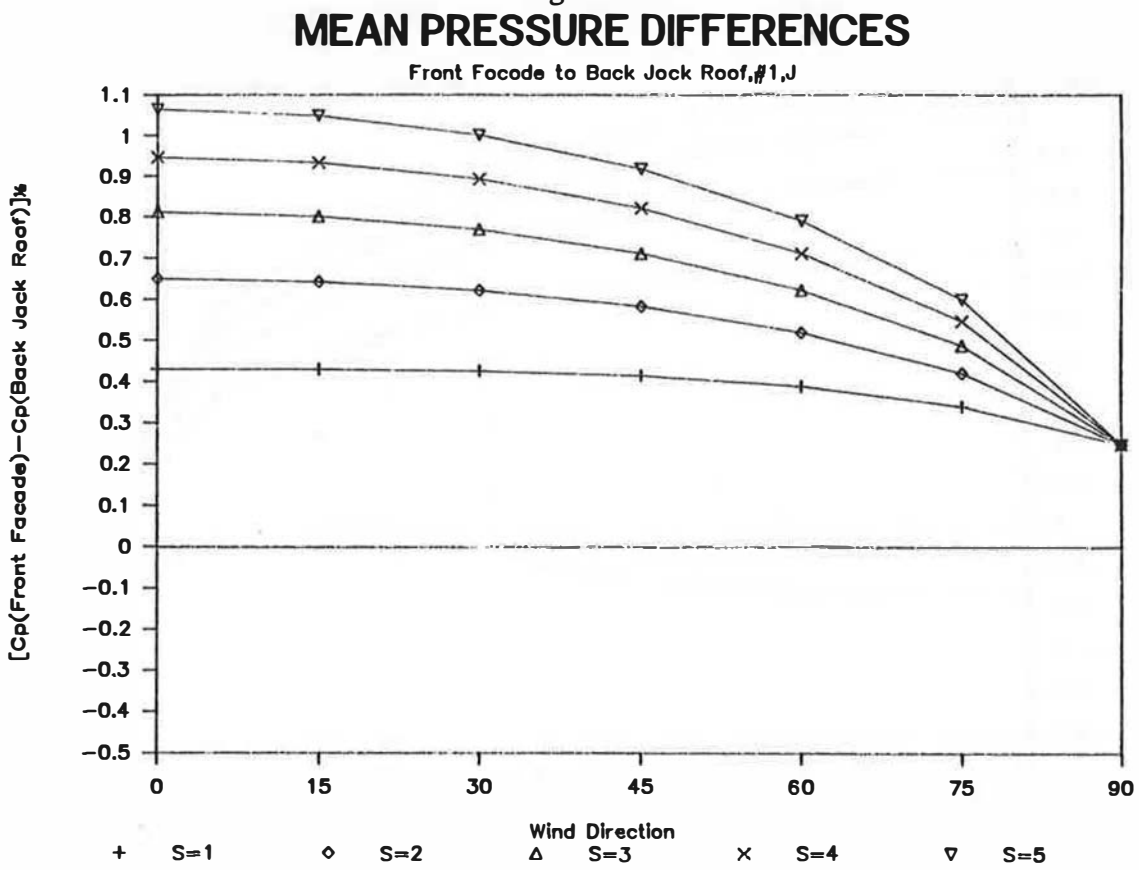

Figure 41

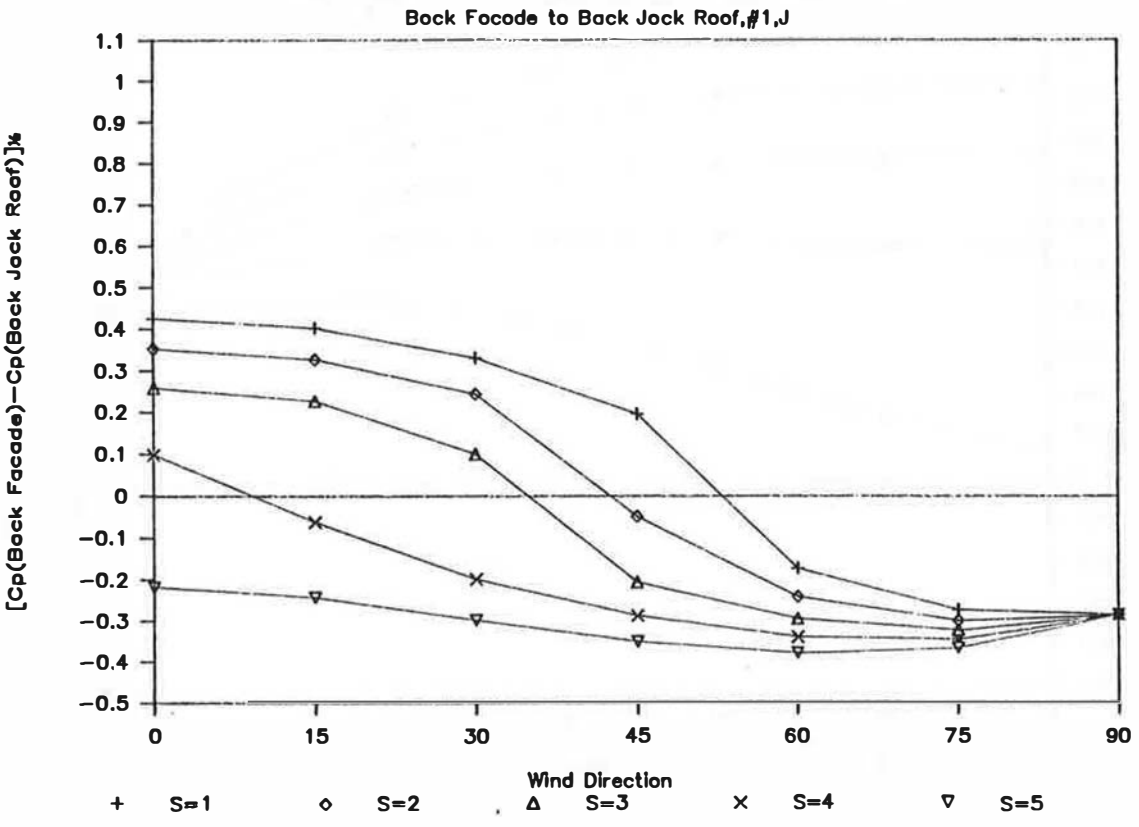

Figure 42

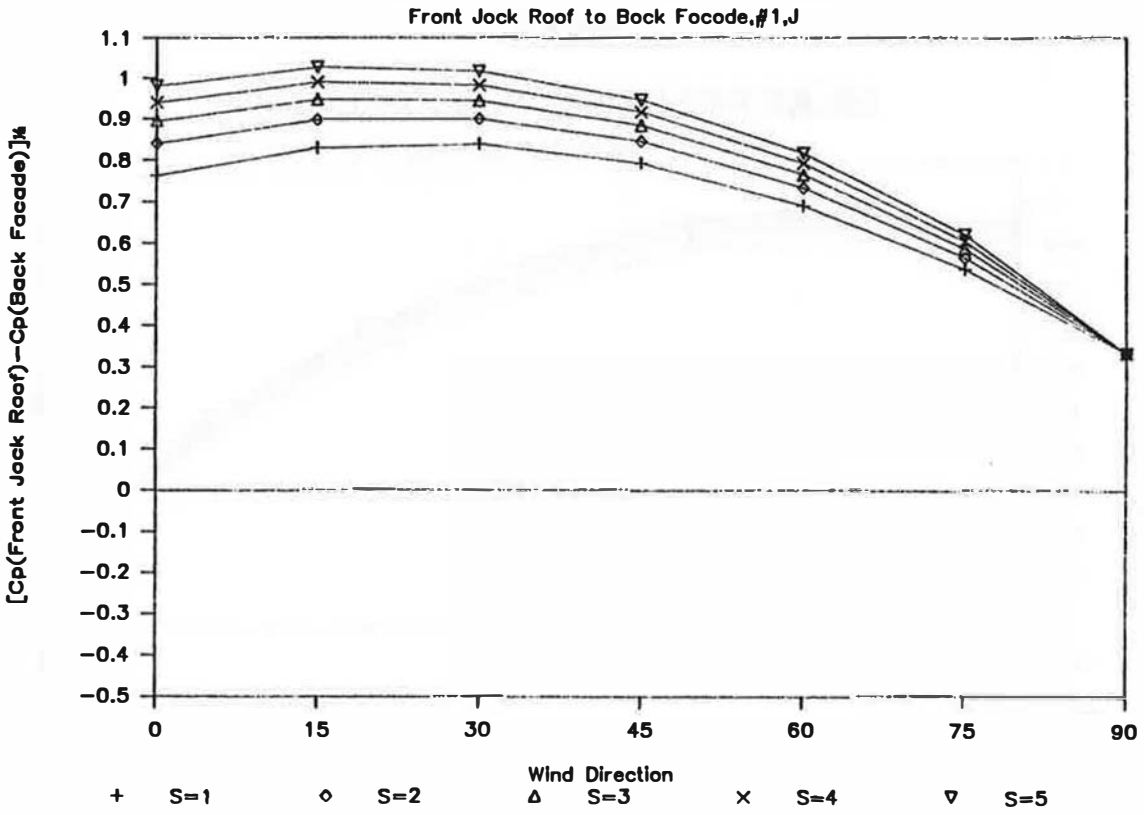

Figure 43

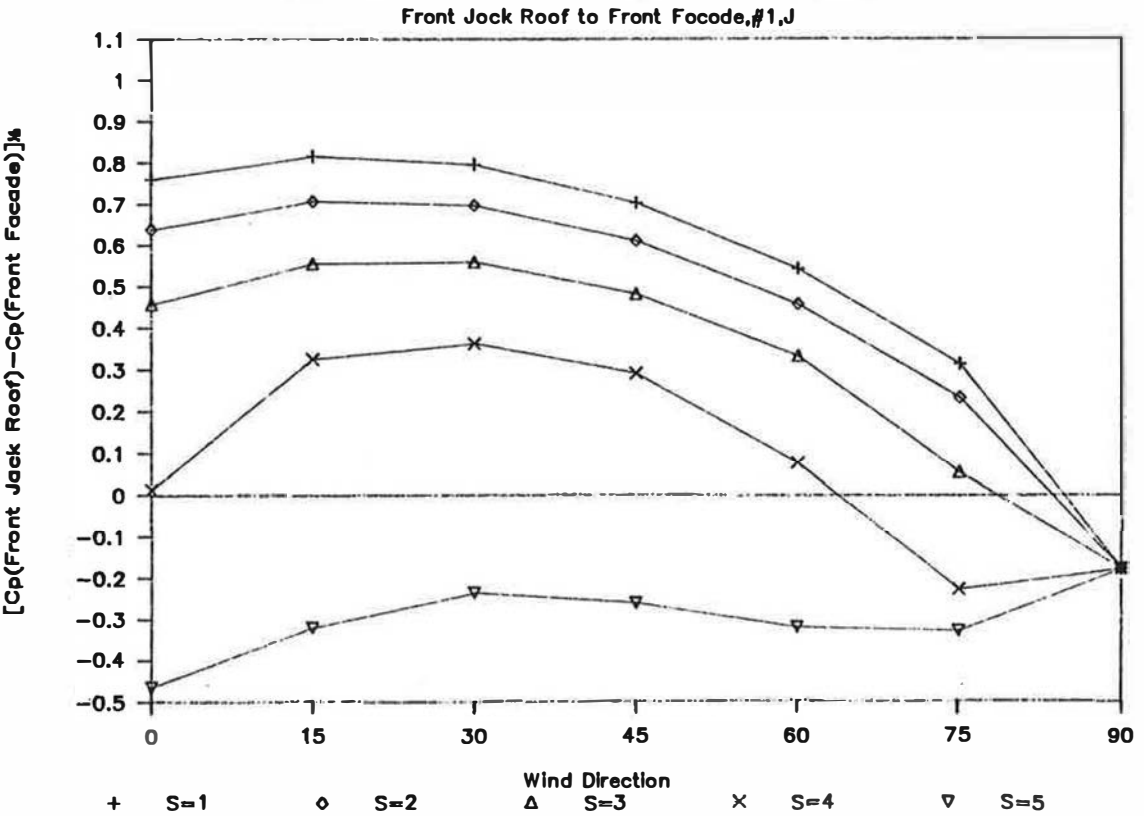

Figure 44

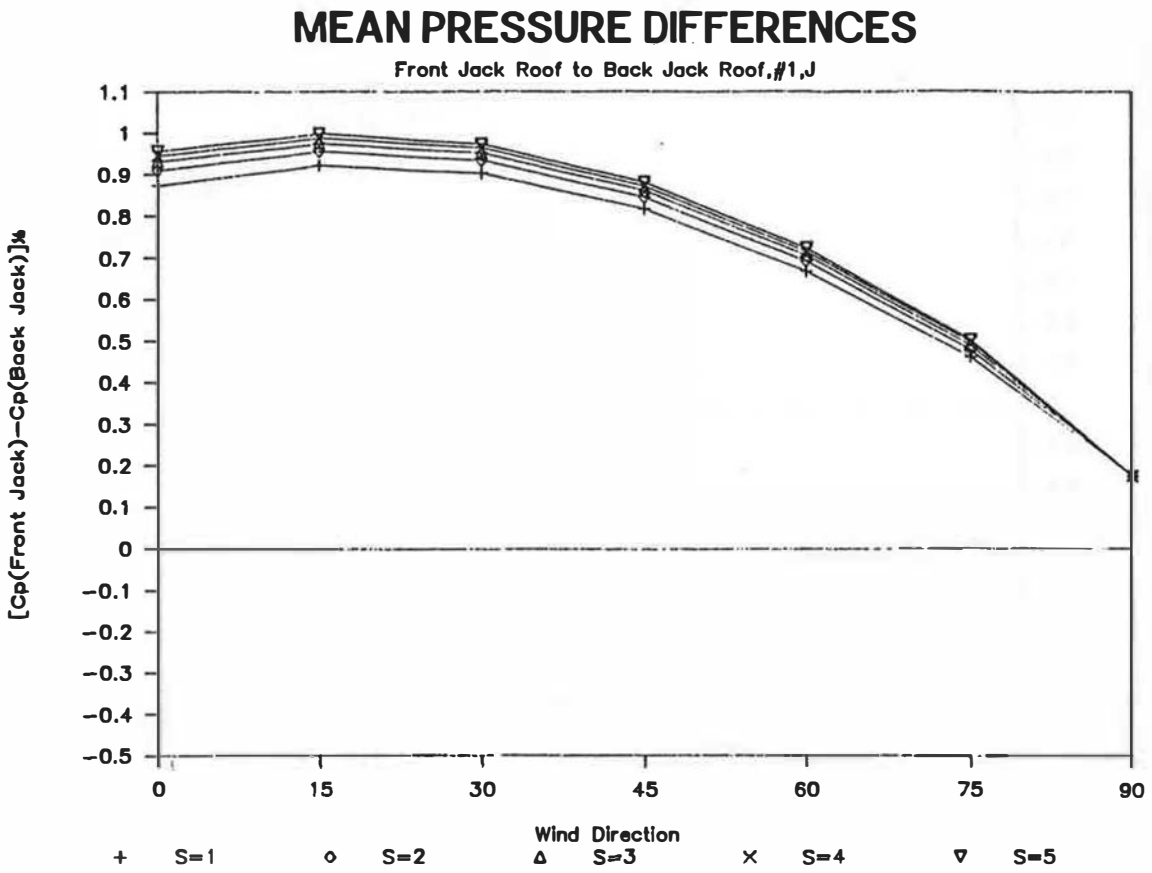
MEAN PRESSURE DIFFERENCES
Front Jack Roof to Back Jack Roof,#1,J
[Cp(Front Jack)−Cp(Back Jack)]
1.1
1
0.9
0.8
0.7
0.6
0.5
0.4
0.3
0.2
0.1
0
−0.1
−0.2
−0.3
−0.4
−0.5
0
15
30
45
60
75
90
Wind Direction
+ S=1
◇ S=2
△ S=3
× S=4
▽ S=5